

Quantifying intermolecular interactions as a basis of domain formation in membranes

Inauguraldissertation

zur

Erlangung der Würde eines Doktors der Philosophie

vorgelegt der

Philosophisch–Naturwissenschaftlichen Fakultät

der Universität Basel

von

Alekos D. Tsamaloukas

aus Hilden, Deutschland

Basel, 2006

Genehmigt von der Philosophisch-Naturwissenschaftlichen Fakultät
auf Antrag von:

PD Dr. Heiko Heerklotz

Prof. Dr. Joachim Seelig

Basel, 24. Januar 2006

Prof. Dr. Hans-Jakob Wirz (Dekan)

Es gibt keine Kunst, welche so schwierig ist, wie die Kunst der Beobachtung: es gehört dazu ein gebildeter nüchterner Geist und eine wohlgeschulte Erfahrung, welche nur durch Übung erworben wird; denn nicht der ist der Beobachter, welcher das Ding vor sich mit seinen Augen sieht, sondern der, welcher sieht, aus welchen Teilen das Ding besteht und in welchem Zusammenhange die Teile mit dem Ganzen stehen. Mancher übersieht die Hälfte aus Unachtsamkeit, ein anderer gibt mehr als er sieht, indem er es mit dem, was er sich einbildet, verwechselt, ein anderer sieht die Teile des Ganzen, aber er wirft Dinge zusammen, die getrennt werden müssen.

J. Liebig

Contents

1	Summary	1
2	Introduction	3
2.1	Lipids as the structural building blocks of membranes	3
2.2	Summary of the topics addressed	5
2.2.1	Differential interactions of cholesterol with different lipids . . .	5
2.2.2	Interaction of detergents with lipid membranes	6
2.2.3	Packing properties of lipid/cholesterol mixtures	7
2.3	Concluding Remarks	8
	Bibliography	9
	Acknowledgements	15
	Published and submitted work	17
	Structural, Volumetric, and Thermodynamic Characterization of a Mi- cellar Sphere-to-Rod Transition	18
	Interactions of Cholesterol with Lipid Membranes and Cyclodextrin Characterized by Calorimetry	34
	A Quantitative Model Describing the Selective Solubilization of Mem- brane Domains	45
	Nonideal mixing in multicomponent lipid/detergent systems	58
	Thermodynamic comparison of the interactions of cholesterol with un- saturated phospholipid and sphingomyelins	78
	Gradual change or phase transition — characterizing liquid lipid- cholesterol membranes on the basis of thermal volume changes	99
	Tabellarischer Lebenslauf	114

1 Summary

Within the last two decades the field of membrane biology has witnessed an increased interest in the function and organization of membrane lipids with a particular focus on the possibility of these to demix into separate domains. The present thesis aimed at providing quantitative information about intermolecular interactions that may be responsible for the formation of such lipid domains in membranes. Vesicular lipid model systems mimicking the composition of the plasma membrane were biophysically characterized by means of modern microcalorimetric techniques as a function of temperature and in the presence (or absence) of detergents.

For the formation and/or existence of one specific type of lipid domain, so called *lipid rafts*, that are under intense scrutiny at present, cholesterol is reasoned to be of paramount importance. To study differential interactions of cholesterol with different lipids, three independent experimental assays for isothermal titration calorimetry (ITC) in conjunction with a novel mathematical formalism to model these were introduced. By means of reversible complexation with methylated- β -cyclodextrin (cyd), sufficient amounts of the hydrophobic cholesterol molecule can be solubilized in the aqueous phase. Thereby it became possible to study the thermodynamics of either uptake of or release of cholesterol from lipid vesicles of various compositions. As one important result a comprehensive set of quantitative data on cholesterol/lipid interactions was obtained including for the first time also information on enthalpic contributions to the differential interactions of cholesterol with different lipids. Additionally, in these studies lipid/cyd interactions could be investigated and suggestions on how to optimize cholesterol extraction from biological membranes were made that could be derived from the different stoichiometries of the complexes formed, i.e., lipid or cholesterol complexed to cyd, respectively.

The possibility to isolate detergent resistant patches is commonly used to argue for the existence of (functional) domains in the original, detergent-free membrane. This kind of reasoning does, however, neglect the possibility of detergent-induced alteration or (in the worst case) induction of domains. In this context, a theoretical model suitable to describe the selective solubilization of a membrane containing two lipid domains (liquid ordered and liquid disordered) was developed. Based on equilibrium thermodynamical relations it was shown that detergent-induced formation of ordered membrane domains can occur if the detergent mixes nonideally with an order preferring lipid and/or cholesterol. Furthermore, both the composition as well

as the mere existence of the liquid ordered domain was shown to be highly variable upon addition of detergent to the membrane. A experimental study was carried out in parallel to these theoretical simulations with the goal to better understand the mixing of a commonly used nonionic detergent with different lipid/cholesterol systems. In order to allow for a quantitative discussion of the experimental results obtained, a theory for nonideal mixing in multicomponent lipid/detergent system was developed that accounts for nonideality in terms of simple pair interaction statistics. The parameters collected imply that a separation of ordered from disordered membrane domains can under certain circumstances occur. A crucial parameter governing the abundance and composition of detergent-resistant membrane patches appeared to be the unfavourable interaction of cholesterol with detergent. Taken together, these two studies provided additional evidence against the simple identification of *lipid rafts* with detergent resistant membrane patches.

The third part of this thesis was devoted to a characterization of different phase equilibria employing a rather new experimental technique, pressure perturbation calorimetry (PPC). A micellar sphere-to-rod transition was characterized in terms of a large set of structural, volumetric, and thermodynamic parameters including the first published data on the change in partial molar volume of a detergent occurring upon the transition. Subsequent to this study, the question whether binary mixtures of an unsaturated lipid and cholesterol should be better described in terms of a phase separation (liquid ordered and liquid disordered phases) or of gradual changes in largely homogenous membranes was addressed with the help of PPC experiments. The possibility of cholesterol to condense lipids not only laterally but also with respect to volume was measured in this study for the first time. Information on the number of condensed lipids per cholesterol were obtained by comparing the results of simulations of expansivity curves according to three theoretical models appropriate to be applied in this context. It was found that the behaviour of the binary mixtures investigated is best described in terms of submicroscopic demixing rather than true phase separation or random mixing.

2 Introduction

2.1 Lipids as the structural building blocks of membranes

Lipids, the structural building blocks of the membrane bilayer, are commonly categorized among three classes: (i) glycerophospholipids, (ii) sphingolipids, and (iii) sterols (cholesterol and related sterols) (1–3). The diversity of species belonging to the first two classes is enormous (4). For example, from an extract of a single cell type it is possible to identify more than 400 different glycerophospholipids by means of modern mass spectrometric methods (5). Given this observation, one may immediately be tempted to ask what purpose is underlying this feature. Why do cells synthesize so many different lipid species, when in principle for a simple bilayer to form, one lipid species would suffice? Why operating many different, energy requiring lipid synthesis pathways, when a single one would be enough?

Among others, one reason could be that specific lipids are needed to create “localized variations in the composition of the cell membrane” (6), in short: **membrane domains**, that in turn have a meaning for proper function of the cell.

The very notion that cell membranes may contain such specialized regions has, however, received only limited attention over the years (7). It gave rise to the concept of so-called “boundary lipids” around certain proteins (8, 9) but this idea had to be abandoned when the results of different experimental techniques were compared. Nevertheless, about 20 years ago a major change in the perception of membrane bilayer architecture occurred again for the following reasons. Firstly, Simons and van Meer (10) proposed in their studies of epithelial cells a lipid sorting mechanism resulting in a lateral and asymmetric separation of sphingolipids and glycerophospholipids, respectively. Secondly, a better understanding of lipid biophysics, lipid sorting processes, and the effects of detergents on biological membranes were combined by some authors to argue for the existence of so-called “lipid rafts” (11–16) in the plasma membrane of cells. These membrane microdomains are proposed to be enriched in sphingolipids, saturated phospholipids with long chains, cholesterol (17, 18), and selected classes of proteins, e.g., glycosylphosphatidylinositol anchored proteins. Furthermore, based on a tentative equivalence with the behaviour observed in model membrane systems, “lipid rafts” are said to be in an liquid ordered phase (19–22) (ℓ_o -phase) thereby distinguishing them from

the otherwise fluid phase membrane (liquid disordered, ℓ_d -phase). They are now implicated to play a pivotal role in many important biological processes like, e.g., signal transduction, apoptosis, cell adhesion and migration and many more (23, 24).

Conclusive experimental evidence regarding the existence of “lipid rafts” *in vivo* is weak at present, despite the thousands of publications related to this topic that accumulated over the last 10–15 years (excellent reviews are, e.g., (25–28)). In addition to the “Seeing is believing” line of argumentation (29), especially two of the main criteria commonly applied to argue for their *in vivo*-existence are likely to be error prone: (i) resistance of certain membrane patches to extraction with cold nonionic detergents, and (ii) loss of detergent-resistance combined with the dissolution of “lipid rafts” by cholesterol-depletion of cells with methylated- β -cyclodextrin (cyd). The first criterion is based on the observation that certain membrane patches remain unsolubilized upon applying cold nonionic detergents to a given membrane of interest (30, 31). These detergent resistant membrane fragments (DRMs) are *inter alia* rich in sphingolipids and cholesterol, in an ℓ_o -phase when isolated from cells and were thus proposed to be derived from pre-existing “raft”-microdomains (12, 32). Cholesterol depletion of cells is used to argue for the existence of “lipid rafts” following an analogy to model membrane systems. In these system it was indeed found that domains disintegrate upon application of cyd, owing to the fact that elevated cholesterol concentrations are necessary to create liquid-liquid (ℓ_o/ℓ_d)-immiscibilities (33–35).

In relation to the detergent resistance criterion, two experimental studies of Heerklotz et al. (36, 37) showed that matters are certainly more complicated than implied by the simple “DRM=raft”-equivalence (critically reviewed in (38)). These authors showed, employing modern microcalorimetric techniques as well as solid-state nuclear magnetic resonance measurements that the proposed existence of ordered, sphingolipid and cholesterol enriched domains, can in fact be induced by the addition of a detergent to a membrane system. Apart from being limited to the study of model-membrane systems approximately resembling the lipid composition of the plasma membrane, these studies have already raised concern about the fact that “detergent resistant membranes should not be assumed to resemble biological rafts in size, structure or even existence.” In the mean time, additional, experimental support for this warning was provided also by studies utilizing biological specimen (39, 40). Related to the second criterion, a reading of the relevant literature largely conveys the impression that little, not to say no, attention is given to the facts that: (i) cholesterol has various biochemical and biophysical effects in cells, and that (ii) cyd is able to extract not only cholesterol but also lipid from a membrane (41).

Given the prevailing controversies in the field of lipid domains in cell membranes, the present thesis pursues the following goals. Employing an approach based on

equilibrium thermodynamics[¶] (an overview about complementary, spectroscopic approaches is given, e.g., in (43)) the present work is aimed at understanding the forces that govern the formation of membrane domains and how these are altered by the addition of detergents. One goal was accordingly to quantify lipid/lipid and lipid/detergent pair-interactions in membranes in terms of simple physical models like, e.g., the model of regular solutions (44). This task was successfully completed resulting in a consistent and detailed picture as published in the attached papers specified by numbers: (II), (IV), and (V) below. In parallel to these experimental studies, a theoretical study was performed that makes use of these parameters in model calculations of domain formation and detergent induced alteration of domains (III). Finally, with the goal to investigate demixed membranes, a rather new experimental method, pressure perturbation calorimetry (PPC) (45–47) was further developed and applied to study a phase equilibrium on the example of a micellar sphere-to-rod transition (I). Subsequently, we then succeeded to employ PPC in a study that characterizes domain equilibria in cholesterol containing membranes (VI).

2.2 Summary of the topics addressed

2.2.1 Differential interactions of cholesterol with different lipids

Quantitative data on differential interactions of cholesterol with different lipids are limited at present, although an urgent need for such data exists given the crucial role cholesterol is supposed to play in membrane domain formation. Especially, thus far only affinity differences were reported in terms of membrane/membrane or cyd/membrane partition coefficients of cholesterol (48–51). Herein, a novel approach based on isothermal titration calorimetry (ITC) (52–54) is presented that also measures cyd/membrane partitioning of cholesterol (the necessity to use cyd in these kind of experiments is due to the poor solubility of cholesterol in water (55, 56)). By virtue of the microcalorimetric approach a complete thermodynamic picture is constructed, i.e., enthalpic and entropic contributions of cholesterol/lipid interactions are quantified in detail. For an analysis of the experimental data, a theoretical model to describe the partitioning of cholesterol between membranes and cyd/cholesterol complexes is introduced. In addition to yielding the predominant stoichiometry of these complexes, i.e., one cholesterol per two cyd, reasonable suggestions on how to optimize the procedure of cholesterol extraction for *in vivo*-studies are made. All of the results obtained with various binary glycerophospholipid/cholesterol mixtures are described in:

[¶]We follow C. Tanford who aptly put it (42): “But science does not progress by startling discoveries alone, and thermodynamic analysis serves its purpose by assimilating the new into the old and the part into the whole. It can create a simple unified conceptual framework for biology, as it has done for chemistry, and has the potential for clarifying research problems and indicating productive pathways for solving them.”

(II): Interactions of Cholesterol with Lipid Membranes and Cyclodextrin Characterized by Calorimetry by Alekos Tsamaloukas, Halina Szadkowska, Peter J. Slotte, and Heiko Heerklotz, *Biophys. J.* 89, 1109–1119 (2005)

Further experimental as well as theoretical developments were necessary to include also sphingolipids in these kind of partitioning experiments. A direct outcome of these efforts is a study of more complex ternary lipid mixtures including a comparative analysis of cholesterol interactions with both glycerophospholipid and different sphingolipids detailed in:

(V): Thermodynamic comparison of the interactions of cholesterol with unsaturated phospholipid and sphingomyelins by Alekos Tsamaloukas, Halina Szadkowska, and Heiko Heerklotz, *Biophys. J.*, *in revision* (2005)

Finally, in relation to these studies the following appears worth to note. Quite generally, the binding of a hydrophobic ligand to a lipid membrane or water soluble receptor is a topic of utmost interest in the pharmaceutical industry. The assays introduced in conjunction with the formalism derived for a mathematical analysis of the experimental data hold good promise to be applicable in binding studies with other hydrophobic ligands than cholesterol.

2.2.2 Interaction of detergents with lipid membranes

To better understand the effects addition of a detergent to a membrane system of interest has, a quantitative model describing the selective solubilization of membrane domains is introduced. Based on simple equilibrium thermodynamical relations, it allows to calculate the abundances and compositions of the four pseudophases involved, i.e., aqueous and micellar phase as well as fluid (ℓ_d), and ordered (ℓ_o) membrane phase. From a comparison of simulations carried out under the assumption of either ideal or nonideal mixing it is shown that in the latter case detergent-induced formation of ordered domains can occur. Hence, the isolation of ℓ_o -phase, detergent resistant patches from a membrane may be a result of the very addition of detergent and does not correspond to anything pre-existing in the detergent-free system. The model calculations and additional results are presented in:

(III): A Quantitative Model Describing the Selective Solubilization of Membrane Domains by Sandro Keller, Alekos Tsamaloukas, and Heiko Heerklotz, *J. Am. Chem. Soc.* 127, 11469–11476 (2005)

Given the important role nonideal mixing may play in the formation of membrane domains, additional experimental input data for the above theoretical model are needed. To this end, the interaction of the commonly used nonionic detergent

Triton X-100 (TX-100) with lipid membranes of different composition was studied in detail employing both ITC and differential scanning calorimetry (DSC) (57). The mixing behaviour of ternary and quaternary lipid/detergent mixtures is analysed within the framework of a simple thermodynamic model based on pairwise interaction parameters between components α and β (44). Based on the parameters obtained, it appears likely that under certain conditions ℓ_d -phase lipid/TX-100 enriched domains demix from ℓ_o -phase lipid/cholesterol enriched ones. In addition, it is proposed that the (large and unfavourable) nonideal interaction of cholesterol and detergent is a crucial parameter governing the mixing behaviour in detergent additive membranes. Further results of this experimental study are provided in:

(IV): Nonideal mixing in multicomponent lipid/detergent systems by Alekos Tsamaloukas, Halina Szadkowska, and Heiko Heerklotz, *J. Phys.: Condens. Matter, in revision* (2005)

2.2.3 Packing properties of lipid/cholesterol mixtures

The differential packing abilities of different lipid species are proposed to be another key parameter for the formation of membrane domains. For example, sphingolipids with their long and largely saturated acyl chains can pack more tightly together than glycerophospholipids that are usually rich in kinked, unsaturated acyl chains. While for such systems a phase separation into a gel-phase (enriched in sphingolipid) and a fluid-phase (enriched in glycerophospholipid) is likely to occur, matters are again complicated by the presence of cholesterol that is able to transform a gel into a ℓ_o -phase. A common physical variable used to specify packing properties in membranes is the apparent mean molecular area of a lipid as determined in Langmuir film balance experiments (58–60). It is well known that cholesterol can increase the order of neighbouring lipid acyl chains, thereby effectively stretching them which in turn results in a increase in membrane thickness (cholesterol “condensing” effect (17, 58, 61)). Studies dealing with the more natural variable when it comes to discuss packing in membranes, i.e., the partial volume of lipid and its cholesterol induced changes, are, however, extremely rare at present. As a consequence, here PPC is introduced in this context since it provides precise data of thermal expansivity of colloidal dispersions.

In a first study to further develop and characterize the PPC-technique, experiments with aqueous solutions of common nonionic detergents were performed. These studies led to the first ever published data on the volumetric properties of a micellar sphere-to-rod transition. In conjunction with further thermodynamic and structural data obtained by both small angle neutron scattering (SANS) and dynamic light scattering (DLS), they are reported in:

(I): Structural, Volumetric, and Thermodynamic Characterization of a Micellar Sphere-to-Rod Transition by Heiko Heerklotz, Alekos Tsamaloukas, Katarzyna Kita-Tokarczyk, Pavel Strunz, and Thomas Gutberlet, *J. Am. Chem. Soc.* 126, 16544–16552 (2004)

In order to help resolving the issue whether binary membrane systems of glycerophospholipid/cholesterol should be better described in terms of a phase separation (ℓ_o/ℓ_d -phase coexistence) or of gradual changes in largely homogenous membranes, the phase behaviour of various binary mixtures was studied with the help of PPC. A detailed comparison of the predictions of three existing theoretical models suitable to be employed in this context (phase model (62), random neighbour model (63), and condensed complex model (64, 65)) with the experimental data obtained, is presented in:

(VI): Gradual change or phase transition — characterizing liquid lipid-cholesterol membranes on the basis of thermal volume changes by Heiko Heerklotz and Alekos Tsamaloukas, *Biophys. J.*, *submitted* (2006)

2.3 Concluding Remarks

The yet unknown “raft stabilizer” (37) remains elusive if one is willing to believe in its existence at all. Despite the *plethora* of experimental techniques that are applied to study the formation and existence of “lipid rafts”, major doubts about the concept itself persist.

In the present thesis, principles of domain formation in model membranes were investigated that are believed to be helpful for resolving some of the ambiguities concerning raft formation in cell membranes (66). A quantitative explanation for detergent induced domain formation, the enhancement or creation of ℓ_o -phase domains in equilibrium is provided by an approach combining both new experimental developments and the invention of suitable theoretical concepts. The limitations of the two most commonly applied methods to prove the *in vivo* existence of “lipid rafts”, detergent insolubility and cholesterol depletion, were investigated and suggestions on how to increase the reliability of these can be drawn on the basis of the results obtained.

I believe that understanding the physical principles of domain formation in complex model systems approximating cell membranes as closely as possible will serve as a proper guideline for a better interpretation and understanding of the phenomena observed *in vivo*. The ternary and quaternary (lipid/detergent) systems studied here are certainly only a starting point in this direction. It is to be expected that lipid/protein interactions are another very important factor in the “lipid raft rubric” (26) that clearly deserve further experimental and theoretical efforts.

Bibliography

1. Koynova, R., and M. Caffrey. 1998. Phases and phase transitions of the phosphatidylcholines. *Biochim. Biophys. Acta* 1376:91–145.
2. Ohvo-Rekilä, H., B. Ramstedt, P. Leppimäki, and J. P. Slotte. 2002. Cholesterol interactions with phospholipids in membranes. *Prog. Lip. Res.* 41:66–97.
3. McMullen, T. P. W., R. N. A. H. Lewis, and R. N. McElhaney. 2004. Cholesterol-phospholipid interactions, the liquid-ordered phase and lipid rafts in model and biological membranes. *Current Opinion in Colloid and Interface Science* 8:459–468.
4. Bretscher, M. S. 1973. Membrane structure: some general principles. *Science* 181:622–629.
5. Pulfer, M., and R. C. Murphy. 2003. Electrospray mass spectrometry of phospholipids. *Mass Spec. Rev.* 22:332–364.
6. Nichols, B. 2005. Without a raft. *Nature* 436:638–639.
7. Edidin, M. 2003. Lipids on the frontier: a century of cell-membrane bilayers. *Nature Rev. Mol. Cell Biol.* 4:414–418.
8. Davoust, J., B. M. Schoot, and P. M. Devaux. 1979. Physical Modifications of Rhodopsin Boundary Lipids in Lecithin-Rhodopsin Complexes: A spin-label study. *Proc. Natl. Acad. Sci. USA* 76:2755–2759.
9. Marsh, D., and L. I. Horvath. 1998. Structure, dynamics and composition of the lipid-protein interface. Perspectives from spin-labelling. *Biochim. Biophys. Acta* 1376:267–296.
10. Simons, K., and G. van Meer. 1988. Lipid sorting in epithelial cells. *Biochemistry* 27:6197–6202.
11. Brown, D. A., and J. K. Rose. 1992. Sorting of GPI-anchored proteins to glycolipid-enriched membrane subdomains during transport to the apical cell surface. *Cell* 68:533–544.

12. Simons, K., and E. Ikonen. 1997. Functional rafts in cell membranes. *Nature* 387:569–572.
13. Rietvald, A., and K. Simons. 1998. The differential miscibility of lipids as the basis for the formation of functional membrane rafts. *Biochim. Biophys. Acta* 1376:467–469.
14. London, E., and D. A. Brown. 2000. Insolubility of lipids in TX-100: physical origin and relationship to sphingolipid/cholesterol membrane domains (rafts). *Biochim. Biophys. Acta* 1508:182–195.
15. Brown, D. A., and E. London. 2000. Structure and function of sphingolipid–and cholesterol–rich membrane rafts. *J. Biol. Chem.* 275:17221–17224.
16. Binder, W. H., V. Barragan, and F. M. Menger. 2003. Domänen und Rafts in Lipid-membranen. *Angew. Chemie* 115:5980–6007.
17. Yeagle, P. L. 1985. Cholesterol and the cell membrane. *Biochim. Biophys. Acta* 822:267–287.
18. Simons, K., and E. Ikonen. 2000. How cells handle cholesterol. *Science* 290:1721–1726.
19. Ipsen, J. H., G. Karlström, O. G. Mouritsen, H. Wennerström, and M. J. Zuckermann. 1987. Phase equilibrium in the phosphatidylcholine–cholesterol system. *Biochim. Biophys. Acta* 905:162–172.
20. Ipsen, J. H., O. G. Mouritsen, and M. J. Zuckermann. 1989. Theory of thermal anomalies in the specific heat of lipid bilayers containing cholesterol. *Biophys. J.* 56:661–667.
21. Vist, M. R., and J. H. Davis. 1990. Phase equilibria of cholesterol/dipalmitoyl-phosphatidylcholine mixtures: ²H nuclear magnetic resonance and differential scanning calorimetry. *Biochemistry* 29:451–464.
22. Sankaram, M. B., and T. E. Thompson. 1990. Interaction of cholesterol with various glycerolipids and sphingomyelin. *Biochemistry* 29:10670–10675.
23. Simons, K., and R. Ehehalt. 2002. Cholesterol, lipid rafts, and disease. *The Journal of Clinical Investigation* 110:597–603.
24. Anderson, R. G. W., and K. Jacobson. 2002. A role for lipid shells in targeting proteins to caveolae, rafts, and other lipid domains. *Science* 296:1821–1825.
25. Silvius, J. R. 2003. Role of cholesterol in lipid raft formation: lessons from lipid model systems. *Biochim. Biophys. Acta* 1610:174–183.
26. Edidin, M. 2003. The state of lipid rafts: From model membranes to cells. *Annu. Rev. Biophys. Biomol. Struct.* 32:257–283.

27. Munro, S. 2003. Lipid rafts: Elusive or Illusive? *Cell* 115:377–388.
28. Simons, K., and W. L. C. Vaz. 2004. Model Systems, Lipid Rafts, And Cell Membranes. *Annu. Rev. Biophys. Biomol. Struct.* 33:269–296.
29. Brown, D. A. 2001. Seeing is believing: Visualization of rafts in model membranes. *Proc. Natl. Acad. Sci. USA* 98:10517–10518.
30. Steck, T. L., and J. Yu. 1973. Selective solubilization of proteins from red blood cell membranes by protein perturbants. *J. Supramol. Struct.* 1:220–232.
31. Yu, J., D. A. Fischman, and T. L. Steck. 1973. Selective solubilization of proteins and phospholipids from red blood cell membranes by nonionic detergents. *J. Supramol. Struct.* 1:233–247.
32. Simons, K., and D. Toomre. 2000. Lipid rafts and signal transduction. *Nat. Rev. Mol. Cell Biol.* 1:31–39.
33. Dietrich, C., L. A. Bagatolli, Z. N. Volovyk, N. L. Thompson, M. Levi, K. Jacobson, and E. Gratton. 2001. Lipid rafts reconstituted in model membranes. *Biophys. J.* 80:1417–1428.
34. Kahya, N., D. Scherfeld, K. Bacia, B. Poolman, and P. Schwille. 2003. Probing lipid mobility of raft-exhibiting model membranes by fluorescence correlation spectroscopy. *J. Biol. Chem.* 278:28109–28115.
35. Bacia, K., D. Scherfeld, N. Kahya, and P. Schwille. 2004. Fluorescence correlation spectroscopy relates rafts in model and native membranes. *Biophys. J.* 87:1034–1043.
36. Heerklotz, H. 2002. Triton promotes domain formation in lipid raft mixtures. *Biophys. J.* 83:2693–2701.
37. Heerklotz, H., H. Szadkowska, T. Anderson, and J. Seelig. 2003. The sensitivity of lipid domains to small perturbations demonstrated by the effect of Triton. *J. Mol. Biol.* 329:793–799.
38. Lichtenberg, D., F. M. Goñi, and H. Heerklotz. 2005. Detergent-resistant membranes should not be identified with membrane rafts. *Trends in Biochemical Sciences* 30:430–436.
39. Schuck, S., M. Honsho, K. Ekroos, A. Shevchenko, and K. Simons. 2003. Resistance of cell membranes to different detergents. *Proc. Natl. Acad. Sci. USA* 100:5795–5800.
40. van Rheenen, J., E. M. Achame, H. Janssen, J. Calafat, and K. Jalink. 2005. PIP₂ signaling in lipid domains: a critical re-evaluation. *The EMBO Journal* 24:1664–1673.

41. Anderson, T. G., A. Tan, P. Ganz, and J. Seelig. 2004. Calorimetric measurement of phospholipid interaction with methyl- β -cyclodextrin. *Biochemistry* 43:2251–2261.
42. Tanford, C. 1978. The hydrophobic effect and the organization of living matter. *Science* 200:1012–1018.
43. Lagerholm, B. C., G. E. Weinreb, K. Jacobson, and N. L. Thompson. 2005. Detecting microdomains in intact cell membranes. *Annu. Rev. Phys. Chem.* 56:309–336.
44. Cevc, G., and D. Marsh. 1987. Phospholipid bilayers: Physical principles and models, volume 5. 1st edition. John Wiley & Sons, Inc., New York.
45. Kujawa, P., and F. M. Winnik. 2001. Volumetric studies of aqueous polymer solutions using pressure perturbation calorimetry: A new look at the temperature-induced phase transition of Poly(N-isopropylacrylamide) in water and D₂O. *Macromolecules* 34:4130–4135.
46. Lin, L.-N., J. F. Brandts, J. M. Brandts, and V. Plotnikov. 2002. Determination of the volumetric properties of proteins and other solutes using Pressure Perturbation Calorimetry. *Anal. Biochem.* 302:144–160.
47. Heerklotz, H., and J. Seelig. 2002. Application of pressure perturbation calorimetry to lipid bilayers. *Biophys. J.* 82:1445–1452.
48. Yeagle, P., and J. Young. 1986. Factors contributing to the distribution of cholesterol among phospholipid vesicles. *J. Biol. Chem.* 261:8175–8181.
49. Lange, Y., J. S. D'Alessandro, and D. M. Small. 1979. The affinity of cholesterol for phosphatidylcholine and sphingomyelin. *Biochim. Biophys. Acta* 556:388–398.
50. Leventis, R., and J. R. Silvius. 2001. Use of cyclodextrins to monitor transbilayer movement and differential lipid affinities of cholesterol. *Biophys. J.* 81:2257–2267.
51. Niu, S.-L., and B. J. Litman. 2002. Determination of membrane cholesterol partition coefficient using a lipid vesicle–cyclodextrin binary system: Effect of Phospholipid Acyl chain unsaturation and headgroup composition. *Biophys. J.* 83:3408–3415.
52. Wiseman, T., S. Williston, J. F. Brandts, and L. N. Lin. 1989. Rapid measurement of binding constants and heats of binding using a new titration calorimeter. *Anal. Biochem.* 179:131–137.
53. Chellani, M. 1999. Isothermal titration calorimetry: biological applications. *Am. Biotechnol. Lab* 17:14–18.
54. Heerklotz, H., and J. Seelig. 2000. Titration calorimetry of surfactant–membrane partitioning and membrane solubilization. *Biochim. Biophys. Acta* 1508:69–85.

55. Haberland, M. E., and J. A. Reynolds. 1973. Self-association of cholesterol in aqueous solution. *Proc. Natl. Acad. Sci. USA* 70:2313–2316.
56. Gilbert, D. B., C. Tanford, and J. A. Reynolds. 1975. Cholesterol in aqueous solution: Hydrophobicity and Self-association. *Biochemistry* 14:444–448.
57. Plotnikov, V. V., J. M. Brandts, L. N. Lin, and J. F. Brandts. 1997. A new ultrasensitive scanning calorimeter. *Anal. Biochem.* 250:237–244.
58. de Kruyff, B., R. A. Demel, A. J. Slotboom, L. L. M. van Deenen, and A. F. Rosenthal. 1973. The effect of the polar headgroup on the lipid-cholesterol interaction: A monolayer and differential scanning calorimetry study. *Biochim. Biophys. Acta* 307:1–19.
59. Smaby, J. M., M. Momsen, V. S. Kulkarni, and R. E. Brown. 1996. Cholesterol-induced area condensations of galactosylceramides and sphingomyelins with identical acyl chains. *Biochemistry* 35:5696–5704.
60. Ramstedt, B., and J. P. Slotte. 1999. Interaction of cholesterol with sphingomyelins and acyl-chain matched phosphatidylcholines: A comparative study of the effect of the chain length. *Biophys. J.* 76:908–915.
61. Demel, R. A., and B. de Kruyff. 1976. The function of sterols in membranes. *Biochim. Biophys. Acta* 457:109–132.
62. Veatch, S. L., and S. L. Keller. 2005. Seeing spots: Complex phase behavior in simple membranes. *Biochim. Biophys. Acta* 1746:172–185.
63. Edholm, O., and J. F. Nagle. 2005. Areas of molecules in membranes consisting of mixtures. *Biophys. J.* 89:1827–1832.
64. Radhakrishnan, A., and H. M. McConnell. 1999. Condensed complexes of cholesterol and phospholipids. *Biophys. J.* 77:1507–1517.
65. Radhakrishnan, A., T. G. Anderson, and H. M. McConnell. 2000. Condensed complexes, rafts and the chemical activity of cholesterol in membranes. *Proc. Natl. Acad. Sci. USA* 97:12422–12427.
66. London, E. 2005. How principles of domain formation in model membranes may explain ambiguities concerning lipid raft formation in cells. *Biochim. Biophys. Acta* 1746:203–220.

Acknowledgements

Die vorliegende Arbeit entstand im Zeitraum April 2003 bis Dezember 2005 in der Arbeitsgruppe von PD Dr. Heiko Heerklotz in der Abteilung Biophysikalische Chemie des Biozentrums der Universität Basel. Den folgenden Personen fühle ich mich zu grösstem Dank verpflichtet:

- ▷ Heiko und Halina für die wunderbare Zeit, die ich mit Euch beiden in den letzten 32 Monaten verbringen durfte. Heiko insbesondere für die mir gebotene Möglichkeit in seiner Gruppe als Doktorand zu arbeiten, die unerschöpfliche Geduld mit mir und die jederzeit ausgezeichnete Betreuung. Desweiteren für die vielen mir unterbreiteten Angebote von denen ich wohl nur wenige wahrgenommen habe sowie vor allem die Toleranz gegenüber meinem ελληνικό χοντροκέφαλο. Halina für die ausgezeichnete Hilfe im Labor bezüglich jedweder anfallender praktischer Arbeiten, die Verbreitung von guter Laune, wenns mal nicht so rund lief, sowie die Bekanntschaft mit dem wohl Besten, was die Basler Konditoreikunst zu bieten hat.
- ▷ Den übrigen, mir in den letzten knapp drei Jahren in der Arbeitsgruppe von Prof. J. Seelig begegneten Mitarbeitern, danke ich für die angenehme Atmosphäre, sowie die mir jederzeit spontan und unkompliziert geleistete Hilfe, wenn ich diese benötigte. Im Besonderen danke ich Bernhard Steinbauer für viele interessante Diskussionen auch in der Zeit nach seinem Ausscheiden aus der Ag sowie Götz Kohler für die angenehmen Mittagsrunden, die vielen kleinen anregenden Diskussionen, sowie die wunderbaren, wenn auch schlauchenden, Radausflüge.
- ▷ Den zwei Strategen aus der Lothringer, Florian Weissbach und Sven Lammers, für viele vergnügliche Stunden zusammen. Meinem Studienkollegen aus Berliner Tagen, Florian, insbesondere dafür, mich positiv bezgl. meines Starts in Basel beeinflusst zu haben, sowie einige, wenn auch teils kontroverse politische Diskussionen.
- ▷ Meiner Familie für die moralische, versorgungstechnische und auch ansonsten in jeder Hinsicht phantastische Unterstützung während meiner gesamten Studienzeit, gebührt mein allergrösster Dank.

Published and submitted work

(I): Structural, Volumetric, and Thermodynamic Characterization of a Micellar Sphere-to-Rod Transition by Heiko Heerklotz, Alekos Tsamaloukas, Katarzyna Kita-Tokarczyk, Pavel Strunz, and Thomas Gutberlet, *J. Am. Chem. Soc.* 126, 16544–16552 (2004)

(II): Interactions of Cholesterol with Lipid Membranes and Cyclodextrin Characterized by Calorimetry by Alekos Tsamaloukas, Halina Szadkowska, Peter J. Slotte, and Heiko Heerklotz, *Biophys. J.* 89, 1109–1119 (2005)

(III): A Quantitative Model Describing the Selective Solubilization of Membrane Domains by Sandro Keller, Alekos Tsamaloukas, and Heiko Heerklotz, *J. Am. Chem. Soc.* 127, 11469–11476 (2005)

(IV): Nonideal mixing in multicomponent lipid/detergent systems by Alekos Tsamaloukas, Halina Szadkowska, and Heiko Heerklotz, *J. Phys.: Condens. Matter*, *in revision* (2005)

(V): Thermodynamic comparison of the interactions of cholesterol with unsaturated phospholipid and sphingomyelins by Alekos Tsamaloukas, Halina Szadkowska, and Heiko Heerklotz, *Biophys. J.*, *in revision* (2005)

(VI): Gradual change or phase transition — characterizing liquid lipid-cholesterol membranes on the basis of thermal volume changes by Heiko Heerklotz and Alekos Tsamaloukas, *Biophys. J.*, *submitted* (2006)

Structural, Volumetric, and Thermodynamic Characterization of a Micellar Sphere-to-Rod Transition

Heiko Heerklotz,^{*,†} Alekos Tsamaloukas,[†] Katarzyna Kita-Tokarczyk,[‡]
Pavel Strunz,[§] and Thomas Gutberlet[§]

Contribution from the Biozentrum, University of Basel, Klingelbergstrasse 70,
CH-4056 Basel, Switzerland, Department of Chemistry, University of Basel,
Klingelbergstrasse 80, CH-4056 Basel, Switzerland, and Paul Scherrer Institute,
CH-5232 Villigen PSI, Switzerland

Received July 26, 2004; E-mail: heiko.heerklotz@unibas.ch

Abstract: The thermotropic sphere-to-rod transition of nonionic surfactants was characterized in terms of a large set of parameters: the transition temperature and width, the partial volume, coefficient of thermal volume expansion, enthalpy, isobaric heat capacity, and structural parameters, such as radius of gyration and hydrodynamic radius. Data were recorded as a function of concentration of surfactants in H₂O and in D₂O. To this end, pressure perturbation calorimetry (PPC), small angle neutron scattering (SANS), dynamic light scattering (DLS), differential scanning calorimetry (DSC), and isothermal titration calorimetry (ITC) were applied in a study of aqueous solutions containing myristyl, tridecyl, and lauryl maltoside and heptaethyleneglycoltetradecyl ether (C₁₄EO₇). Small changes in the thermodynamic and volumetric parameters (e.g., the partial volume change is ~+2%) are discussed in detail as the result of three effects governing the transition. (i) Reduction of the water accessible hydrophobic surface area (ASA_{ap}) drives the transition. (ii) Shrinking in headgroup size by thermal dehydration triggers the transition. (iii) Hypothesized gradual ordering of the chains may control the effect of chain length on the transition.

Introduction

In this paper, we present a comprehensive description including the first data on the volumetric properties of micellar sphere-to-rod transitions. Volume changes were measured by means of pressure perturbation calorimetry (PPC), a method which has only recently been introduced and applied to study proteins,^{1–3} polymers,⁴ and phospholipids.^{5,6} A criticism of the technique⁷ was shown to be irrelevant.^{8,9} PPC is based on the measurement of the heat response of a solution to a small pressure jump of 5 bar and yields the temperature-dependent coefficient of thermal expansion and, in turn, the volume change accompanying a thermotropic transition of solutes or colloids.

The transition of spherical surfactant micelles in solution to a cylindrical geometry was already described by Luzzati¹⁰ in 1964 and has been thoroughly studied since then by light scattering,^{11,12} SANS,^{13–16} and electron microscopy.¹⁷ A par-

ticular issue of scattering data has been to distinguish between the continuous rodlike structures and the effects of critical fluctuations and attractive interactions between small micelles.^{16,18} The terms cylindrical, rodlike, threadlike, or polymer-like micelles describe the same general geometry but may emphasize different properties with respect to length, flexibility, or branching; we will however use the term rodlike for any micelle with a locally cylindrical structure, regardless of these specific properties.

Most sphere-to-rod transitions can be explained in terms of a simple but useful *packing model* described by Israelachvili,¹⁹ which is based on three criteria: (i) the surface-to-volume ratio of the aggregates in relation to the molecular dimensions, (ii) the fact that the radius of the core cannot exceed the maximum projected chain length, and (iii) that smaller aggregates are entropically favored over larger ones. First, the surface-to-volume ratio of the hydrophobic core of the aggregate, A/V , agrees with the ratio of the surface increment covered by the

[†] Biozentrum.

[‡] Department of Chemistry.

[§] Paul Scherrer Institute.

- (1) Lin, L. N.; Brandts, J. F.; Brandts, J. M.; Plotnikov, V. *Anal. Biochem.* **2002**, *302*, 144–160.
- (2) Sasisanker, P.; Oleinikova, A.; Weingartner, H.; Ravindra, R.; Winter, R. *Phys. Chem. Chem. Phys.* **2004**, *6*, 1899–1905.
- (3) Ravindra, R.; Winter, R. *ChemPhysChem* **2004**, *5*, 566–571.
- (4) Kujawa, P.; Winnik, F. M. *Macromolecules* **2001**, *34*, 4130–4135.
- (5) Wang, S. L.; Eppard, R. M. *Chem. Phys. Lipids* **2004**, *129*, 21–30.
- (6) Heerklotz, H.; Seelig, J. *Biophys. J.* **2002**, *82*, 1445–1452.
- (7) Randzio, S. L. *Thermochim. Acta* **2003**, *398*, 75–80.
- (8) Heerklotz, H. *J. Phys.: Condens. Matter* **2004**, *16*, R441–467.
- (9) Brandts, J.; Lin, L. *Thermochim. Acta* **2004**, *414*, 95–100.
- (10) Reiss-Husson, F.; Luzzati, V. *J. Phys. Chem.* **1964**, *68*, 3504–3511.
- (11) Cirkel, P. A.; Koper, G. J. M. *Langmuir* **1998**, *14*, 7095–7103.

- (12) von Berlepsch, H.; Dautzenberg, H.; Rother, G.; Jaeger, J. *Langmuir* **1996**, *12*, 3613–3625.
- (13) He, L. Z.; Garamus, V. M.; Funari, S. S.; Malfois, M.; Willumeit, R.; Niemeier, B. *J. Phys. Chem. B* **2002**, *106*, 7596–7604.
- (14) He, L. Z.; Garamus, V.; Niemeier, B.; Helmholz, H.; Willumeit, R. *J. Mol. Liq.* **2000**, *89*, 239–248.
- (15) Stradner, A.; Glatter, O.; Schurtenberger, P. *Langmuir* **2000**, *16*, 5354–5364.
- (16) Glatter, O.; Fritz, G.; Lindner, H.; Brunner-Popela, J.; Mittelbach, R.; Strey, R.; Egelhaaf, S. U. *Langmuir* **2000**, *16*, 8692–8701.
- (17) Bernheim-Groswasser, A.; Wachtel, E.; Talmon, Y. *Langmuir* **2000**, *16*, 4131–4140.
- (18) Lindman, B.; Wennerstrom, H. *J. Phys. Chem.* **1991**, *95*, 6053–6054.
- (19) Israelachvili, J. N. *Intermolecular and Surface Forces*, 2nd ed.; Academic Press: London, 1991.

headgroup, a_0 , to the partial volume of the hydrophobic tail, v_{chain} (i.e., $A/V = a_0/v_{\text{chain}}$). The optimum area per headgroup, a_0 , depends not only on steric properties but also on electrostatic interactions, hydration, and other forces governing the packing density of the headgroups. It is straightforward to verify that the surface-to-volume ratio, A/V , is inversely proportional to the radius (or half bilayer thickness), R , amounting to $1/R$ for a lamella, $2/R$ for a cylinder, and $3/R$ for a sphere. The second criterion requires that a tail must be able to reach the center of the micelle so that the radius R is limited by the maximum projected length of the tail, l_{max} : $R \leq l_{\text{max}}$. Hence, spheres can be formed for a so-called packing parameter $\gamma \equiv v_{\text{chain}}/(a_0 l_{\text{max}}) \leq 1/3$, cylinders for $\gamma \leq 1/2$, and bilayer vesicles for $\gamma \leq 1$. Finally, the model assumes that more, smaller particles are entropically favored over fewer, larger ones (e.g., spheres over rods).

This concept explains why sphere-to-rod transitions of micelles can proceed (i) upon addition of a hydrophobic compound or a cosurfactant with large v_{chain} and small a_0 , such as alcohols and diacyl phospholipids,^{15,20–22} and (ii) by reducing a_0 of ionic surfactants by addition of salt¹² or counterionic surfactants.²³ For nonionics, it may be induced (iii) with increasing temperature since thermal dehydration diminishes a_0 ,^{24,25} but for ionic surfactants, it was observed (iv) with decreasing temperature.²⁶ Being a growth or association phenomenon, the transition can also proceed (v) with increasing concentration.^{27–29}

Grell et al.²⁴ established thermotropic sphere-to-rod transitions for $C_{14}EO_6$ and $C_{16}EO_8$ by SANS and measured the *enthalpy change* ($\sim +2$ kJ/mol) by differential scanning calorimetry (DSC). DSC scans of lipid–surfactant mixtures showed endotherms related to micellar growth or association below the cloud point.³⁰ Isothermal titration calorimetry (ITC) in which the lipid POPC was injected into micelles of $C_{12}EO_n$ at room temperature revealed transitions at a lipid mole fraction of 12% for $C_{12}EO_7$ ³¹ and of 24% for $C_{12}EO_8$ ²¹ that were accompanied by an increase in excess enthalpy ($\sim 1–2$ kJ/mol)³¹ and also identified as sphere-to-rod transitions by SANS.²² Since ionic surfactants, such as SDS, exhibit a sphere-to-rod transition with decreasing temperature,¹⁸ the enthalpy changes are exothermic.^{26,32}

Volumetric data on the sphere-to-rod transition are extremely rare, most likely since the accompanying changes in the absolute volume or density of the solution are very small. Gonzalez-Perez et al.³³ found slight discontinuities in the partial molar volume of myristoyldimethylbenzylammonium chloride as a

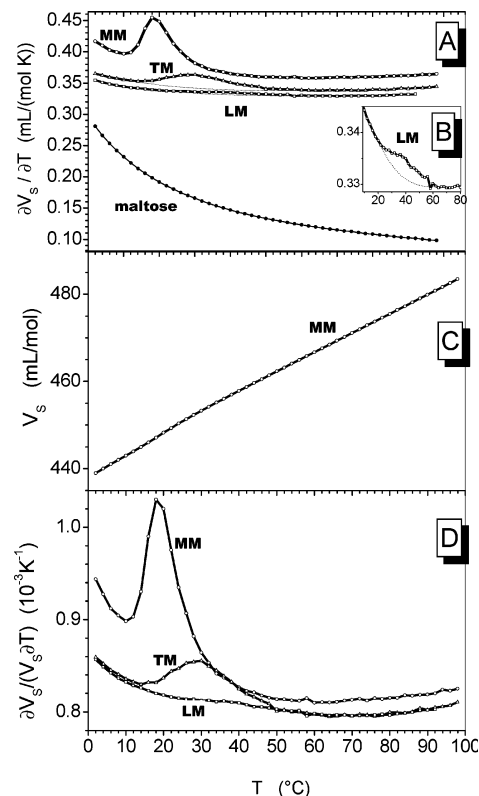


Figure 1. (A) PPC curves of lauryl (LM), tridecyl (TM), and myristyl (MM) maltosides and maltose in water (100 mM), showing the thermal expansion of the partial molar volume of the surfactants, $\partial V_s/\partial T$, as a function of temperature, T . (B) Zoomed reproduction of the curve of LM shown in A. (C) Partial molar volume of MM, $V_s(T)$, obtained by integration of the PPC curve using a value of $V_s(20\text{ °C}) = 448$ mL/mol for the integration constant (cf. Experimental Section in the Supporting Information). Note that the transition is hardly visible in the integral curve. (D) Temperature-dependent coefficient of thermal expansion, $\alpha = \partial V_s/(V_s \partial T)$, corresponding to the curves shown in panel A.

function of concentration, suggesting a volume change of $\sim +0.45$ mL/mol at 25 °C and decreasing with increasing temperature. They interpreted this finding in terms of a partial dehydration of headgroups and counterions (due to stronger binding to the surfactant). Application of 2.5 kbar to solutions of flexible, branched rodlike micelles of $C_{12}E_5$ did not induce a transition to spheres, as one might expect if the volume expands at a sphere-to-rod transition, but a freezing of the hydrophobic core leading to hexagonally packed, stiff, unbranched cylinders.³⁴

Results

PPC. Figure 1A shows curves of the molar expansivity, for example, the change in partial molar volume of the solute, V_s , with temperature, T , of micellar dispersions of alkyl maltosides in water. Pronounced peaks are observed, in particular, for myristyl maltoside (MM) and tridecyl maltoside (TM), representing thermal transitions that are accompanied by an increase in volume. The peaks become larger, narrower, and shifted to a lower temperature with increasing length of the alkyl chain.

Integration of the PPC curve from an arbitrarily defined baseline (cf. dotted lines in the figure) yields the volume change of the transition, ΔV_s , which amounts to ~ 1 mL/mol for MM

- (20) Walter, A.; Vinson, P. K.; Kaplun, A.; Talmon, Y. *Biophys. J.* **1991**, *60*, 1315–1325.
- (21) Heerklotz, H.; Lantzsch, G.; Binder, H.; Klose, G.; Blume, A. *J. Phys. Chem.* **1996**, *100*, 6764–6774.
- (22) Gutberlet, T.; Kiselev, M.; Heerklotz, H.; Klose, G. *Physica B* **2000**, *276*, 381–383.
- (23) Raghavan, S. R.; Fritz, G.; Kaler, E. W. *Langmuir* **2002**, *18*, 3797–3803.
- (24) Grell, E.; Lewitzki, E.; Schneider, R.; Ilgenfritz, G.; Grillo, I.; von Raumer, M. *J. Therm. Anal.* **2002**, *68*, 469–478.
- (25) Brigantii, G.; Bonincontro, A. *J. Non-Cryst. Solids* **1998**, *235*, 704–708.
- (26) Mazer, N. A.; Olofsson, G. *J. Phys. Chem.* **1982**, *86*, 4584–4593.
- (27) Miura, M.; Kodama, M. *Bull. Chem. Soc. Jpn.* **1972**, *45*, 428–431.
- (28) May, S.; Ben-Shaul, A. *J. Phys. Chem. B* **2001**, *105*, 630–640.
- (29) Al-Anber, Z. A.; Avalos, J. B. I.; Floriano, M. A.; Mackie, A. D. *J. Chem. Phys.* **2003**, *118*, 3816–3826.
- (30) Kresheck, G. C.; Mihelich, J. *J. Chem. Phys. Lipids* **2003**, *123*, 45–62.
- (31) Heerklotz, H. H.; Binder, H.; Schmiedel, H. *J. Phys. Chem. B* **1998**, *102*, 5363–5368.
- (32) Gu, G. X.; Yan, H. K.; Chen, W. H.; Wang, W. Q. *J. Colloid Interface Sci.* **1996**, *178*, 614–619.
- (33) Gonzalez-Perez, A.; Czpakiewicz, J.; Del Castillo, J. L.; Rodriguez, J. R. *Colloid Surf., A* **2001**, *193*, 129–137.

- (34) Bossev, D. P.; Kline, S. R.; Israelachvili, J. N.; Paulaitis, M. E. *Langmuir* **2001**, *17*, 7728–7731.

Table 1. Results of PPC and DSC Experiments^a

		C_S (mM)	T_{sr} (°C)	ΔT_{sr} (K)	ΔV_S (mL/mol)	$\Delta V_S/V_S$ (‰)	ΔH (kJ/mol)	c.u.
LM	H ₂ O	100	40	24	0.1	0.2		
TM	H ₂ O	100	30	20	0.5	1.1		
	H ₂ O	37	37	23	0.3	0.7	0.2	600
	D ₂ O	37	30	20	0.3	0.7	0.2	800
MM	H ₂ O	300	13.5	7	1.1	2.5	0.6	600
		100	19.4	9	1.0	2.2	0.6	500
		37	23.1	11	1.0	2.2	0.6	300
		10	30.0	16	1.0	2.2		
	D ₂ O	37	19.6	8	0.9	2.0	0.5	600
C ₁₄ E ₇	H ₂ O	100	18.7	9	0.7	1.5	1.9	140
	D ₂ O	100	17.4	8		1.5	1.5	230

^a Estimated errors are typically ± 1 , at the most ± 2 , of the last digit. T_{sr} and ΔT_{sr} are obtained consistently from DSC (high resolution in T) and PPC (low resolution) curves.

(cf. Table 1). The temperature at the maximum of $\partial V_S/\partial T$, T_{sr} , and the full width at half-height, ΔT_{sr} , are listed in Table 1. The PPC curve of lauryl maltoside (LM) shows only a very weak discontinuity (enlarged in Figure 1B). The expansivity curve for maltose is shown for comparison.

Figure 1C shows the partial molar volume, V_S , of MM as a function of temperature, which was derived by integrating the PPC curve (Figure 1A) with an integration constant chosen to reach a specific volume of 0.83 mL/g at 20 °C (cf. Experimental Section in the Supporting Information). It is noteworthy that PPC is far more sensitive to reveal the transition than methods determining the absolute volume or density since a slight ($\sim 10\%$) increase of the slope of $V_S(T)$ in a certain temperature range (Figure 1C) gives rise to a sharp peak in the PPC curve (Figure 1A). *Relative* volume changes (Figure 1D) are quantified in terms of the coefficient of the isobaric volume expansion, α :

$$\alpha \equiv \left. \frac{\partial V_S}{V_S \partial T} \right|_p \quad (1)$$

Considering, for instance, the values at 60 °C, it turns out that the larger absolute expansion of TM compared to LM arises simply from the larger size of TM; the relative expansion is $\sim 0.8\%/K$ in both cases. MM, however, shows also a somewhat higher $\alpha(60\text{ °C})$, which could be interpreted in terms of a larger contribution to α of the tail compared to that of the headgroup.

Figure 2A illustrates that the micellar transition becomes broader and is shifted to higher temperature upon dilution from 300 to 10 mM. Each data point shown for 10 mM MM is the average of the results obtained after 8 pressure jumps (4 up and 4 down). When the uncertainty in defining a baseline is taken into account, particularly for the 10 mM curve, there is no significant change in ΔV_S as a function of concentration. Exchange of H₂O by D₂O promotes the formation of rods, as indicated by a downshift in the transition temperature by ~ 4 K (cf. Figure 2C and data for 37 mM TM and MM in Table 1). The evaluation of the curve in D₂O was based on the reference-specific volume of 0.83 mL/g as in H₂O (cf. Experimental Section in the Supporting Information); the uncertainty of this value leads to an increased error of the absolute values of $\partial V_S/\partial T$ but does not affect the result for the transition volume, ΔV_S , substantially, which shows no significant deviation from the corresponding values in H₂O.

DSC. Figure 3 shows DSC curves of 37 mM MM in H₂O and D₂O. The transitions are endothermic, like all equilibrium

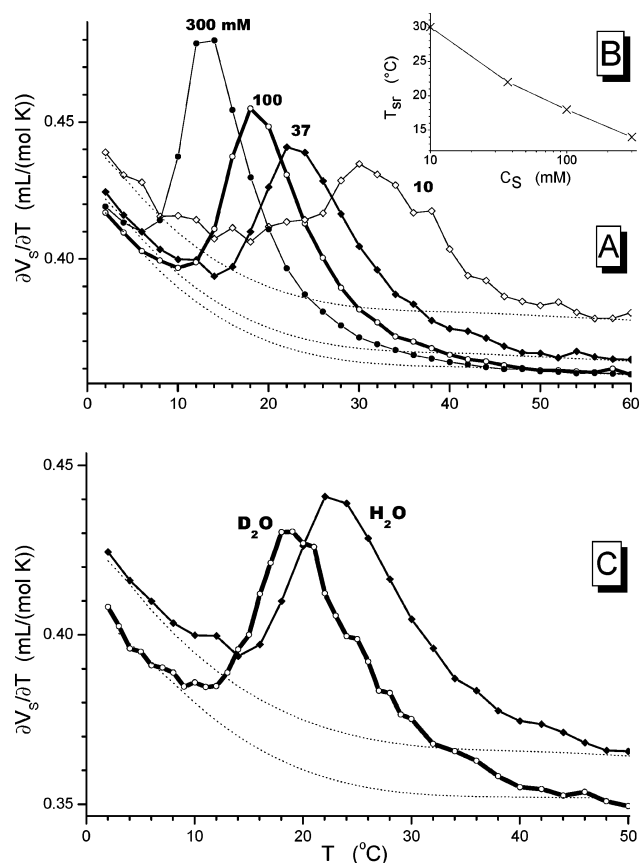


Figure 2. PPC curves of dispersions of MM as a function of concentration (A and B) and H₂O/D₂O substitution (C). (A) Experiments in H₂O at concentrations given in the plot. The inset in B shows the decrease in transition temperature, T_{sr} , as a function of the concentration on a semilogarithmic scale. (C) PPC curves of dispersions of 37 mM MM in H₂O and D₂O.

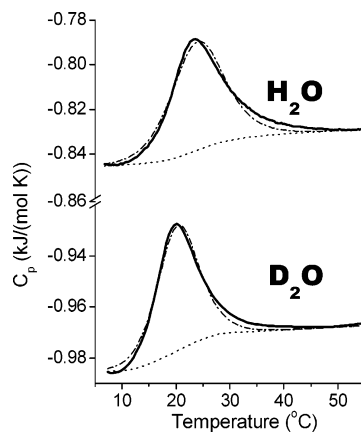


Figure 3. Raw DSC curves of 37 mM micellar dispersions of MM in H₂O and D₂O (bold solid lines) and the progress baselines (dotted) used for integration to derive ΔH (see Table 1). The curves were fitted by a model (dash-dot lines) based on a two-state transition of a single type of cooperative unit.

transitions driven by increasing temperature. The absolute values of the apparent C_p are not corrected for the heat capacity of excess H₂O/D₂O in the reference cell and, therefore, are not straightforward to interpret. The arbitrary assignment of progress baselines (cf. dotted curves in Figure 3) makes it possible to integrate the DSC peaks (yielding the enthalpy of the transition) and to estimate the step-height between the baselines extrapo-

lated from below and above the transition, which corresponds to the molar heat capacity change of the transition, ΔC_p . It seems to be slightly positive (0.010 ± 0.005 J/mol K), but the very small value and the uncertainty of the baseline hinder a precise determination. For a two-state transition, the width and shape of the peaks are determined by the van't Hoff enthalpy change, ΔH_{vH} .^{35,36} It describes the same process as the calorimetric enthalpy change, ΔH (corresponding to the area underneath the peak), but is normalized per mole of cooperative units (c.u.) rather than per mole of monomers (as for ΔH). The size of a cooperative unit, c.u., is the number of monomers that undergoes the transition as a single unit. We obtained satisfactory fits assuming a single type of cooperative units (cf. dash-dot lines in Figure 3) with van't Hoff enthalpies of 220 and 280 kJ/mol c.u. for H₂O and D₂O, respectively, yielding c.u. = $\Delta H_{vH}/\Delta H \approx 300$ and 600. Other c.u. values are included in Table 1. Consistent with the PPC curve, the transition is shifted to lower T_{sr} and narrowed (larger c.u.) in D₂O compared to that in H₂O, and the enthalpy change, ΔH , is slightly smaller.

Comparison of the volume and enthalpy changes accompanying a transition allows one to estimate the dependence of the transition temperature, T_{sr} , on pressure, p , according to

$$\frac{\partial T_{sr}}{\partial p} = -T_{sr} \frac{\Delta V_S}{\Delta H} \quad (2)$$

as derived from the Clausius–Clapeyron equation^{6,37,38} (note that 1 mL/kJ converts into 1/10 kbar). The DSC curves recorded for TM and MM at different concentrations and in H₂O and D₂O correspond to a common pressure dependence of 50 ± 5 K/kbar, and C₁₄EO₇ in H₂O yields a significantly smaller value of 11 K/kbar.

It is noteworthy that PPC and DSC transition peaks (after baseline subtraction) have virtually the same shape (not explicitly shown). This is a consequence of the fact that the changes in volume and enthalpy occurring during the transition are coupled. The same observation was made for chain melting transitions of phospholipids^{6,39,40} and explained theoretically.³⁹ The identity of the shapes makes it also possible to determine ΔH_{vH} from the PPC curves. Independent evaluations of the shape of the relatively pronounced PPC and DSC peaks of MM and C₁₄EO₇ yielded fairly consistent results. A comparison of PPC and DSC curves is particularly useful for the broad peaks of TM where the uncertainty in assigning a baseline limits the precision of the data evaluation.

DLS. Figure 4 shows the progress of the sphere-to-rod transition as obtained from DLS and integration of the PPC curve, both indicating a micellar transition of MM at about 20 °C, but only a much weaker thermotropic growth of TM micelles (at higher temperature) and hardly any significant growth of LM micelles.

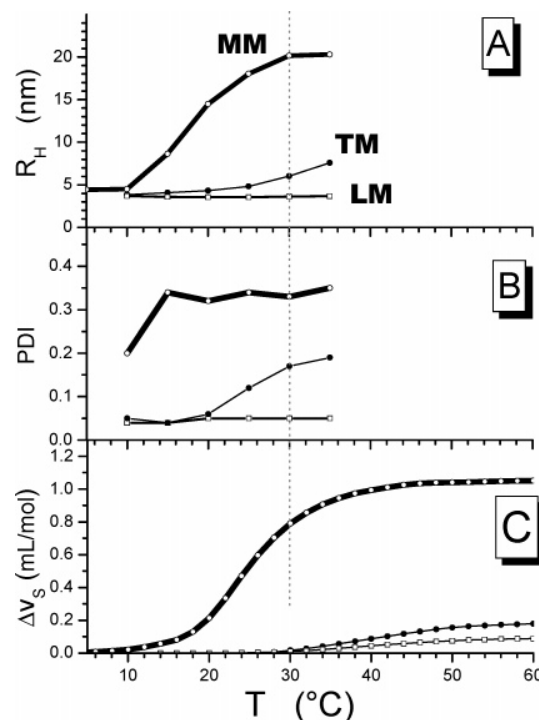


Figure 4. Progress of the sphere-to-rod transition of MM, TM, and LM (as labeled in panel A, all 37 mM) as reflected by the increase in the hydrodynamic radius, R_H , (A) and polydispersity index (B) measured by dynamic light scattering (DLS) and the volume change (integrated PPC curve after baseline subtraction, panel C). The maximum error of R_H is ± 3 nm.

The DLS data of MM at 5 °C provide good evidence for an essentially spherical geometry. The fact that the hydrodynamic radius, R_H , of about 4.5 nm is somewhat larger than the maximum projected length of a surfactant molecule (~ 3 nm) can be explained by bound water contributing to R_H , the roughness of the micellar surface, and perhaps minor deviations from an ideally spherical shape. This is in line with the polydispersity index (PDI) of ~ 0.2 , indicating only minor deviations from a monodisperse sample. With increasing temperature, DLS reveals a growth and shape transition of the micelles. R_H increases strongly to about 20 nm at 35 °C, which cannot be realized by spherical micelles since the molecules are only ~ 3 nm “long”. The intensity distribution in the transition range (not shown here) shows two populations with different form factors, which is indicative of a coexistence of different shapes (in varying proportions) rather than a gradual elongation of the spheres. This polydispersity is also reflected by the large PDI.

TM shows a much weaker but significant increase of R_H (from 4 to 7 nm) and the PDI, showing a slight increase in the average size and polydispersity at about 25 °C.

LM micelles form a fairly monodisperse population (PDI $\ll 0.1$) of spherical micelles of $R_H \approx 3.5$ –4 nm (effective length of LM ≈ 2.6 nm) over the whole temperature range that is accessible to our DLS instrument. PPC suggests that a slight growth might take place at higher temperatures, but the effect is extremely weak and its significance is questionable.

For comparison, panel C of Figure 4 shows the transition curves obtained by integrating the PPC peaks after subtraction of the baseline. Generally, a good agreement is observed with the DLS data. It should, however, be noted that the effective

- (35) Leharne, S. A.; Chowdhry, B. Z. In *Bio-calorimetry*; Chowdhry, B. Z., Ladbury, J. E., Eds.; John Wiley and Sons: Chichester, U.K., 1998; pp 157–182.
- (36) Blandamer, M. J.; Briggs, B.; Brown, H. R.; Burgess, J.; Butt, M. D.; Cullis, P. M.; Engberts, J. *J. Chem. Soc., Faraday Trans.* **1992**, *88*, 979–984.
- (37) Anthony, F. H.; Biltonen, R. L.; Freire, E. *Anal. Biochem.* **1981**, *116*, 161–167.
- (38) Landwehr, A.; Winter, R. *Ber. Bunsen-Ges. Phys. Chem.* **1994**, *98*, 214–218.
- (39) Ebel, H.; Grabitz, P.; Heimburg, T. *J. Phys. Chem. B* **2001**, *105*, 7353–7360.
- (40) Heerklotz, H.; Szadkowska, H.; Anderson, T.; Seelig, J. *J. Mol. Biol.* **2003**, *329*, 793–799.

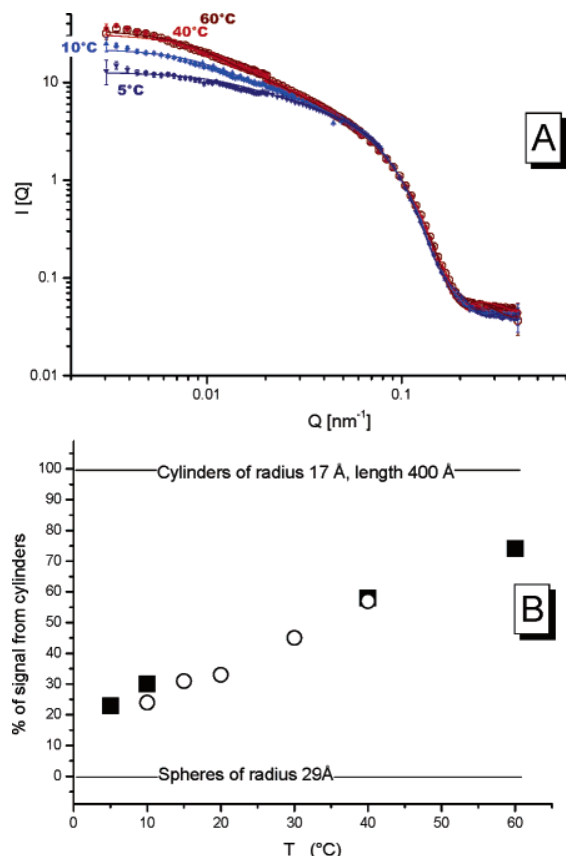


Figure 5. SANS data of 100 mM MM in D₂O at 60 °C (○), 40 °C (●), 10 °C (▲), and 5 °C (▼) and fit curves (A). The fits were based on a fixed scattering length density of $\eta = 1.048 \times 10^{-6} \text{ cm}^{-2}$ and a fixed scaling factor of $\sigma = 0.1$ in the LogNorm distribution (see Experimental Section in the Supporting Information). All fits indicated a coexistence of spheres and cylinders with the same geometry ($R_S = 28.7 \pm 0.9 \text{ \AA}$, $R_C = 16.9 \pm 1.0 \text{ \AA}$, $L_C = 402 \pm 75 \text{ \AA}$; ranges are standard deviations) but varying proportions. The percentage of cylinders is illustrated by panel B for samples of 37 mM (○) and 100 mM (■).

value of R_H and the scattering intensity are not directly proportional to the number of molecules being localized in rods compared to that in spheres. This is essentially the case for progress curves obtained by integrating PPC or DSC curves.

SANS. The neutron scattering intensity, I , as a function of scattering vector, Q (Figure 5), shows a slope depending on the dimensionality of the system. The increasing negative slope at low Q ($Q < 0.07 \text{ \AA}^{-1}$) is indicative of a change from a zero-dimensional system (small spherical micelles) to a one-dimensional geometry (long thin cylinders).

A detailed model evaluation of the scattering curves implies that they can be described in terms of a *coexistence* of spherical and cylindrical particles of virtually temperature- and concentration-independent radii (standard deviations $\leq 1 \text{ \AA}$) but with the fraction of cylinders increasing strongly with temperature (cf. Figure 5B).

The interpretation of the SANS model parameters has to take into account the limitations of the model. The dispersions might contain a great variety of particles: rough and dynamic spherical, ellipsoidal, peanut-shaped,²⁸ and longer, flexible, and possibly branched rodlike micelles. The model reduces this possible variety to two ideal, smooth geometries: spheres and stiff cylinders. However, the fact that this simple model yields a good fit of the scattering curves implies that the deviations

from these ideal shapes are not pronounced and that a more complex, more realistic model with additional adjustable parameters is not warranted by the data. Nevertheless, it is obvious that the deviations of the micelles from the two ideal shapes must affect the fit parameters. One may speculate that the effective length of the quasi-cylindrical parts, L_C , is related to the persistence length rather than the total length of the flexible rods. The fact that the values obtained for L_C are about 20 times the radius R_C suggests that the curvature of the rods is relatively weak and the local geometry is indeed close to a cylinder. A sophisticated quantitative characterization of the flexibility of the rods of a mixture of similar compounds, alkylpolyglucosides, with hexanol has revealed a Kuhn length of $\sim 100\text{--}150 \text{ \AA}$.¹⁵ Deviations of the small particles from an ideal spherical geometry and those of the cylinders from an ideally circular cross-section are likely to give rise to an overestimation of the radii.

Second, the micelles do not have a homogeneous scattering length density, η . Instead, η decreases gradually from $6.3 \times 10^{-6} \text{ cm}^{-2}$ in bulk D₂O to $\eta \approx 0.1 \times 10^{-6} \text{ cm}^{-2}$ in the core of the micelle (as in oil). The model distinguishes only between the background and “effective particles” with a pre-set, homogeneous η of $1.0 \times 10^{-6} \text{ cm}^{-2}$. This operational definition of the particle boundaries includes not only hydrocarbon but also some water and headgroups.

These limitations of the model account for the fact that the effective radius of the spherical micelles, R_S , is larger than the maximum projected chain length ($\sim 19 \text{ \AA}$), which would not be realistic for the hydrophobic core of an ideal, smooth sphere. Note also that the fraction of the scattering arising from cylinders (Figure 5B) is not the fraction of all molecules that are residing within cylinders (Figure 4C).

Despite these issues, the SANS data clearly demonstrate that the transition of MM micelles at about 20 °C is a sphere-to-rod transition. The rods have a relatively long persistence length, and the effective radius is significantly smaller ($\sim 2/3$) than that of the spheres. With increasing temperature, the number of rods increases on the expense of spheres, but the geometric parameters of the two types of micelles remain virtually unchanged.

ITC. The concentration-dependent enthalpy changes of MM were measured using ITC at various temperatures (cf. Figure 6A) The micelles dissociate upon injection into the cell until the CMC is reached, giving rise to a quasi-sigmoidal curve with the point of inflection at the CMC.

In particular, ionic detergents have been found to show a three-step behavior forming spherical micelles at the CMC which then grow cooperatively to rodlike micelles at the “second CMC” at, for example, $3 \cdot \text{CMC}$.^{28,41} Such a pattern is not observed for the nonionic detergents studied here.

A plot of the enthalpies of micelle formation, ΔH^{mic} , of MM versus temperature yields a linear dependency (Figure 6B). The slope is the heat capacity change of micelle formation, $\Delta C_p^{\text{mic}} = -0.60 \text{ kJ/mol K}$, which is a large negative value, as is typical for processes driven by the hydrophobic effect. The temperature at which the CMC is minimum corresponds to the point where ΔH^{mic} vanishes, that is, the point of intersection of the fit line with the abscissa, $T(\Delta H^{\text{mic}} = 0) = 19.5 \text{ °C}$. The CMC at 25 °C amounts to 10 μM . Again, no significant deviations from

(41) Kubota, Y.; Kodama, M.; Miura, M. *Bull. Chem. Soc. Jpn.* **1973**, *46*, 100–103.

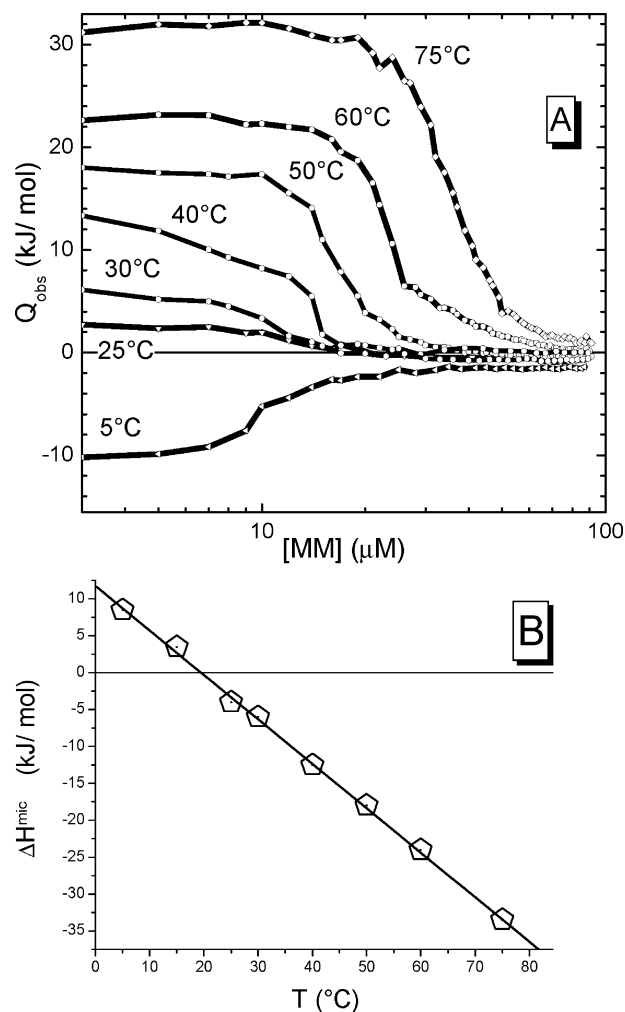


Figure 6. (A) ITC curves obtained upon demicellization experiments injecting micellar solutions of MM (0.5 mM) into water at different temperatures. (B) Enthalpies of micelle formation, ΔH^{mic} , as a function of temperature. The linear fit yields the heat capacity change, ΔC_p^{mic} (slope), and the temperature at the intercept with the abscissa, $T(\Delta H^{\text{mic}} = 0)$, where the CMC is minimum.

linearity are found that could be interpreted in terms of different structural states of the micelles at different temperatures.

For the micelle formation of TM, we obtained $\text{CMC}(25\text{ }^{\circ}\text{C}) = 35\mu\text{M}$, $\Delta C_p^{\text{mic}} = -0.53\text{ kJ/mol K}$ and $T(\Delta H^{\text{mic}} = 0) = 24\text{ }^{\circ}\text{C}$; the results for C_{14}EO_7 are $\text{CMC}(25\text{ }^{\circ}\text{C}) = 7\mu\text{M}$, $\Delta C_p^{\text{mic}} = -0.8\text{ kJ/mol K}$ and $T(\Delta H^{\text{mic}} = 0) = 36\text{ }^{\circ}\text{C}$.

Discussion

The various parameters of the sphere-to-rod transition determined here imply that the process is governed by a complex scheme of interrelated changes in headgroup hydration, ASA_{ap} , and chain order. An interpretation of the data requires all of these effects to be taken into account because each of the effects dominates some of the observable properties.

Headgroup Dehydration Triggers the Thermotropic Transition. A straightforward explanation why, for example, MM shows a thermotropic sphere-to-rod transition can be obtained in terms of the packing concept. Combination of Tanford's⁴² empirical rules (cf. Materials) yields for the compounds studied

(42) Tanford, C. *The Hydrophobic Effect: Formation of Micelles and Biological Membranes*, 2nd ed.; Wiley: New York, 1980.

here a virtually constant $v_{\text{chain}}/l_{\text{max}} \approx 21\text{ \AA}^2$ so that the packing parameter becomes controlled exclusively by a_0 , with a critical $a_0 \approx 60\text{--}65\text{ \AA}^2$, corresponding to the transition between rods and spheres ($\gamma \approx 0.5$). A temperature-dependent variation of a_0 arises from a thermally activated dehydration of the headgroups, as shown for other nonionic surfactants, for example, using dielectric spectroscopy.^{25,33} Kujawa and Winnik⁴ characterized the thermal dehydration of a polymer in terms of a volume increase ($\sim +1\%$) measured by PPC because water bound to polar groups has a larger density than does the characteristic hydrogen-bonded structure of bulk water (cf. also Chalikian⁴³). The gradual, thermal dehydration of maltose in solution gives rise to a strong thermal volume expansion particularly below room temperature (Figure 1A). As expected, the sphere-to-rod transitions studied here are also accompanied by a positive ΔV_s , but the small absolute values suggest a partial compensation by other effects (changes in chain packing and ASA_{ap}).

It should be noted that in contrast to the sphere-to-rod transition, thermal dehydration is not a cooperative process that is initiated when a certain temperature is reached. No substantial peak of the PPC curve is found for maltose and LM, which show (virtually) no sphere-to-rod transition. That means that headgroup hydration inhibits the sphere-to-rod transition up to a certain temperature, that is, when it becomes too weak to overcompensate another force that promotes the transition. It is a temperature-dependent trigger but not the driving force of the transition.

The Chain Ordering Hypothesis. What cannot be understood in terms of the packing concept is why the tendency to form rodlike micelles decreases clearly with decreasing chain length. Although all long-chain alkyl maltosides share virtually the same packing parameter (cf. previous section), the tendency to form rods decreases from MM to TM and further to LM (Figure 1) and vanishes for octyl maltoside.¹³ Furthermore, C_{16}EO_8 exhibits a T_{sr} lower than that of C_{14}EO_8 ²⁴, and the lyotropic micelle-to-hexagonal (i.e., rodlike) phase transition is promoted by longer chains comparing octyl, decyl, and lauryl maltoside.⁴⁴

A key parameter of the alkyl chains that is not taken into account by the packing parameter is their degree of order, which is related to the average number of gauche defects. Molecules with a stronger propensity for a more ordered chain conformation will prefer micelle geometries inducing a higher degree of chain order and vice versa. However, the relationships between chain order and (i) chain length as well as (ii) spherical versus cylindrical geometry are not obvious.

(i) Unfortunately, there are no direct measurements of the order of methylene segments of different surfactants in micelles, but some clue of chain length effects on order can be derived from fluid phospholipid bilayers, which are well characterized by ^2H NMR.^{45–47} Comparison of dilauroyl-, dimyristoyl-, and dipalmitoylphosphatidylcholine at a given temperature shows that the probability of a chosen C–C bond to form a gauche defect is higher for the longer chains,⁴⁷ suggesting that MM

(43) Chalikian, T. V. *J. Phys. Chem. B* **2001**, *105*, 12566–12578.

(44) Boyd, B. J.; Drummond, C. J.; Krodziewska, I.; Grieser, F. *Langmuir* **2000**, *16*, 7359–7367.

(45) Seelig, A.; Seelig, J. *Biochemistry* **1974**, *13*, 4839–4845.

(46) Seelig, J. *Q. Rev. Biophys.* **1977**, *10*, 353–418.

(47) Douliez, J. P.; Leonard, A.; Dufourc, E. J. *Biophys. J.* **1995**, *68*, 1727–1739.

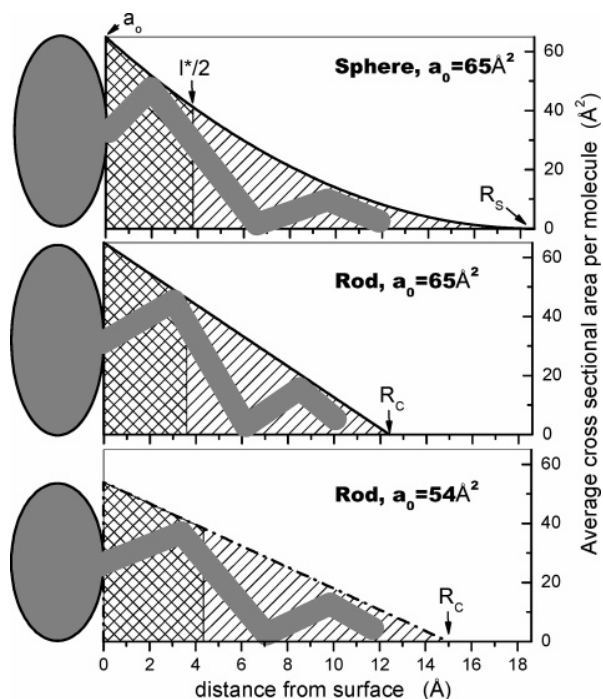


Figure 7. Mass distribution of a myristyl chain as function of distance from the surface in a sphere (top), in a cylinder with the same cross-sectional area at the interface ($a_0 = 65 \text{ Å}^2$, middle), and a cylinder with a reduced interfacial area (54 Å^2 , bottom). The intercept with the ordinate corresponds to the incremental surface area per molecule, a_0 , and the area underneath the curves represents the incremental volume, $v_{\text{chain}} \approx 400 \text{ Å}^3$, of a myristyl chain (outer 200 Å^3 crosshatched, inner 200 Å^3 hatched). The radius of the micelle core follows from the point where the curve reaches zero (midpoint of the micelle).

can be assumed to prefer a higher average degree of chain order than does LM.

(ii) Whether the effective order of the chains is higher or lower in a rodlike micelle compared to a sphere is also not straightforward to predict. A principal difference between spheres and rods is the area-to-volume ratio, amounting to $A/V = a_0/v_{\text{chain}} = 3/R_s$ for spheres and $A/V = a_0/v_{\text{chain}} = 2/R_c$ for cylinders. These two relations imply that for a sphere-to-rod transition, the radius should shrink to $R_c = 2R_s/3$ if a_0 and v_{chain} are conserved. Such a reduction of R , but to a somewhat lesser extent, was indeed observed in our study and measured¹⁶ as well as theoretically predicted²⁸ in the literature. It is graphically illustrated in the top and middle panel of Figure 7, where the intercept with the ordinate corresponds to an arbitrarily chosen $a_0 = 65 \text{ Å}^2$; the area under the curves (hatched + crosshatched) represents $v_{\text{chain}} = 400 \text{ Å}^3$, and the points where the curves reach the abscissa are the corresponding radii, $R_s = 3v_{\text{chain}}/a_0 = 18.5 \text{ Å}$ and $R_c = 2v_{\text{chain}}/a_0 = 12.3 \text{ Å}$.

The figure shows also that the distribution of mass (i.e., the volume increment of a thin shell) as a function of the distance from the surface follows a parabola for a sphere (which is curved in two dimensions) but a straight line for the cylinder. In contrast to the more homogeneous cylinder packing, the sphere must contain very few highly ordered/stretched chains with a projected length close to l_{max} but also a considerable number of highly disordered chains that fill the large volume fraction close to the surface (cf. also ref 28). On average, both systems seem to have similar degrees of order. As an indirect measure of chain order, let us define an effective projected chain length,

l^* , so that half of the chain resides, on average, within a depth of $l^*/2$ from the surface. This value of $l^*/2$ is just the abscissa value which cuts the area under the curve in two halves (left crosshatched, right hatched in Figure 7). It is intriguing that $l^*/2$ (cf. Figure 7) and, in turn, l^* is very similar for the sphere ($l^* = 7.6 \text{ Å}$) and the rod ($l^* = 7.2 \text{ Å}$).

The bottom panel of Figure 7 illustrates the more realistic case that a_0 is smaller in the rod due to headgroup dehydration. Then, the radius is closer to that of the sphere, and the chain is more stretched. Already for a slightly dehydrated headgroup with $a_0 = 60 \text{ Å}^2$, one obtains an $l^* = 7.8 \text{ Å}$, which suggests a higher average order than in a sphere with $a_0 = 65 \text{ Å}^2$.

Although a quantitative treatment in terms of the effect of changes in chain order on the free energy is not possible in the frame of our study, we conclude that there may well be a net stretching/ordering of the hydrocarbon chains accompanying the sphere-to-rod transition. Combined with the assumption that MM prefers an average chain order higher than that of LM, this would explain the findings of surfactants with longer chains showing a stronger tendency to form rodlike micelles.

The available information led us to the hypothesis that the sphere-to-rod transition increases the order of the chains, but we cannot rule out that a disordering (if MM would prefer less order than LM) or another parameter (not order) govern the chain length dependence of the transition. The hypothesis of increasing order accompanying the sphere-to-rod transition gives rise to the apparent paradox that increasing temperature promotes a process that reduces the entropy of the system. Such a chain ordering could neither account for driving nor for triggering the transition, but the phenomenon could be explained in terms of another “force”, the hydrophobic effect, driving the transition and overcompensating the exothermic chain ordering enthalpy.

The Hydrophobic Effect Drives the Transition. A driving force for the sphere-to-rod transition arises from the coupling between the ideal geometrical surface area of the micellar core, a_0 , and the water accessible apolar surface area (ASA_{ap}). Hence, the energy required for a reduction of a_0 by headgroup dehydration is provided by the hydrophobic effect favoring a small ASA_{ap} .

Good evidence for this reduction in ASA_{ap} is provided by our observation of a T_{sr} in D_2O that is lower than that in H_2O . Due to a more stable hydrogen-bond network, D_2O shows a stronger hydrophobic effect and promotes processes that are accompanied by a reduction in ASA_{ap} , such as micelle formation,^{48,49} protein folding,^{1,2,50} and the freezing of fluid lipids to a gel phase.⁵¹ Micelle clustering was found to show a transition temperature higher in D_2O than in water.^{36,52} We found no significant isotope effect on ΔV_s , which is similar to the freezing of lipid bilayers to a gel phase (cf. Wiener et al.⁵⁵) but in contrast with the dehydration of polar groups upon protein folding and

(48) Kresheck, G. C. *J. Phys. Chem. B* **1998**, *102*, 6596–6600.

(49) Kresheck, G. C. *J. Am. Chem. Soc.* **1998**, *120*, 10964–10969.

(50) Hermans, J., Jr.; Scheraga, H. A. *Biochim. Biophys. Acta* **1959**, *36*, 534–535.

(51) Lipka, G.; Chowdhry, B. Z.; Sturtevant, J. M. *J. Phys. Chem.* **1984**, *88*, 5401–5406.

(52) Blandamer, M. J.; Briggs, B.; Burgess, J.; Cullis, P. M.; Eaton, G. *J. Chem. Soc., Faraday Trans.* **1991**, *87*, 1169–1175.

(53) Likhodi, O.; Chalikian, T. V. *J. Am. Chem. Soc.* **1999**, *121*, 1156–1163.

(54) Likhodi, O.; Chalikian, T. V. *J. Am. Chem. Soc.* **2000**, *122*, 7860–7868.

(55) Wiener, M. C.; Tristram-Nagle, S.; Wilkinson, D. A.; Campbell, L. E.; Nagle, J. F. *Biochim. Biophys. Acta* **1988**, *938*, 135–142.

the polymer globule formation.^{4,53,54} Both the sphere-to-rod transition and lipid freezing involve coupled changes in chain order, ASA_{ap} , and headgroup hydration, which may have compensating isotope effects.

The reduction in ASA_{ap} explains why a sphere-to-rod transition can occur spontaneously, but it does not control whether it occurs and at which temperature. One might speculate that the transition is initiated when the hydrophobic effect reaches a certain, critical strength, but this idea is ruled out by the observation that increasing temperature drives the transition of TM at $T_{sr} \approx 30$ °C, where the driving force for hydrophobic association decreases (minimum of CMC is at 24 °C). Empirical rules for proteins given by Murphy^{56,57} suggest that the reduction in ASA_{ap} could also account for the *endothermic* enthalpy change, whereas the gradual dehydration of the polar headgroups and an ordering of the chains should be exothermic.

Sphere-Rod Coexistence. On the basis of the most simple model describing a rodlike micelle as a cylinder with spherical end caps, one might expect that the sphere-to-rod transition is a continuous process since a gradual variation of the total length, L_C , can describe a transformation of a sphere (formally, $L_C = 2R_C$; i.e., the end caps touch each other) to a rod ($L_C > 2R_C$). Such a micelle could assume all aggregation numbers equal or larger than about 70 (corresponding to an ideal sphere formed by myristyl chains).

Our data provide strong evidence that this scenario is wrong (at least for the compounds studied here). DLS and SANS report a two-state transition between two distinct, coexisting geometries, which are spheres and rods of a minimum length, $L_C \geq 20R_C$ (SANS for MM). This is in line with the information from the van't Hoff enthalpy of the transition (DSC of MM, TM) that the formation of a stable rod requires the concerted association of 300–600 molecules (i.e., about 4–8 spherical micelles).

The energetic barrier which inhibits the formation of very short rods can be explained in terms of the different equilibrium radii of rods, R_C , and spheres (and spherical end caps, R_S). Such a barrier was indeed predicted by May and Ben Shaul²⁸ who calculated the interfacial bending energy of a peanut-shaped micelle with quasi-spherical end caps connected by a thinner, cylindrical part. They showed that the cylindrical part must have a minimum length to avoid strongly unfavorable interferences between the ends. One may wonder whether the smaller cooperative unit of rod formation by $C_{14}EO_7$ can be explained in terms of a different bending modulus of the micellar interface or other headgroup properties.

Effects of Concentration, Transition Temperature, and Pressure. The fact that the sphere-to-rod transition is promoted (i.e., T_{sr} is lowered) with increasing surfactant concentration (cf. Figure 1) follows the rule arising from the mass-action law that an increase in concentration promotes association or growth. At a lower concentration, the transition proceeds at higher temperature, T_{sr} , and less cooperatively (smaller c.u.), but the accompanying volume change remains virtually constant. This observation is important because it provides some insight into the temperature dependence of ΔV_S and ΔT_{sr} . In contrast to the micellar shape transition studied here, the temperature of micelle clustering increases with increasing temperature.^{36,52} The con-

centration dependence of T_{sr} implies also the existence of a concentration-driven sphere-to-rod transition, but this turns out to be very gradual. Figure 2A shows that, for example, at 20 °C, the transition to rods starts at ~ 10 mM and is largely completed at 300 mM. When this is taken into account and the fact that ΔH is small compared to the enthalpy of demicellization, it becomes clear why there is no “second CMC” for MM which could be detected by ITC.

It is the nature of the transition studied here that the number of rods increases at the expense of spheres with increasing temperature. The structural parameters of the spheres and rods as well as the volume and enthalpy changes accompanying the sphere-to-rod transition are, however, virtually independent of T_{sr} . In agreement with this fact, ΔC_p and $\Delta\alpha$ are small, and ΔC_p^{mic} is virtually independent of T .

The effect of *elevated pressure* on the sphere-to-rod transition temperature, $\partial T_{sr}/\partial p$, can be assessed on the basis of the DSC and PPC data (ΔH , T_{sr} , and ΔV_S). Since the sphere-to-rod transition increases the volume, it is opposed by enhanced pressure. The effect is relatively strong for MM and TM (~ 50 K/kbar) but weaker for $C_{14}EO_7$ (~ 10 K/kbar). Values of ~ 40 K/kbar were reported for the lamellar-to-inverse hexagonal transition of lipids, which is also accompanied by a change in interfacial curvature and tighter packing of the headgroups.³⁸ The pressure dependence of phospholipid melting is somewhat weaker (~ 20 K/kbar).^{38,58} It is interesting to note that this parameter seems to be conserved for the melting of phospholipids with saturated chains irrespective of chain length and headgroup, despite major differences in ΔH , ΔV , and T_m . This can be considered as a clue that this pressure dependence is a characteristic property of *trans-gauche* isomerization of the chains. In contrast, the sphere-to-rod transitions and the Krafft points⁵⁹ of different surfactants do not obey a common pressure dependence.

Conclusions

It was shown that a combined thermodynamic, volumetric, and structural approach can provide a new level of understanding of a phenomenon, such as the sphere-to-rod transition. Volumetric data could be obtained very precisely and conveniently using PPC. This study gives rise to the following conclusions:

- (1) The thermotropic sphere-to-rod transition is driven by a reduction in the water accessible apolar surface area, ASA_{ap} , which is favored by the hydrophobic effect. This is indicated by a downshift of the transition temperature in D_2O compared to H_2O and may account for the endothermic enthalpy change.
- (2) The transition is triggered by a weaker hydration of the surfactant at higher temperature, which allows the hydrophobic effect to reduce the interfacial area per molecule. Like other phenomena of polar group dehydration, the sphere-to-rod transition is accompanied by an increase of the partial volume.
- (3) The characteristic chain length dependence of the thermotropic sphere-to-rod transition gives rise to the hypothesis that the sphere-to-rod transition is accompanied by an ordering of the alkyl chains; that is, chains in a cylindrical aggregate pack more favorably than in a sphere.

(58) Prasad, S. K.; Chandrasekhar, S.; Shashidhar, R.; Gaber, B. P. *Biophys. J.* **1990**, *57*, A557.

(59) Kaneshina, S.; Yamanaka, M. *J. Colloid Interface Sci.* **1990**, *140*, 474–480.

(56) Baker, B. M.; Murphy, K. P. *Methods Enzymol.* **1998**, *295*, 294–314.

(57) Murphy, K. P. *Med. Res. Rev.* **1999**, *19*, 333–339.

(4) The nonionic surfactants studied here show a concentration-dependent micellar structure but not as a cooperative phenomenon like a "second CMC".

(5) The sphere-to-rod transition is opposed by increasing pressure with a shift of the transition temperature by ~ 50 K/kbar for MM and TM, but this value does not seem to characterize all sphere-to-rod transitions.

Acknowledgment. We are indebted to Halina Szadkowska for excellent technical assistance, and to Joachim Kohlbrecher for providing the sasfit program. We thank a reviewer for

suggesting a van't Hoff analysis of the DSC peaks. Financial support from the Swiss National Science Foundation is gratefully acknowledged by H.H. and A.T. (Grant 31-67216.01). Part of this work was performed at SINQ, Paul Scherrer Institute, Villigen, Switzerland.

Supporting Information Available: Experimental details in the Experimental Section. This material is available free of charge via the Internet at <http://pubs.acs.org>.

JA045525W

EXPERIMENTAL

Materials and their molecular parameters

The detergents n-dodecyl- β -D-maltopyranoside (lauryl maltoside, LM), n-tridecyl- β -D-maltopyranoside (TM), and n-tetradecyl- β -D-maltopyranoside (myristyl maltoside, MM) were purchased from Anatrace Inc. (Maumee, OH, USA) in the highest available (AnagradeTM) purity. Heptaethyleneglycoltetradecylether (C₁₄EO₇) was purchased from Fluka (Buchs, Switzerland).

Micellar dispersions were obtained by dispersing appropriate amounts of dry surfactant in water or heavy water, respectively, followed by vortexing. At least at concentrations of 100 mM, surfactant monomers in solution are negligible taking into account the critical micellar concentrations of 170 μ M (LM), 33 μ M (TM), and 10 μ M (MM).¹

The structure of MM is illustrated by Fig. 8.

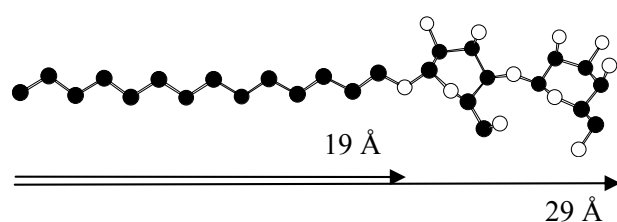


Fig. 8: Possible chemical structure of MM with estimates of the dimensions. Carbon atoms are black, oxygen white, hydrogen omitted.

For data evaluation and interpretation the following assumptions for several molecular parameters have been used. Tanford² has established empirical rules for the partial volumes,

v_{chain} , of n-alkyl chains in micelles and the effective length of an all-trans chain, l_{max} , containing n_{C} carbons:

$$v_{\text{chain}} \approx 26.9 \text{ \AA}^3 \cdot n_{\text{C}} + 27.4 \text{ \AA}^3 \quad (1)$$

$$l_{\text{max}} \approx 1.265 \text{ \AA} \cdot n_{\text{C}} + 1.5 \text{ \AA} \quad (2)$$

yielding e.g. $v_{\text{chain}} \approx 403 \text{ \AA}^3$ and $l_{\text{max}} \approx 19 \text{ \AA}$ for MM. Eq. (1) corresponds to partial molar volumes of $V_{\text{chain}} = 211, 227, 243 \text{ mL/mol}$ for lauryl, tridecyl, and myristyl chains. Comparing the partial molar volume of LM (416 mL/mol^3) and octyl maltoside (353 mL/mol^3) with the corresponding values of V_{chain} yields a common difference of $V_{\text{malt}} = 206 \pm 1 \text{ mL/mol}$ arising from the maltoside head group. Based on this V_{malt} and V_{chain} for $n_{\text{C}} = 13, 14$ one obtains $V_{\text{S}} = 432 \text{ mL/mol}$ for TM and 448 mL/mol for MM and partial specific volumes of 0.81 mL/g (LM), 0.82 mL/g (TM) and 0.83 mL/g (MM). For C_{14}EO_7 , we used 0.99 mL/g based on a head group contribution of 0.84 mL/g as for polyethyleneglycol.

Pressure perturbation calorimetry (PPC) and differential scanning calorimetry (DSC)

PPC and DSC measurements were carried out in a VP DSC calorimeter⁴ from MicroCal (Northampton, MA, USA), equipped with a PPC accessory⁵ from the same manufacturer. The sample cell ($\approx 0.5 \text{ mL}$) was filled with the micellar dispersion and the reference cell with water. The PPC controller applies pressure jumps between 5 bars and 0 bar above ambient and back. A power compensation system keeps the temperature of the cells constant and measures the difference in heat responses of sample versus reference. Such isothermal pressure jumps are automatically performed at a series of, e.g., 50 selected temperatures.

The heat signals obtained after pressure increase and decrease and those of repeated pressure jumps at the same temperature were virtually identical in absolute value, indicating that the processes under study were reversible; these heat values were averaged to improve the signal-to-noise ratio.

A detailed description of the data evaluation is given elsewhere.^{5,6} Briefly, the heats q_{obs} produced or consumed by the sample after isothermal pressure changes were measured as a

function of temperature with the sample and reference cells filled with sample and water. Very small heats obtained in a blank experiment with water in both cells were subtracted to correct for minimal differences between the two cells. The unperturbed water in the sample cell has no effect on the corrected heats, $q_{\text{obs}}(T, \Delta p)$, since it is present also in the reference cell. The difference between both cells arises only from the partial volume of the solute, the product of solute mole number n_s and its partial molar volume, V_s . This partial volume is occupied by n_s solute molecules in the sample cell and by $n_s V_s / V_w$ water molecules in the reference cell (V_w is the partial molar volume of water). Introducing molar heats of solute and water, Q_s and Q_w , we obtain:

$$Q_s = \frac{q_{\text{obs}}}{n_s} + \frac{V_s}{V_w} Q_w \quad (3).$$

The molar heat response and volume of water are considered by the instrument software on the basis of literature data. The molar, isobaric, thermal volume expansion of the surfactants, $\partial V_s / \partial T$, is calculated according to the Maxwell relation:

$$-T \left. \frac{\partial V_s}{\partial T} \right|_p = \left. \frac{\partial Q_s}{\partial p} \right|_T \quad (4).$$

Since the transitions are fully reversible and repeatable, DSC curves could be recorded after PPC experiments without re-filling the cells. The scan rate was 60 K/h and the instrument was in the high gain mode. The shape of the DSC peaks after subtraction of the baseline was modelled by the eq.

$$C_p(T) = \frac{K(T) \Delta H_{\text{vH}}}{(1 + K(T))^2 RT^2} \Delta H \quad (5)$$

with

$$K(T) = \exp \left\{ \frac{-\Delta H_{\text{vH}}}{RT} \left(1 - \frac{T}{T_{\text{sr}}} \right) \right\} \quad (6)$$

using Origin 5.0TM for DSC.

Isothermal titration calorimetry (ITC)

ITC measurements of concentration-dependent micelle dissolution were performed on a VP ITC instrument from MicroCal (Northampton, MA, USA). The demicellization protocol was described in detail in the literature.⁷⁻¹⁰ Briefly, the injection syringe (300 μ L) was loaded with a micellar solution of the surfactant at a concentration about 20-50 times larger than the critical micelle concentration (CMC) and the cell (1.4 mL) was filled with water. After equilibration at the desired temperature, a series of small injections of 1-15 μ L, each, were done and the heat response was measured by the instrument using a power-compensation mechanism. One obtains a quasi-sigmoidal curve with the point of inflection at the cmc. Below the cmc, injected micelles are diluted and dissolve, giving rise to heats of demicellization and dilution. Above the CMC, micelles do no longer disintegrate in the cell and only heats of dilution are measured.

The enthalpies of micelle formation were determined from the curves in Fig. 4 (top) according to:

$$\Delta H^{\text{mic}} = -\left[Q_{\text{obs}}(C_S \ll \text{cmc}) - Q_{\text{obs}}(C_S \gg \text{cmc})\right] \cdot \frac{C_S^{\text{sy}}}{C_S^{\text{sy}} - \text{cmc}} \quad (7)$$

with the minus sign converting the data measured upon demicellization into values for micelle formation. Q_{obs} stands for the observed heat normalized per mole of surfactant added. The heat measured well above the cmc (heat of dilution of the micelles) is subtracted from the heats measured at low concentration, C_S , in the cell, which includes both demicellization and dilution heats. The syringe contains a total surfactant concentration C_S^{sy} including monomers (cmc) and surfactant molecules in micelles ($C_S^{\text{sy}} - \text{cmc}$). The term $C_S^{\text{sy}} / (C_S^{\text{sy}} - \text{cmc})$ amounts to 1.02-1.09 and serves to re-normalize the values of Q_{obs} to the moles of *micellar* surfactant injected since injected monomers do not contribute to the heat of demicellization.

Dynamic light scattering (DLS)

Dynamic light scattering (DLS) was measured using an ALV-500 Multiple Tau Correlator equipped with a 632 nm laser. Scattered light intensity was detected within the angle range from 30° to 150° in steps of 10°. Aqueous solutions (37mM) were placed in cylindrical cuvettes and inserted into the thermostated sample cell; after temperature stabilization (usually ca. 10 minutes), the intensity curve was measured during a 3-min run. Light scattering measurements were performed in the temperature range from 10 to 35°C. Higher temperatures were not available due to the limitations of the instrument.

In DLS, the time decay of an electric field correlation function, $g(Q,t)$, which corresponds to the Fourier transform of the fluctuating number density of scattering particles is measured. The angular dependence allows detection of the phenomena occurring in the system on large and small scale. At each angle, the intensity curve is fitted to yield the apparent aggregate radius, R , and from the extrapolation of the $1/R=f(\theta)$ plot to $\theta=0$, the hydrodynamic radius of particles is obtained. In this study, two different fitting methods were applied, namely the cumulant and double exponential; and both proved to be appropriate fits (evidenced by very small residuals) and yielded practically identical results.

Small angle neutron scattering (SANS)

Small angle neutron scattering measurements were performed at the SANS II beam line of the Swiss Spallation Neutron Source, SINQ. Wavelengths used were 4.55 Å and 10.61 Å with a $\Delta\lambda/\lambda$ of 10 %. Distances between the sample and the 2D He³ multi-wire detector were 0.97 m, 5.0 m, and 6.0 m, respectively, covering a complete range of the scattering vector of $3 \cdot 10^{-3} \leq Q \leq 0.3 \text{ \AA}^{-1}$. The measurement time for the different detector positions varied between 20-65 minutes to collect sufficient counts with a neutron beam illuminating a sample size of 1 cm². Samples were held in a closed, thermostated quartz cell with 1 mm sample thickness. The raw data were corrected for background from sample cell, solvent and electronic noise. Corrected intensities were circularly averaged to obtain $d\Sigma/d\Omega(Q)$.

Fits of $d\Sigma/d\Omega(Q)$ to obtain structural parameters of the micellar aggregates were performed with the program sasfit (ASQ, PSI, Villigen). The implemented scattering functions used for a spherical and a rod-like cylinder structure were

$$\frac{d\Sigma}{d\Omega} = I(Q) = \left\{ \frac{4}{3} \pi R_s^3 \Delta\eta \frac{3 \left[\sin(QR_s) - QR_s \cos(QR_s) \right]}{(QR_s)^3} \right\}^2 \quad (8)$$

and

$$\frac{d\Sigma}{d\Omega} = I(Q) = \left\{ 4\pi R_c^2 L_c \cdot \Delta\eta \frac{J_1 \left(QR_c \sqrt{1-x^2} \right) \cdot \sin \left(0.5QL_c x \right)}{Q^2 R_c L_c x \sqrt{1-x^2}} \right\}^2 \quad (9),$$

respectively. R_s and R_c are the radii of sphere and cylinder, Q the scattering vector, η the scattering length density, J_1 the spherical Bessel function, L_c the length of the cylinder and x the volume fraction of the micellar aggregates. A log-normal distribution was used for smearing of the applied scattering functions with

$$\text{LogNorm}(R, \mu, \sigma, p) = \frac{N}{c_{LN}} \frac{1}{R^{-p}} \exp \left\{ \frac{-\log \left(\frac{R}{\mu} \right)^2}{2\sigma^2} \right\} \quad (10)$$

$$c_{LN} = \sqrt{2\pi} \sigma \mu^{1-p} \exp \left\{ (1-p)^2 \frac{\sigma^2}{2} \right\} \quad (11)$$

with R radius of sphere or cylinder, N particle number, μ variable scaling factor and fixed scaling factors $p=0$, $\sigma=0.1$.

REFERENCES

- (1) Anatrace_Inc. www.anatrace.com.
- (2) Tanford, C. *The hydrophobic effect: formation of micelles and biological membranes*; 2. ed.; Wiley: New York, 1980.
- (3) He, L. Z.; Garamus, V. M.; Funari, S. S.; Malfois, M.; Willumeit, R.; Niemeyer, B. *J. Phys. Chem. B* **2002**, *106*, 7596-7604.
- (4) Plotnikov, V. V.; Brandts, J. M.; Lin, L. N.; Brandts, J. F. *Anal Biochem* **1997**, *250*, 237-244.
- (5) Lin, L. N.; Brandts, J. F.; Brandts, J. M.; Plotnikov, V. *Anal Biochem* **2002**, *302*, 144-160.
- (6) Heerklotz, H.; Seelig, J. *Biophys J* **2002**, *82*, 1445-1452.
- (7) Kresheck, G. C.; Hargraves, W. A. *J. Coll. Interf. Sci.* **1974**, *48*, 481-493.
- (8) Olofsson, G. *J. Phys. Chem.* **1985**, *89*, 1473-1477.

- (9) Paula, S.; Süss, W.; Tuchtenhagen, J.; Blume, A. *J. Phys. Chem.* **1995**, *99*, 11742-11751.
- (10) Heerklotz, H.; Eppand, R. M. *Biophys J* **2001**, *80*, 271-279.

Interactions of Cholesterol with Lipid Membranes and Cyclodextrin Characterized by Calorimetry

Alekos Tsamaloukas,* Halina Szadkowska,* Peter J. Slotte,[†] and Heiko Heerklotz*

*Biozentrum of the University of Basel, Division of Biophysical Chemistry, Basel, Switzerland; and [†]Åbo Akademi University, Department of Biochemistry and Pharmacy, Turku, Finland

ABSTRACT Interactions of cholesterol (cho) with different lipids are commonly believed to play a key role in the formation of functional domains in membranes. We introduce a novel approach to characterize cho-lipid interactions by isothermal titration calorimetry. Cho is solubilized in the aqueous phase by reversible complexation with methyl- β -cyclodextrin (cyd). Uptake of cho into the membrane is measured upon a series of injections of lipid vesicles into a cyd/cho solution. As an independent assay, cho release from membranes is measured upon titrating lipid/cho mixed vesicles into a cyd solution. The most consistent fit to the data is obtained with a mole fraction (rather than mole ratio) partition coefficient and considering a cho/cyd stoichiometry of 1:2. The results are discussed in terms of contributions from 1), the transfer of cho from cyd into a hypothetical, ideally mixed membrane and 2), from nonideal interactions with POPC. The latter are exothermic but opposed by a strong loss in entropy, in agreement with cho-induced acyl chain ordering and membrane condensation. They are accompanied by a positive heat capacity change which cannot be interpreted in terms of the hydrophobic effect, suggesting that additive-induced chain ordering itself increases the heat capacity. The new assays have a great potential for a better understanding of sterol-lipid interactions and yield suggestions how to optimize cho extraction from membranes.

INTRODUCTION

There is evidence that membrane constituents do not move freely and do not distribute homogeneously over cell membranes, a fact that has enormous consequences for biological functions such as signaling and others. The raft hypothesis (1–4) explains functional inhomogeneities or domains in terms of a spontaneous demixing of membrane lipids forming different local pseudo-phases. The recent view combines the concept of functional domains (lipid rafts) with those of liquid-ordered phases in model membranes and detergent-resistant membranes (DRM). A major link between these originally unrelated models is cholesterol (cho). Application of the detergent Triton X-100 at 4°C to cell membranes solubilizes part of the lipids and proteins into small micelles but leaves cho-rich DRMs behind that are large enough to be separated by centrifugation (5,6). In model membranes, large amounts of cholesterol induce the formation of coexisting domains (7) that are described as a phase separation between liquid-ordered and liquid-disordered phases (8–10). These findings have tempted many researchers to take it for granted that lipid rafts are functional, liquid-ordered domains that can be isolated from cell membranes by cold Triton. However, recent studies have suggested that DRMs may be substantially different from functional domains in vivo (rafts) (3,11,12).

An assay for studying functions of cho is based on the effects of removing cho from cells (or model membranes) by means of cyclodextrin (cyd). Cyd is a ring-shaped molecule

consisting of glucose units (seven units for β -cyd), which is well soluble in water but contains a hydrophobic cavity that binds (and thus solubilizes) small hydrophobic molecules including cho. Many biological studies have utilized this phenomenon on a semi-empirical basis for extracting cho from cells or (re-)supplying it to them (e.g., 13,14). The interpretation of such experiments is, however, complicated by the fact that cho has multiple biochemical and biophysical effects in cells and that cyd interacts also with other membrane constituents, including phospholipids.

Our study pursues two major goals. First, we establish an optimized model describing the partitioning of cho between a cyd solution and a membrane phase and show its importance for avoiding artifacts in cho extraction assays. Second, we are using cyd as a tool to investigate the key thermodynamic parameters of nonideal interactions between cho and phospholipid in the membrane.

Much insight in the membrane effects of cho has been gained from scanning calorimetry and other studies of the phase behavior of lipid-cho mixtures (7,15–17). A classical approach to the problem of cho-lipid affinities has been based on measuring the equilibrium distribution of cho between two fractions of vesicles with different lipid composition (18). This technique may, however, suffer from problems due to slow kinetics of cho transfer and difficulties to separate the two vesicle fractions from each other. One sophisticated solution to this problem was described by Huster et al. (19), who measured differences in cho-lipid affinities within the same membrane in terms of the NMR cross-relaxation rates between cho and different lipids. NMR served also to determine differential affinities of cho to different lipids expressed in terms of tie lines in ternary phase

Submitted March 3, 2005, and accepted for publication May 19, 2005.

Address reprint requests to Heiko Heerklotz, E-mail: heiko.heerklotz@unibas.ch.

© 2005 by the Biophysical Society

0006-3495/05/08/1109/11 \$2.00

doi: 10.1529/biophysj.105.061846

diagrams (20). Other authors solved the problem of slow cho exchange kinetics between different lipid vesicles by cyd. Steck and co-workers (21) used cyd-extraction kinetics to provide additional evidence for a fast transbilayer flip-flop of cho in the red cell membrane. Leventis and Silvius (22) showed that small amounts of cyd act as a potent catalyst for cho exchange so that, for example, 1 mM cyd speeds up the intervesicle transfer of cho by a factor of ~ 60 . Hence, cho can become equilibrated between different glycerolipid vesicles within a few minutes. Given the almost exclusive catalytic role of cyd in this approach, interactions between cyd and cho need not be quantified (see also Silvius' general review (23)). Niu and Litman (24) pointed out that problems in separating the two fractions of vesicles can be avoided by studying the different vesicles in separate experiments. They used cyd not as a catalyst but as a means to solubilize substantial amounts of cho. Then, the partitioning of cho between vesicles and cyd (as a common reference state) was measured and quantified in terms of a mole-ratio partition coefficient. Assuming implicitly a 1:1 stoichiometry of cho-cyd complexes, they obtained, e.g., a partition coefficient of 6.7 for cho between cyd and POPC at 37°C. The partitioning of cho between two different lipid membranes is then derived as the ratio between the two lipid-cyd partition coefficients.

Here we establish similar assays measuring the partitioning of cho between cyd and lipid vesicles using isothermal titration calorimetry (ITC). The major advantage of this technique is that it yields the affinity of cho for a lipid species as well as the enthalpic and entropic contribution to the cho-lipid interaction—shedding light on the generalized forces governing mixing or demixing in cho-lipid membranes. Furthermore, it is fast and straightforward and does not require the use of labeled compounds. Two protocols are introduced, analogously to the ITC uptake and release protocols for membrane-water partitioning of soluble compounds (25). The cho-uptake protocol is based on a titration of lipid vesicles into a solution of cyd and cyd-cho complexes. After each injection, some cho is transferred into the membrane. For the cho-release protocol, mixed lipid-cho vesicles are injected into a cyd solution so that part of the membrane-bound cho is extracted by cyd. The data are evaluated in terms of four alternative models, comparing mole-ratio with mole-fraction partition coefficients and allowing for different stoichiometries of the cho-cyd complex. The study gives rise to a comprehensive thermodynamic understanding of the system and to rules to be considered upon application of cyd to membranes. The new protocols can now be applied to vesicles of other lipids.

THEORY

The affinity of a hydrophobic or amphiphilic molecule to insert into a membrane in a nonspecific manner is usually described in terms of a membrane-water partition coefficient.

The formation of a complex of two compounds is quantified by a binding constant given by the mass action law. The distribution of cho between cyd complexes and membranes must therefore be modeled by a combination of the two formalisms. Such a combined model is derived making use of the fact that both partitioning and complex formation contain cho in aqueous solution as a common reference state. The fact that this cho concentration in water, C_{cho}^w , is extremely small and cannot be determined experimentally is no problem, since it does not show up in the final equation relating membrane-bound and cyd-complexed cho with one another.

Membrane-water partitioning

There are many different definitions of membrane-water partition coefficients used in the literature. This is due to the fact that the application of Nernst's partitioning law (26) for dilute solutions in two macroscopically separate phases (such as octanol/water) can only approximately be applied to substantial contents of additives in microheterogeneous systems such as vesicle suspensions.

The mole fraction partition coefficient, $K_X^{b/w}$, between bilayer and water (b/w) is constant if the additive mixes ideally with the host lipid (27),

$$K_x^{b/w} \equiv \frac{X^b}{X^w} = \frac{C_{\text{cho}}^b \times C_W^w}{(C_{\text{cho}}^b + C_L) \times C_{\text{cho}}^w}, \quad (1)$$

with X^b and C_{cho}^b denoting mole fractions and molar concentrations, respectively, of cho in bilayers (superscript b) and water (w) and X^w the mole fraction of cholesterol in aqueous solution (note that $C_W^w + C_{\text{cho}}^w \sim C_W^w$). The concentration of a dilute aqueous solution is generally $C_W^w + C_{\text{cho}}^w = 55.5 \text{ M}$. The phospholipid concentration is C_L and all lipids are assumed to be in the bilayer.

Many amphiphilic compounds partitioning into membranes can be well described assuming a constant mole ratio partition coefficient, $K_R^{b/w}$ (28–30),

$$K_R^{b/w} \equiv \frac{R^b}{C_{\text{cho}}^w} = \frac{C_{\text{cho}}^b}{C_L C_{\text{cho}}^w}, \quad (2)$$

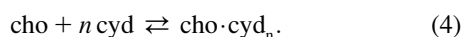
based on the cho/lipid mole ratio within the membrane, R^b . A constant $K_R^{b/w}$ corresponds to a characteristic nonideal mixing represented by a decreasing $K_X^{b/w}$:

$$\frac{K_x^{b/w}}{55.5 \text{ M}} = K_R^{b/w} \times (1 - X^b). \quad (3)$$

Systems with a mole fraction partition coefficient that is constant or even increases with X^b should not be treated assuming a constant mole ratio partition coefficient.

Stoichiometric binding of cho to cyd

For the binding process of cho to cyd, we may write



The equilibrium constant $K^{\text{cyd/w}}$ is given by the mass action law,

$$K^{\text{cyd/w}} = \frac{C_{\text{cho}}^{\text{cyd}}}{C_{\text{cho}}^{\text{w}} (C_{\text{cyd}} - n C_{\text{cho}}^{\text{cyd}})^n} \approx \frac{C_{\text{cho}}^{\text{cyd}}}{C_{\text{cho}}^{\text{w}} (C_{\text{cyd}})^n}, \quad (5)$$

where $C_{\text{cho}}^{\text{cyd}}$ stands for the concentration of cho bound to cyd which is equal to the concentration of $\text{cho} \cdot \text{cyd}_n$ complexes (assuming that each complex contains one cho molecule), n is the stoichiometry of the complex, and C_{cyd} is the total cyd concentration. The approximation in the last part of Eq. 5 applies to the case of negligible saturation of the cyd, $C_{\text{cyd}} \gg n \cdot C_{\text{cho}}^{\text{cyd}}$, which is generally fulfilled in our experiments.

Membrane-cyd partitioning of cho

Relating either Eq. 1 or Eq. 2 with Eq. 5 eliminates $C_{\text{cho}}^{\text{w}}$ and yields the bilayer/cyd mole fraction partition coefficient,

$$K_X \equiv \frac{K_X^{\text{b/w}}}{K^{\text{cyd/w}} \times C_{\text{w}}^{\text{w}}} = \frac{C_{\text{cho}}^{\text{b}} (C_{\text{cyd}})^n}{(C_{\text{L}} + C_{\text{cho}}^{\text{b}}) C_{\text{cho}}^{\text{cyd}}}, \quad (6)$$

and the mole ratio partition coefficient,

$$K_R = \frac{C_{\text{cho}}^{\text{b}} (C_{\text{cyd}})^n}{C_{\text{L}} C_{\text{cho}}^{\text{cyd}}}. \quad (7)$$

Assuming $n = 1$, Eq. 7 becomes equivalent to the model used by Niu and Litman (24). Substituting $C_{\text{cho}}^{\text{cyd}} = C_{\text{cho}} - C_{\text{cho}}^{\text{b}}$ we may solve Eqs. 6 and 7 for the membrane-bound cholesterol concentration,

$$C_{\text{cho}}^{\text{b}} = \frac{C_{\text{L}} - C_{\text{cho}} + (C_{\text{cyd}})^n / K_X}{2} \times \left(\sqrt{1 + 4 \frac{C_{\text{L}} C_{\text{cho}}}{[C_{\text{L}} - C_{\text{cho}} + (C_{\text{cyd}})^n / K_X]^2}} - 1 \right), \quad (8)$$

$$C_{\text{cho}}^{\text{b}} = \frac{K_R C_{\text{L}} C_{\text{cho}}}{(C_{\text{cyd}})^n + K_R C_{\text{L}}}. \quad (9)$$

MATERIALS AND METHODS

Substances and sample preparation

1-Palmitoyl-2-oleoyl-*sn*-glycero-3-phosphocholine (POPC) was purchased from Avanti Polar Lipids (Alabaster, AL) and cholesterol (cho) and randomly methylated β -cyclodextrin (cyd) were from Fluka (Buchs, Switzerland). Mixtures of POPC and cho were prepared by addition of cho to the dry lipid powder, resuspension in chloroform/methanol, and consecutive drying under a gentle stream of nitrogen. The sample was then held under vacuum for at least 12 h for further drying. The composition of the sample was checked by weighing the dry material before and after an addition. The dry lipid mixtures were suspended in 100 mM NaCl, 10 mM Tris buffer at pH 7.4 by gentle vortexing to reach a POPC concentration of 10 mM. After five consecutive freeze-thaw cycles, large unilamellar vesicles were prepared by

10 extrusion runs through a Nucleopore polycarbonate filter with a pore diameter of ~ 100 nm in a Lipex extruder (Northern Lipids, Vancouver, Canada). Extrusion was performed at 50°C . Our results imply in agreement with the literature (31,32) that cho flip-flop between the outer and inner lipid leaflet is fast (a few minutes or less), so that cho is homogeneously distributed over the membrane. Samples containing 50 mol % cho have been reported to be subject to artifacts arising from a separation of the dry substances leading to a heterogeneous distribution of cho between the vesicles (33). For homogenization, we have therefore sonicated these samples before freeze-thawing (restoring the multilamellar state) and extrusion. Large unilamellar vesicles were stored in the dark under nitrogen and used for a week at maximum.

ITC measurements

ITC experiments were performed on a VP ITC calorimeter from MicroCal (Northampton, MA) (34,35). The calorimeter performs a series of injections from a computer-controlled, $300\text{-}\mu\text{L}$ injection syringe into the calorimeter cell (1.4 mL). The temperature of the cell is kept constant by a power compensation feedback. Each injection leads to a peak of the power of the compensation heater, which is integrated to obtain the heat response of the system.

Both uptake and release assays are based on a titration of lipid vesicles (10 mM POPC) into a solution of cyd (2.5–10 mM). Cholesterol is either included in the titrant (release assay) or in the initial cell content (uptake assay). The cho/cyd ratio was always below 1:20 so that free cyd was in large excess and saturation with cho remained negligible. Mixing after each injection leads to an equilibration of cho between membranes and cyd which, in turn, gives rise to the heat signal.

All solutions were degassed before filling to avoid air bubbles. The typical sequence of injections was $1 \times 1 \mu\text{L}$, $3 \times 5 \mu\text{L}$, and $\sim 10 \times 10 \mu\text{L}$. The first injection is subject to larger errors, therefore its volume is chosen very small and its heat is not taken into account upon curve fitting. The three $5\text{-}\mu\text{L}$ injections are performed to increase the resolution in the beginning of the titration, where the heats are largest and vary strongly from one to another.

After each injection, the heat power of reaction was recorded for a sufficient time to ensure that the signal returns to the baseline level. Depending on the kinetics of cho exchange between membrane and cyd, waiting times ranged between 10 min (in particular at 50°C) and 1 h (25°C) giving rise to a total time of $\sim 2\text{--}14$ h per titration.

The primary data analysis was performed using Origin for ITC (MicroCal) provided with the instrument. Integration of the power peaks after each injection (see Fig. 1, top) from a manually adjusted baseline yields the differential heat response of the system to the injection. These data are normalized with respect to the number of moles of lipid injected. The results of a blank run, i.e., titration of pure lipid into a cyd solution for both protocols, were subtracted from each data set of cho partitioning. The resulting corrected, normalized heats were exported into an Excel spreadsheet for curve fitting.

Curve fitting

The data were evaluated using a Microsoft Excel spreadsheet (Microsoft, Seattle, WA) in a stepwise mode. The spreadsheet contains information about the experimental setup (initial concentrations in the cell and syringe and injection volumes). It calculates the concentration of all components, cho, cyd, and lipid after each injection in the cell assuming that injection of a volume of ΔV_i changes each concentration by

$$C_i - C_{i-1} = \frac{\Delta V_i}{V_{\text{cell}}} \left(C^{\text{sytr}} - \frac{C_i + C_{i-1}}{2} \right), \quad (10)$$

where C^{sytr} , C_i , and C_{i-1} denote concentrations of the respective compound in the syringe, after and before the i^{th} injection, respectively. The equation takes into account the addition of compound from the syringe (if $C^{\text{sytr}} \neq 0$)

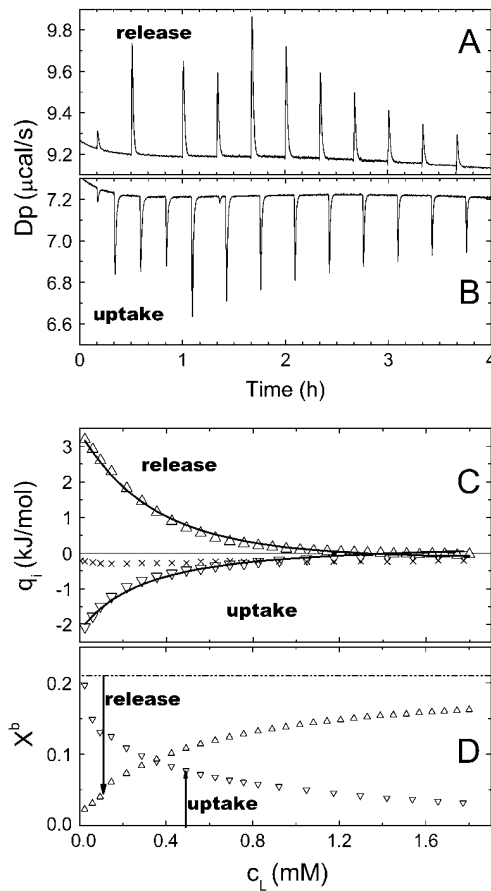


FIGURE 1 Data of cho uptake and cho release experiments at 37°C, 5 mM cyd. (A) Detail of the raw data of a release experiment, showing the compensation heat power versus time t . The injection volumes are $1 \times 1 \mu\text{L}$, $3 \times 5 \mu\text{L}$, and others $10 \mu\text{L}$, respectively. (B) Detail of raw data of an uptake experiment (analogous to A). (C) Integrated, normalized heats of uptake (∇) and release (Δ) after subtraction of the blank (\times). The fit curves correspond to a global fit (setup and fit parameters given in the text). (D) Average X^b in the cell during the experiments (symbols as in C) calculated using K_X obtained in C. X^b in the syringe is 0.21 (release) and 0 (uptake).

and the displacement of ΔV_i of cell content (average concentration $(C_i + C_{i-1})/2$) out of the completely filled cell. Eq. 10 is based on the assumption that overflow material is no longer in contact with the cell content as recommended by the manufacturer. Solving Eq. 10 for C_i yields

$$C_i = \frac{C_{i-1} \left(1 - \frac{\Delta V_i}{2V_0}\right) + C^{\text{syrr}} \frac{\Delta V_i}{V_0}}{1 + \frac{\Delta V_i}{2V_0}}. \quad (11)$$

Based on arbitrarily chosen initial values for K (either K_R or K_X), the table also calculates the corresponding concentration of membrane-bound cho after the i^{th} injection, $C_{\text{cho}}^b(i)$ (Eqs. 8 or 9), and the corresponding mole fraction of cho in the membrane, $X^b(i)$. The difference between C_{cho}^b after and before a given injection, $C_{\text{cho}}^b(i) - C_{\text{cho}}^b(i-1)$, results from several effects:

$$C_{\text{cho}}^b(i) - C_{\text{cho}}^b(i-1) = \frac{\Delta V_i}{V_{\text{cell}}} \left(C_{\text{cho}}^{\text{b, syr}} - \frac{C_{\text{cho}, i}^b + C_{\text{cho}, i-1}^b}{2} \right) + [C_{\text{cho}}^b]_i^{\text{transfer}}. \quad (12)$$

First, membrane-bound cho is added from the syringe (only for the release protocol) and flows over from the cell content. This contribution, which does not give rise to any heat, is calculated analogously to Eq. 10 replacing the total concentrations C^{syrr} , C_i , and C_{i-1} by the membrane-bound ones. Second, the re-equilibration in the cell after disturbing the equilibrium by the injection leads to a transfer of cho from cyd into the membrane or vice versa; the corresponding contribution $[C_{\text{cho}}^b]_i^{\text{transfer}}$ is the source of the measured heat.

The absolute heat measured after the i^{th} injection, q_i , is linearly related to the mole number of transferred cho, which is obtained from $[C_{\text{cho}}^b]_i^{\text{trans}}$ by multiplication with the cell volume, V_{cell} , and the molar enthalpy of transfer, ΔH :

$$q_i = [C_{\text{cho}}^b]_i^{\text{trans}} \times V_{\text{cell}} \times \Delta H + q_{\text{dil}}. \quad (13)$$

Note that both ΔH and ΔC_{cho}^b are generally defined for the membrane uptake of cho from cyd. The fact that the sign of the heat, q_i , is different for cho release is considered by $[C_{\text{cho}}^b]_i^{\text{trans}}$ becoming negative. Since q_i should correspond to experimental data after subtraction of a blank that covers most heats of dilution and other unwanted heat effects, the remaining dilution heat q_{dil} should be very small. However, tests have shown that the precision of the fit parameters is improved by allowing for a small constant q_{dil} to account for imperfections of the blank or of the model (36).

Eq. 13 could be used for fitting data, but we prefer using heats that are normalized with respect to the mole number of injected lipid, Q_i , yielding (V_{cell} cancels out)

$$Q_i = \frac{[C_{\text{cho}}^b]_i^{\text{trans}}}{C_L(i) - C_L(i-1)} \Delta H + Q_{\text{dil}}, \quad (14)$$

where Q_{dil} also becomes a value given per mole of lipid injected. Eq. 14 is used to fit K , ΔH , and Q_{dil} by the Excel solver tool to the experimental data.

RESULTS

Uptake and release experiments at 37°C

Fig. 1 shows part of the raw data (Fig. 1 A) and normalized differential heats (Fig. 1 C) of a release experiment titrating 10 mM POPC including 19 mol % (2.3 mM) cho into the calorimeter cell loaded with 5 mM cyd. After each injection, part of the cho located in the injected vesicles is extracted by cyd, giving rise to an endothermic heat of transfer. The steps in the peak heights (Fig. 1 A) are due to different injection volumes and vanish upon normalization (Fig. 1 B). The values of Q_i (Δ) are obtained after subtraction of those measured in a blank run, injecting cho-free 10 mM POPC into 5 mM cyd. These blank heats presented as the symbol “ \times ” are small and almost constant. Larger, more variable blanks are obtained for experiments utilizing 7.5 mM and in particular 10 mM cyd.

Fig. 1 B shows raw data of an uptake experiment injecting 10 mM POPC vesicles into a mixture of 5 mM cyd and 90 μM cho. The injected lipid vesicles take up part of the cho from cho-cyd_n complexes. As the reverse transfer of the cho release, the accompanying heats must of course be exothermic. The blank is the same as for the release.

The fit curves in Fig. 1 are obtained by a global fit of both uptake and release data using Eq. 14 and correspond to $K_X = (37 \pm 7)$ mM, $n = 2$ (set), $\Delta H = -(16 \pm 2)$ kJ/mol, and small constant heats of dilution $Q_{\text{dil}}(\text{uptake}) = 0.2$ kJ/mol

and $Q_{\text{dil}}(\text{release}) = -0.16$ kJ/mol. The uncertainties are estimated maximum errors. The fit is good, showing that the data are consistent and that the system reaches equilibrium after each injection. Comparing data of many experiments, the data of independent uptake, independent release, and global fits agree often within experimental error. In some cases, there seems to be a trend of independent uptake fits to overestimate K and yield a ΔH that is somewhat less exothermic than obtained by global and release fits. Separate fits of the two curves in Fig. 1 yield, for example, $K_X = 41$ mM (release) and 49 mM (uptake), and $\Delta H = -16$ kJ/mol (release) and -11 kJ/mol (uptake).

A global evaluation of the same data based on Eq. 8 and n set to 1 yields similarly good fit curves with $K_R = 7$, $\Delta H = -17$ kJ/mol, $q_{\text{dil}}(\text{uptake}) = 0.2$ kJ/mol, and $q_{\text{dil}}(\text{release}) = -0.5$ kJ/mol. The value of K_R agrees with the literature (6.7, as published by Niu and Litman (24)) and ΔH is in line with the result of the model described above. The data could also be fitted by the models based on K_X , $n = 1$ and on K_R , $n = 2$ (results not shown). The selection of the best model requires a variety of data sets measured under different conditions (see below).

Using K_X determined by the fit one can calculate the membrane composition in the calorimeter cell during the titration (Fig. 1 D). In the beginning of the release assay, the membrane-bound cho ($X^b = 0.21$ in the syringe) is almost fully extracted, but at the end, the injections cause only a reduction to $X^b \sim 0.15$. Therefore the heat of titration decreases in the course of the titration. In the beginning of the uptake assay, all cho is already in the cell but there is very little POPC yet so that X^b is maximum, ~ 0.2 . In the course of the titration, the membrane-bound cho distributes over more vesicles and X^b decreases.

The effect of the cyclodextrin concentration

Cholesterol uptake experiments injecting POPC vesicles into cyd-cho solutions were performed at varying cyd concentrations. Technical constraints limit the applicable cyd concentration in our assays to the range from 2.5 mM through 10 mM. The lower limit is determined by the sensitivity of the calorimeter, because the cho/cyd ratio was always kept below 1:20 (mol/mol) and at least 30–50 μM cho are required to obtain a sufficient signal/noise ratio.

The maximum applicable cyd concentration of ~ 10 mM is determined by the requirement to keep factors other than cholesterol transfer negligible. Blank experiments titrating POPC into cyd solutions excluding cho showed small, almost constant heats at cyd concentrations of up to 5 mM but increasing, variable signals at higher cyd concentrations. These blank heats were always subtracted from the experimental data of cholesterol uptake and release experiments, but at >10 mM cyd they were no longer small compared to the experimental signal, thus adding substantial experimental error. The origin of these heat effects at $C_{\text{cyd}} > 10$ mM

probably relate to the binding of PC to cyd (24,37), possible minute impurities of the cyd, heats of dilution of the cyd solution by the injection, and others.

The dilution of cyd in the cell by the injection could be avoided (only in the uptake protocol) by including cyd in the syringe. However, a test titrating a POPC dispersion including 7.5 mM cyd into 7.5 mM cyd showed similar heats like the usual blank, injecting cyd-free POPC into 7.5 mM cyd. Test experiments titrating POPC/cyd into cyd/cho yielded consistent but somewhat less reproducible results for K and ΔH , possibly due to vesicle changes caused by long-term incubation with cyd. We therefore decided to use cyd-free titrants.

Apart from these technical limits for the cyd concentration, the interaction parameters determined by the fit procedure should not depend on the experimental cyd concentration if the model is correct. Both panels of Fig. 2 show the same results of release experiments injecting vesicles including 21 mol % of cho into cyd solutions of 2.5, 5, 7.5, and 10 mM at 50°C. The upper panel shows curves of a good global fit of all data sets based on a stoichiometry of $n = 2$, $K_X = 32$ mM, $\Delta H = -5.0$ kJ/mol and individual, small Q_{dil} values ranging from -0.1 to 0.01 kJ/mol. Global fits as shown in Fig. 2 allow also for an additional, free fit of the stoichiometry, yielding values of $n = 2.0 \pm 0.2$ for several data sets. The bottom panel illustrates the best fit that is possible with n

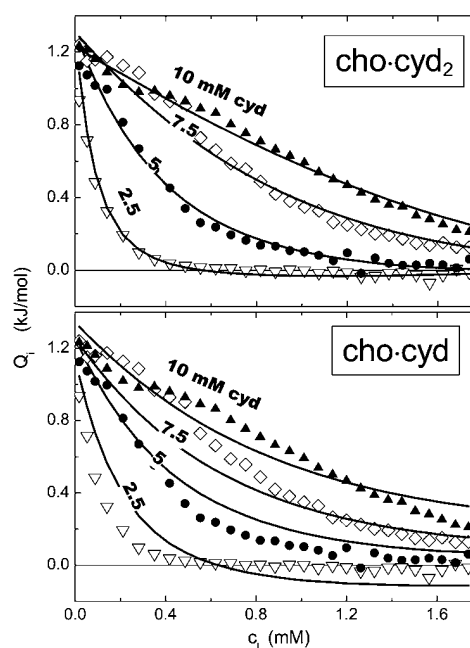


FIGURE 2 A stoichiometry of cho-cyd₂ ($n = 2$) agrees with the data much better than cho-cyd. The data represent release experiments injecting vesicles of 10 mM POPC, 21 mol % cho, into cyd solutions of 2.5 mM (∇), 5 mM (\bullet), 7.5 mM (\diamond), and 10 mM (\blacktriangle) at 50°C (same in both panels). The fit curves in the top panel are obtained by a global fit assuming a stoichiometry of cho-cyd₂ ($n = 2$) (parameters given in text), those in the bottom panel illustrate the best fit possible assuming $n = 1$.

set to 1; there is no doubt that the assumption of exclusive cho-cyd (1:1) complexes is inconsistent with these data. Analogous measurements at $X^b = 0.1$ and 0.3 yield the same result (not shown).

The effect of the cholesterol content in the membrane

The cholesterol content in the membrane specified in terms of the mole fraction, X^b , varies during a titration. If cho mixes nonideally with POPC, K and ΔH are a function of X^b . This appears to be in conflict with our model, which is based on constant values of K and ΔH . However, previous membrane partitioning studies of surfactants and peptides have shown that ITC data are usually not very sensitive to composition-dependent variations of K or ΔH (36). Instead, it was found that the formal application of an ideal model (K and ΔH constant) to a nonideal system yields rather good fits with parameters corresponding to an effective membrane composition, X^b , in the beginning of the titration. For example, the shape of the curves in Fig. 1 *C* is mainly determined by injections inducing changes in X^b from ~ 0.2 to ~ 0 (release) or vice versa (uptake) (Fig. 1 *D*). The results of both experiments correspond, thus, to an effective X^b of ~ 0.2 . It should be noted that a global fit of uptake and release data with substantially different effective X^b would be less consistent.

The fact that X^b changes only moderately during an experiment and the results can be approximately associated with one effective X^b makes the data rather insensitive to composition-dependent phenomena and makes it virtually impossible to derive information regarding nonideal effects from a single run. Imagine, for example, a formation of POPC₂-cho complexes of relatively high affinity. Most cho molecules up to $X^b \sim 0.33$ (and practically all up to $X^b = 0.2$) would form such complexes so that ΔH and K_X in the experiments shown in Fig. 1 would be constant and provide no clue of complex formation.

Instead of refining the model for evaluating single ITC curves, we have to compare the results of different experiments with different effective X^b if we want to shed light on nonideal, composition-dependent phenomena. We have therefore performed series of uptake and release experiments at varying cho concentrations and evaluated the data using the ideal model. For release experiments, it is straightforward to assign the effective X^b to the known cho content in the titrant. For uptake experiments, we calculated X^b ($C_L \rightarrow 0$) as an estimate (upper limit) of the effective X^b using the K_X value obtained by the fit. For global fits of uptake and release data, we chose data sets with a similar effective X^b . A plot of the results as a function of the effective membrane composition is shown in Fig. 3.

For effective $X^b \leq 0.3$, the composition-dependent variation of the data is smaller than the estimated maximum errors of $\pm 20\%$ for K_X and ± 2 kJ/mol for ΔH , indicating that deviations from ideal mixing are relatively small. For

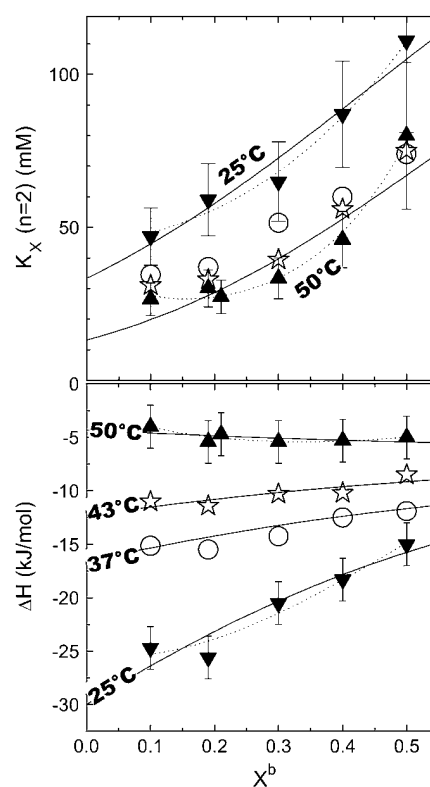


FIGURE 3 The cyclodextrin-membrane partition coefficient, K_X (*top*) and the molar enthalpy change of transfer, ΔH (*bottom*) as a function of the effective cholesterol content in the membrane, X^b (see text for definition). The data correspond to experiments at different temperatures as indicated in the plot. Estimated maximum errors are generally 20% for K_X and ± 2 kJ/mol for ΔH , some error bars are omitted for clarity. The lines correspond to best fits according to Eqs. 19 and 18 considering only pairwise (*solid*) and also multibody (*dotted*) interactions, respectively (see Discussion).

higher cho contents, nonideal mixing effects become significant at least for K_X (increasing with X^b) and ΔH (25°C) (becoming less exothermic with increasing X^b).

Temperature dependency

Results obtained at different temperatures are included in Fig. 3.

Fig. 4 shows the corresponding thermodynamic potentials of transfer of cho from cho-cyd₂ complexes into POPC-cho vesicles as a function of temperature. The enthalpy changes, ΔH , were measured directly in the calorimeter; the points displayed in Fig. 4 refer to small cho contents in the membrane ($X^b = 0.1$ –0.2). The changes in the standard Gibbs free energy, ΔG^0 , were calculated from K_X according to

$$\Delta G^0 = -RT \ln \frac{K_X}{1 \text{ mM}}, \quad (15)$$

where R is the ideal gas constant and T the absolute temperature. The standard state of all compounds used to derive an activity-based, dimensionless value of K was chosen a

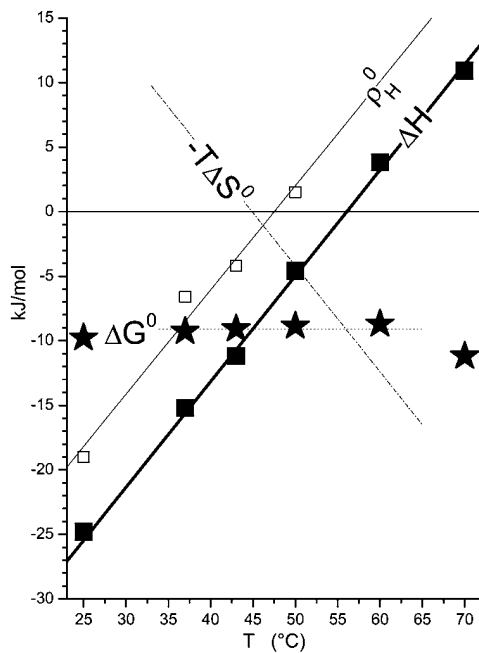


FIGURE 4 The standard Gibbs free energy, ΔG^0 (★), and enthalpy, ΔH (■), of transfer of cho from cho-cyd₂ complexes into POPC membranes as a function of temperature. The average ΔG^0 (dotted line) and linear fit of ΔH (thick solid line, slope $\Delta C_p = 0.8$ kJ/(mol K)) correspond to an entropic contribution of $-T\Delta S^0$ illustrated by the dash-dotted line. The enthalpic nonideality parameter, ρ_H^0 (□), exhibits the same slope as a function of T as ΔH (see Nonideal Mixing of POPC and Cho, in text).

1-mM solution at the given temperature. Referring all activities to 1 M, all values of ΔG^0 would be larger by ~ 7 RT. A linear regression of $\Delta H(T)$ yields a positive heat capacity change of $\Delta C_p = (0.8 \pm 0.1)$ kJ/(mol K) and a temperature of vanishing ΔH of 56°C. Above 56°C, the transfer of cho into the membrane becomes endothermic. The ΔG^0 data could, in the frame of the experimental uncertainty, be well described by a temperature-independent value of $\Delta G^0 = (-9.1 \pm 0.2)$ kJ/mol (at least, within 37–50°C). From these fit lines, the entropic contribution to ΔG^0 , $-T\Delta S^0$, was calculated according to

$$-T\Delta S^0 = \Delta G^0 - \Delta H, \quad (16)$$

assuming the enthalpy of transfer to be virtually independent of concentrations so that $\Delta H = \Delta H^0$. Fig. 4 also includes enthalpic nonideality parameters which are discussed in Nonideal Mixing of POPC and Cho, in the next section.

DISCUSSION

Distinguishing between effects of cyd-to-membrane transfer and nonideal mixing in the membrane

One of our goals is to discuss the thermodynamic phenomena that govern the mixing or demixing behavior in lipid-cho

membranes. To this end, we have to distinguish two contributions to, e.g., ΔH :

$$\Delta H(X^b) = \Delta H^{\text{cyd} \rightarrow \text{b, id}} + \Delta H^{\text{nonid}}(X^b). \quad (17)$$

The first, $\Delta H^{\text{cyd} \rightarrow \text{b, id}}$, corresponds to the transfer of cho from cyd complexes into a hypothetical ideally mixed membrane; it is by definition independent of the membrane composition X^b . The second, $\Delta H^{\text{nonid}}(X^b)$ arises from specific, nonideal interactions between cho and POPC within the bilayer. Generally, $\Delta H^{\text{nonid}} = 0$ for pure phases which would allow for a direct measurement of $\Delta H^{\text{cyd} \rightarrow \text{b, id}} = \Delta H(X^b \rightarrow 1)$. However, since pure cho forms no fluid bilayers, we have to compute ΔH^{nonid} using a model describing the composition-dependence of ΔH at lower X^b . The limited X^b -range and precision of the data do, unfortunately, not warrant a complex model. We have chosen a statistical model (see next section for a discussion of other possible concepts) with one or two nonideality parameters, yielding for the enthalpy (38,39),

$$\Delta H^{\text{nonid}}(X^b) = (1 - X^b)^2 \times (\rho_H^0 + 2\rho_H^1 X^b \dots), \quad (18)$$

and, taking into account Eq. 15, for K_x ,

$$K_x(X^b) = K_x^{\text{id}} \times \exp \left\{ -\frac{(1 - X^b)^2}{RT} (\rho_G^0 + 2\rho_G^1 X^b + \dots) \right\}, \quad (19)$$

where ρ_H^i and ρ_G^i ($i = 0, 1, \dots$) denote nonideality parameters of the enthalpy and of the free energy of mixing, respectively. For $\rho_H^0 = \rho_G^0$ and vanishing higher order terms, ρ^i ($i > 0$) = 0, these equations correspond to the model of regular solutions, describing nonideality in terms of pairwise interactions. For lipid bilayers, we have to consider $\rho_H^0 \neq \rho_G^0$ since the entropy is not governed by the arrangement of the molecules alone (which is assumed to be random), but includes major contributions from intramolecular degrees of freedom. Higher order terms in ρ_H^i, ρ_G^i ($i = 1, 2, \dots$) account for nonpairwise, multibody interactions of cooperative units of $i + 2$ molecules. It should be noted that such multibody interactions are equivalent to stoichiometric complexes of $i + 2$ molecules (i.e., lipid-cho₂, and lipid₂-cho in our case) provided the association constant of the complex is weak.

Fitting Eqs. 18 and 19 to the data (curves in Fig. 3) allows us to approximately split the enthalpy and K_x value of transfer to nonideal membranes into contributions from transfer into hypothetical, ideally mixed membranes (see The effect of acyl chain order on heat capacity, below) and from nonideal mixing of POPC and cho (see below).

Nonideal mixing of POPC and cho

The hypothesis that biological membranes contain lipid rafts, functional domains that are formed by a spontaneous demixing of different lipids in the presence of cholesterol, has led to an enormous interest in the nonideal mixing

behavior of cho with phospholipids. In the case of ideal mixing of cho and POPC, the partition coefficients K_X and enthalpies of uptake, ΔH , should be independent of the membrane composition, X^b . Nonideal systems may either show a tendency 1), to demix into different domains if cho-rich environments are favorable; 2), to arrange into superlattices if cho-rich environments are unfavorable; or 3), to form stoichiometric complexes.

Radhakrishnan and McConnell (40) have found that saturated lipids can form stoichiometric complexes with cho, whereas unsaturated lipids do not. Indeed, our data show no evidence for the formation of high-affinity, cholesterol-rich complexes which should give rise to a drop in K_X at a stoichiometric composition $X^b \leq 0.5$ (41,42). Superlattice formation should also give rise to rather sudden drops of K_X at specific X^b (43,44), which are not observed here. A real phase separation into coexisting liquid-ordered and liquid-disordered phases as reported by de Almeida et al. (45) should be represented by jumps of ΔH at the boundaries but constant ΔH in between. This general behavior was explained in detail for the example of membrane-micelle coexistence (39,46) and would apply (qualitatively) analogously to an liquid-ordered/liquid-disordered coexistence. The value $K_X(X^b)$ should increase within the coexistence range, since cho affinity would be higher in the liquid-ordered, than in the liquid-disordered, phase. Again, we do not find evidence for such behavior.

Our data show the thermodynamic behavior as discussed for cho-induced chain ordering in a largely randomly mixed membrane. Fitting $K_X(X^b)$ excluding higher order terms (all $\rho^i = 0$ for $i > 0$) is, within experimental error, compatible with the data but systematic deviations remain (*solid lines* in Fig. 3). These fits suggest pairwise interactions that are somewhat unfavorable by $\rho_G^0 \sim (5 \pm 1)$ kJ/mol at all temperatures investigated. This means that each molecule in a mixture containing 30% cho has, on average, an increased free energy of ~ 1 kJ/mol as a result of unfavorable POPC-cho interactions (excess free energy; see Heerklotz et al. (39)). Hence, the cost of nonideal mixing is less than, but on the same order of magnitude as, the gain due to the entropy of ideal mixing, $-T\Delta S_{\text{mix}}^{\text{id}} \sim -1.6$ kJ/mol for $X^b = 0.3$. At room temperature, the nonideal interaction is highly exothermic ($\rho_H^0 = -19$ kJ/mol), suggesting that the unfavorable Gibbs free energy is dominated by a large loss in intramolecular entropy. The nonideal interaction causes a strong increase in heat capacity by $d\rho_H^0/dT = +(0.8 \pm 0.1)$ kJ/(mol K) (see *open square* in Fig. 4). The precision and particularly the limited composition range of the data in Fig. 3 do not strictly justify a fit with more adjustable parameters but we have, nevertheless, repeated the fits allowing also for ρ_H^1 and ρ_G^1 , respectively (*dotted lines* in Fig. 3). These fits yield substantial values for ρ_G^1 (4 and 13 kJ/mol at 25 and 50°C, respectively), suggesting slightly unfavorable POPC₂-cho units but two- to threefold more unfavorable POPC-cho₂ units.

The nonideal behavior observed here (unfavorable but exothermic) has been described to accompany the chain-ordering, membrane condensing effect of cho, since tighter packing and increased order cost entropy but improve enthalpically favorable interactions and conformations. The cooperative, multibody character of this interaction is also illustrated by the umbrella model (31). This suggests that cholesterol intercalates between lipids without occupying much space in the headgroup region, so that it is screened from water by the headgroups like under an umbrella. The thermodynamic pattern (unfavorable but exothermic) has also been described for the transfer of cho from gel to fluid bilayers, which is also accompanied by chain ordering (47).

The effect of acyl chain order on heat capacity

A surprising result is the positive heat capacity change. A generally accepted rule relates a positive ΔC_P to either an increase in water-exposed hydrophobic surface area or to a dehydration of polar groups (48). The intercalation of cho between lipids should, however, reduce the exposure of hydrophobic groups to water (umbrella) and allow for a better hydration of the surrounding lipid headgroups (since the polar group of cho needs very little space). This paradox suggests the hypothesis that the ordering of the lipid chains itself causes a strong increase in heat capacity. This is surprising, taking into account that lipid melting, which is accompanied by a dramatic change in chain order, has virtually no ΔC_P (15,49). However, melting is a complex process including many phenomena which are different from gradual changes in order in a fluid membrane. This hypothesis also provides an explanation for the negative $d\rho_H^0/dT$ (50) and anomalously negative values of ΔC_P observed for the membrane uptake of membrane-disordering compounds such as detergents (50,51) and alcohols (52), which could not be explained in terms of the hydrophobic effect alone.

The transfer of cho from cyd into hypothetical, ideally mixed membranes

The fit parameter $\Delta H^{\text{cyd} \rightarrow \text{b,id}}$ excludes specific cho-POPC interactions and allows us to interpret the dissociation of the cho-cyd₂ complex and the transfer of cho to a state corresponding to a hypothetical ideally mixed membrane. The standard free energy gain of $\sim -(12 \pm 1)$ kJ/mol is essentially of enthalpic nature ($\Delta H^{\text{cyd} \rightarrow \text{b,id}} \sim -(11 \pm 2)$ kJ/mol) at 25°C. The entropy change ($-T\Delta S^0 = -(1 \pm 3)$ kJ/mol) and the heat capacity change $d[\Delta H^{\text{cyd} \rightarrow \text{b,id}}]/dT = -(0.1 \pm 0.1)$ kJ/(mol K) are negligible. This means that the transfer of cho between cyd and the membrane is neither promoted nor opposed by the hydrophobic effect. One has, however, to keep in mind that the hydrophobic surface of cyd is fully exposed to water in the absence of cho whereas the membrane anneals after removal of cho and does not expose a free hydrophobic binding site to water. Hence, the screening

of cho from water must be better in the membrane to compensate for the accessible hydrophobic surface of free cyd.

The cho-cyd₂ complex

The binding of cho to cyd is governed by the hydrophobic effect as discussed in the previous section. That means that cho covers most of the hydrophobic surface area of cyd and vice versa, thus avoiding its exposure to water. Given the molecular dimensions, two stacked cyd molecules seem to be required to largely screen a cho molecule from water, taking into account that a cho molecule is ~ 18 Å long, whereas the cavity of cyd is only ~ 8 Å long.

The section on the effect of the cyclodextrin concentration has indeed provided strong evidence that the cho-cyd interaction can be described much better in terms of the formation of a cho-cyd₂ than cho·cyd complex. The comparison of these two most simple cases does, of course, not exclude more complex behavior such as sequential binding leading to a coexistence of cho·cyd, cho·cyd₂, and maybe even cho·cyd₃ complexes, but cho-cyd₂ seems at least to be the dominating species.

The idea that more than one cyd molecule binds one cho is further supported by our observation that a stock solution of 100 mM cyd, 10 mM cho is stable, but dilution to 10 mM cyd, 1 mM cho leads to precipitation. This is very likely due to the formation of aggregates of free cho which are formed when the free cho concentration, C_{cho}^w , supersedes the solubility limit. The mass action law (Eq. 5) yields (replacing $C_{\text{cho}}^{\text{cyd}} = C_{\text{cho}} - C_{\text{cho}}^w$):

$$C_{\text{cho}}^w = \frac{C_{\text{cho}}}{K^{\text{cyd/w}} \times (C_{\text{cyd}})^n + 1}. \quad (20)$$

Let us consider Eq. 20 for the case that both C_{cho} and C_{cyd} are reduced by the same factor upon dilution. If $n = 1$, dilution decreases C_{cho}^w or leaves it unchanged (if $K^{\text{cyd/w}} \cdot C_{\text{cyd}} \gg 1$). An increase in C_{cho}^w upon dilution, as suggested by the precipitation, implies a higher stoichiometry, $n > 1$.

Pointing out that a model based on K_X and $n = 2$ is clearly superior, we note that the conclusions drawn by Niu and Litman (24) working with K_R and $n = 1$ are not questioned. They have related cho affinities for different lipids to each other that were measured at identical cyd and cho concentrations. Errors appear only if one used their K -values for calculating the cyd-membrane distribution at a different cyd concentration.

The application of cyd to the selective extraction of cho from membranes

Extraction of cho from cell and model membranes by cyd has become a widely used approach to study the function of cho. Our results imply that the cyd concentration used for this purpose must be carefully chosen. Our model parameters

(K , n) allow calculating the fraction of cho that remains membrane-bound, $C_{\text{cho}}^b/C_{\text{cho}}$, at a given cyd concentration. We calculated curves showing this fraction assuming membranes of 1 and 0.1 mM POPC + cho (30 mol % cho) as shown in Fig. 5.

For comparison, we simulated the retention of POPC in these membranes, C_L^b/C_L , in the same range of cyd concentrations on the basis of the results of Anderson et al. (37). These authors established a model for PC binding to cyd, which implies a membrane-retained fraction of lipid as

$$\frac{C_L^b}{C_L} = 1 - \frac{K(C_{\text{cyd}})^4}{C_L}, \quad (21)$$

with a temperature-dependent K yielding, by interpolation, a value of 192 M^{-3} at 37°C .

Let us, at first, consider a sample of 0.3 mM cho, 0.7 mM POPC (*top panel* of Fig. 5). At a cyd concentration of 1 mM, the removal of molecules from the membrane is negligible as discussed already by Leventis and Silvius (22). A cyd concentration of 5 mM extracts 40%, and one of 10 mM removes $\sim 75\%$ of the cho from the membrane, without binding significant amounts of phospholipid. The range

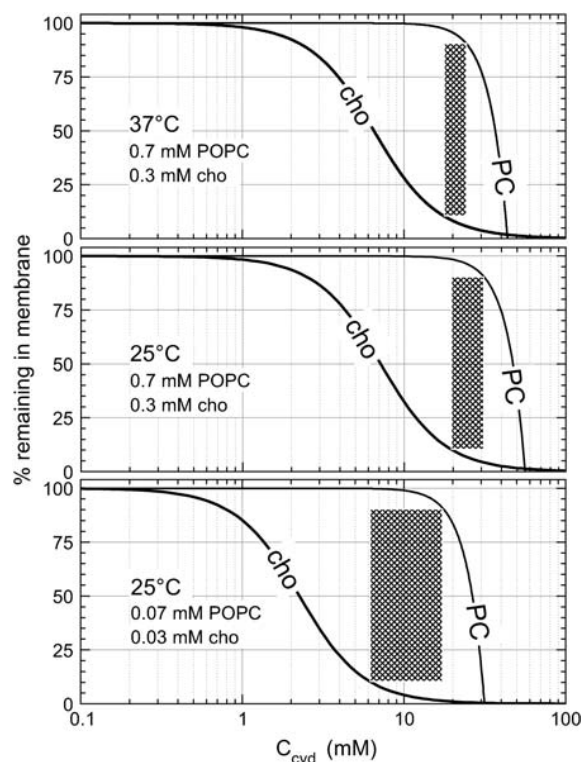


FIGURE 5 Retention of cho and POPC in membranes as a function of the cyd concentration at different cho and POPC concentrations and temperatures as indicated in the plot. The curves for cho are calculated on the basis of $n = 2$, $K_X \sim 60 \text{ mM}$ (25°C) and 50 mM (37°C), and those for PC are based on Eq. 21 with $K = 192 \text{ M}^{-3}$ (37°C) and 71 M^{-3} (25°C) derived from Anderson et al. (37). The cross-hatched areas indicate the range where $>90\%$ of the cho, but $<10\%$ of the POPC, are extracted.

where $\geq 90\%$ of cho but $\leq 10\%$ of POPC are extracted (*cross-hatched* in Fig. 5, *top*) is quite narrow, $\sim 18\text{--}24$ mM cyd. At 40 mM cyd, most of the membrane is destroyed by cyd.

Our calculations suggest two strategies for broadening the applicable range in cyd concentrations in which a substantial extraction of cho is reached without removal of lipid. These are dilution of the membrane system and lower extraction temperature. For example, a 10-fold dilution and extraction at 25°C increases the cross-hatched range to $6\text{--}18$ mM cyd (Fig. 5, *bottom*).

Fig. 5 cannot, of course, specify an optimum cyd concentration window that would be applicable to all membrane systems. For example, preliminary data suggest that sphingomyelin seems to be more susceptible to extraction by cyd but to attenuate the extraction of cho. Hence, the available window of cyd concentrations for selective removal of cho would become even narrower. The discussion of Fig. 5 illustrates, at least, the problem of optimizing the cyd concentration, and provides typical concentrations and optimization strategies that may also be worth trying when biological membranes are concerned.

Another technically important problem is how much time is needed for cho extraction from or cho loading into membranes. We could show that both cho extraction from membranes and cho loading into membranes (of POPC) equilibrate largely within <1 h at 25°C and within a few minutes at 50°C . The observation that the same state is reached by both uptake and release is a strict criterion for equilibration, confirming the suggestion from Niu and Litman (24), who found that no further uptake is detectable after ~ 1 h.

CONCLUSIONS

1. Isothermal titration calorimetry is an excellent new technique to study the interaction of cho with lipid membranes in detail.
2. Cho exhibits a nonideal interaction with POPC which is exothermic but entropically unfavorable and accompanied by a positive heat capacity change. This nonideal behavior corresponds to the well-known membrane-ordering effect of cho.
3. An anomalous increase in heat capacity accompanying the nonideal interaction gives rise to the hypothesis that additive-induced membrane ordering yields a positive, and disordering a negative, contribution to ΔC_p . Hence, heat capacities of additive partitioning into membranes may deviate markedly from the otherwise well-established rule relating ΔC_p to changes in water-exposed surface area.
4. Complexes of cho with cyd have a dominant stoichiometry of cho-cyd₂.
5. There is only a very narrow window of cyd concentrations that allow for a substantial extraction of cho from membranes without destroying the membrane. At least

for POPC, this window becomes broader upon dilution of the membrane dispersion and at lower temperature.

We are indebted to Dr. Fredrik Ollila (now at Novartis AG, Basel, Switzerland) for his help at the beginning of the project. We thank Dr. Thomas Anderson (Biozentrum Basel) and Sandro Keller (Forschungsinstitut für Molekulare Pharmakologie, Berlin) for their important comments on the manuscript.

Financial support from the Swiss National Science Foundation (grant No. 31-67216.01) and from Prof. Joachim Seelig (Biozentrum Basel) is gratefully acknowledged.

REFERENCES

1. Simons, K., and E. Ikonen. 1997. Functional rafts in cell membranes. *Nature*. 387:569–572.
2. Edidin, M. 2003. The State of lipid rafts: from model membranes to cells. *Annu. Rev. Biophys. Biomol. Struct.* 16:257–283.
3. Munro, S. 2003. Lipid rafts: elusive or illusive? *Cell*. 115:377–388.
4. Simons, K., and W. L. Vaz. 2004. Model systems, lipid rafts, and cell membranes. *Annu. Rev. Biophys. Biomol. Struct.* 33:269–295.
5. Brown, D. A., and J. K. Rose. 1992. Sorting of GPI-anchored proteins to glycolipid-enriched membrane subdomains during transport to the apical cell surface. *Cell*. 68:533–544.
6. London, E., and D. A. Brown. 2000. Insolubility of lipids in Triton X-100: physical origin and relationship to sphingolipid/cholesterol membrane domains (rafts). *Biochim. Biophys. Acta*. 1508:182–195.
7. Vist, M. R., and J. H. Davis. 1990. Phase equilibria of cholesterol/dipalmitoylphosphatidylcholine mixtures: ^2H nuclear magnetic resonance and differential scanning calorimetry. *Biochemistry*. 29:451–464.
8. Ipsen, J. H., O. G. Mouritsen, and M. J. Zuckermann. 1989. Theory of thermal anomalies in the specific-heat of lipid bilayers containing cholesterol. *Biophys. J.* 56:661–667.
9. Ohvo-Rekila, H., B. Ramstedt, P. Leppimäki, and J. P. Slotte. 2002. Cholesterol interactions with phospholipids in membranes. *Prog. Lipid Res.* 41:66–97.
10. McMullen, T. P. W., R. N. A. H. Lewis, and R. N. McElhaney. 2004. Cholesterol-phospholipid interactions, the liquid-ordered phase and lipid rafts in model and biological membranes. *Current Opinion Colloid Interface Sci.* 8:459–468.
11. Heerklotz, H. 2002. Triton promotes domain formation in lipid raft mixtures. *Biophys. J.* 83:2693–2701.
12. van Rheenen, J., E. Mulugeta Achame, H. Janssen, J. Calafat, and K. Jalink. 2005. PIP₂ signaling in lipid domains: a critical re-evaluation. *EMBO J.* 24:1664–1673.
13. Kilsdonk, E. P., P. G. Yancey, G. W. Stoudt, F. W. Bangerter, W. J. Johnson, M. C. Phillips, and G. H. Rothblat. 1995. Cellular cholesterol efflux mediated by cyclodextrins. *J. Biol. Chem.* 270:17250–17256.
14. Ohvo, H., and J. P. Slotte. 1996. Cyclodextrin-mediated removal of sterols from monolayers: effects of sterol structure and phospholipids on desorption rate. *Biochemistry*. 35:8018–8024.
15. Blume, A. 1980. Thermotropic behavior of phosphatidylethanolamine-cholesterol and phosphatidylethanolamine-phosphatidylcholine-cholesterol mixtures. *Biochemistry*. 19:4908–4913.
16. McMullen, T. P. W., R. Lewis, and R. N. McElhaney. 1999. Calorimetric and spectroscopic studies of the effects of cholesterol on the thermotropic phase behavior and organization of a homologous series of linear saturated phosphatidylethanolamine bilayers. *Biochim. Biophys. Acta Biomembr.* 1416:119–134.
17. Nyholm, T. K., M. Nylund, and J. P. Slotte. 2003. A calorimetric study of binary mixtures of dihydrosphingomyelin and sterols, sphingomyelin, or phosphatidylcholine. *Biophys. J.* 84:3138–3146.

18. Yeagle, P. L., and J. E. Young. 1986. Factors contributing to the distribution of cholesterol among phospholipid vesicles. *J. Biol. Chem.* 261:8175–8181.
19. Huster, D., K. Arnold, and K. Gawrisch. 1998. Influence of docosahexaenoic acid and cholesterol on lateral lipid organization in phospholipid mixtures. *Biochemistry.* 37:17299–17308.
20. Veatch, S. L., I. V. Polozov, K. Gawrisch, and S. L. Keller. 2004. Liquid domains in vesicles investigated by NMR and fluorescence microscopy. *Biophys. J.* 86:2910–2922.
21. Steck, T. L., J. Ye, and Y. Lange. 2002. Probing red cell membrane cholesterol movement with cyclodextrin. *Biophys. J.* 83:2118–2125.
22. Leventis, R., and J. R. Silvius. 2001. Use of cyclodextrins to monitor transbilayer movement and differential lipid affinities of cholesterol. *Biophys. J.* 81:2257–2267.
23. Silvius, J. R. 2003. Role of cholesterol in lipid raft formation: lessons from lipid model systems. *Biochim. Biophys. Acta Biomembr.* 1610: 174–183.
24. Niu, S. L., and B. J. Litman. 2002. Determination of membrane cholesterol partition coefficient using a lipid vesicle-cyclodextrin binary system: effect of phospholipid acyl chain unsaturation and headgroup composition. *Biophys. J.* 83:3408–3415.
25. Heerklotz, H. 2004. Microcalorimetry of lipid membranes. *J. Phys. Cond. Matter.* 16:R441–R467.
26. Nernst, W. 1891. Distribution of a material between two solvents and between solvent and vapor. *Ztschr. Phys. Chem.* 8:110.
27. Tanford, C. 1980. The hydrophobic effect: formation of micelles and biological membranes. Wiley, New York.
28. Seelig, J., and P. Ganz. 1991. Nonclassical hydrophobic effect in membrane binding equilibria. *Biochemistry.* 30:9354–9359.
29. Schurtenberger, P., N. Mazer, and W. Känzig. 1985. Micelle to vesicle transition in aqueous solutions of bile salt and lecithin. *J. Phys. Chem.* 89:1042–1049.
30. Heerklotz, H., and J. Seelig. 2000. Titration calorimetry of surfactant-membrane partitioning and membrane solubilization. *Biochim. Biophys. Acta.* 1508:69–85.
31. Huang, J., and G. W. Feigenson. 1999. A microscopic interaction model of maximum solubility of cholesterol in lipid bilayers. *Biophys. J.* 76:2142–2157.
32. Lange, Y., J. Dolde, and T. L. Steck. 1981. The rate of transmembrane movement of cholesterol in the human erythrocyte. *J. Biol. Chem.* 256:5321–5323.
33. Huang, J., J. T. Buboltz, and G. W. Feigenson. 1999. Maximum solubility of cholesterol in phosphatidylcholine and phosphatidylethanolamine bilayers. *Biochim. Biophys. Acta.* 1417:89–100.
34. Chellani, M. 1999. Isothermal titration calorimetry: biological applications. *Am. Biotechnol. Lab.* 17:14–18.
35. Wiseman, T., S. Williston, J. F. Brandts, and L.-N. Lin. 1989. Rapid measurement of binding constants and heats of binding using a new titration calorimeter. *Anal. Biochem.* 179:131–137.
36. Heerklotz, H. 1998. Thermodynamics of hydrophobic and steric lipid/additive interactions. In *Bio-calorimetry*. J. Ladbury and B. Chowdhry, editors. Wiley, Chichester, UK. 89–100.
37. Anderson, T. G., A. Tan, P. Ganz, and J. Seelig. 2004. Calorimetric measurement of phospholipid interaction with methyl- β -cyclodextrin. *Biochemistry.* 43:2251–2261.
38. Cevc, G., and D. Marsh. 1985. Phospholipid Bilayers. E. Bittar, editor. John Wiley and Sons, New York.
39. Heerklotz, H. H., H. Binder, and H. Schmiedel. 1998. Excess enthalpies of mixing in phospholipid-additive membranes. *J. Phys. Chem. B.* 102:5363–5368.
40. Radhakrishnan, A., T. G. Anderson, and H. M. McConnell. 2000. Condensed complexes, rafts, and the chemical activity of cholesterol in membranes. *Proc. Natl. Acad. Sci. USA.* 97:12422–12427.
41. Radhakrishnan, A., and H. M. McConnell. 2000. Chemical activity of cholesterol in membranes. *Biochemistry.* 39:8119–8124.
42. Radhakrishnan, A., and H. M. McConnell. 1999. Condensed complexes of cholesterol and phospholipids. *Biophys. J.* 77:1507–1517.
43. Huang, J. 2002. Exploration of molecular interactions in cholesterol superlattices: effect of multibody interactions. *Biophys. J.* 83:1014–1025.
44. Cannon, B., G. Heath, J. Huang, P. Somerharju, J. A. Virtanen, and K. H. Cheng. 2003. Time-resolved fluorescence and Fourier transform infrared spectroscopic investigations of lateral packing defects and superlattice domains in compositionally uniform cholesterol/phosphatidylcholine bilayers. *Biophys. J.* 84:3777–3791.
45. de Almeida, R. F., A. Fedorov, and M. Prieto. 2003. Sphingomyelin/phosphatidylcholine/cholesterol phase diagram: boundaries and composition of lipid rafts. *Biophys. J.* 85:2406–2416.
46. Heerklotz, H., G. Lantzsch, H. Binder, G. Klose, and A. Blume. 1996. Thermodynamic characterization of dilute aqueous lipid/detergent mixtures of POPC and C12EO8 by means of isothermal titration calorimetry. *J. Phys. Chem.* 100:6764–6774.
47. Spink, C. H., S. Manley, and M. Breed. 1996. Thermodynamics of transfer of cholesterol from gel to fluid phases of phospholipid bilayers. *Biochim. Biophys. Acta.* 1279:190–196.
48. Murphy, K. P. 1999. Predicting binding energetics from structure: looking beyond δG degrees. *Med. Res. Rev.* 19:333–339.
49. Chapman, D., and J. Urbina. 1974. Biomembrane phase transitions. Studies of lipid-water systems using differential scanning calorimetry. *J. Biol. Chem.* 249:2512–2521.
50. Heerklotz, H., H. Binder, G. Lantzsch, G. Klose, and A. Blume. 1997. Lipid/detergent interaction thermodynamics as a function of molecular shape. *J. Phys. Chem. B.* 101:639–645.
51. Keller, M., A. Kerth, and A. Blume. 1997. Thermodynamics of interaction of octyl glucoside with phosphatidylcholine vesicles: partitioning and solubilization as studied by high sensitivity titration calorimetry. *Biochim. Biophys. Acta.* 1326:178–192.
52. Rowe, E. S., F. Zhang, T. W. Leung, J. S. Parr, and P. T. Guy. 1998. Thermodynamics of membrane partitioning for a series of *n*-alcohols determined by titration calorimetry: role of hydrophobic effects. *Biochemistry.* 37:2430–2440.

A Quantitative Model Describing the Selective Solubilization of Membrane Domains

Sandro Keller,[†] Alekos Tsamaloukas,[‡] and Heiko Heerklotz^{*,‡}

Contribution from the Research Institute of Molecular Pharmacology FMP, Robert-Rössle-Strasse 10, 13125 Berlin, Germany, and the Biozentrum der Universität Basel, Klingelbergstrasse 50/70, 4056 Basel, Switzerland

Received April 28, 2005; E-mail: heiko.heerklotz@unibas.ch

Abstract: The classical three-stage model of membrane solubilization, including mixed membranes, membrane–micelle coexistence, and mixed micelles, is not applicable to demixed, domain-forming membranes and must, therefore, fail to describe the phenomenon of detergent-resistant membranes (DRMs). In lack of a quantitative model, it has often been assumed that ordered, detergent-depleted domains are inert, whereas fluid domains are solubilized. We establish a quantitative model based on equilibrium thermodynamics that is analogous to the three-stage model but comprises three components (two lipids and one detergent) in four phases (liquid-ordered and liquid-disordered membranes, micelles, and detergent in aqueous solution). For a given set of total concentrations and input parameters (initial abundance of ordered domains, solubilization boundaries of the pure lipids, etc.), it serves to calculate the phase boundaries and partial concentrations of all components in all phases. The results imply that the abundance and composition of ordered domains may vary substantially upon addition of detergent, both before and during solubilization of the fluid phase. It seems that gel-phase or order-preferring lipids are thermodynamically “resistant” regardless of the presence of a second, fluid phase. However, thermodynamic or kinetic resistance is not sufficient for obtaining DRMs because the resistant particles may be too small to be isolated. Cholesterol may be crucial for rendering the fragments large enough and, furthermore, enhance the formation of ordered domains by nonideal interactions with the detergent.

Introduction

The solubilization of biological membranes by detergents has long been used as the main method for the isolation and purification of membrane proteins and other constituents. Recently, considerable interest has been attracted by the finding that biological membranes can be solubilized selectively. Certain membrane constituents are incorporated into small micelles, whereas others remain in so-called detergent-resistant membrane fragments that are large enough to be separated by centrifugation.¹ This provides a unique tool to preselect classes of proteins to be isolated and to study the preferences of proteins for certain membrane environments, and it will undoubtedly be of great value also for future large-scale studies of membrane proteins. Apart from that, it has stimulated the hypothesis that the resistant fragments resemble functional domains, so-called “lipid rafts”, existing already in the original, detergent-free membrane. Thousands of studies addressing this issue have been published.^{2–5}

The solubilization of homogeneous fluid membranes is described by what is often referred to as the three-stage

model.^{6–8} In the first stage, detergent micelles added to a lipid membrane dispersion dissolve into monomers, and the latter partition between membrane and aqueous solution. When a critical detergent mole fraction, X_e^{sat} , is reached in the membrane, mixed micelles appear in coexistence with these saturated membranes during the second stage. The mole fraction of detergent in the micelles is X_e^{sol} . Addition of more detergent increases the number of micelles at the expense of membranes but leaves their internal compositions, X_e^{sol} and X_e^{sat} , unchanged. When the average detergent mole fraction in micelles and membranes, X_e , approaches X_e^{sol} , the last membranes disappear, and at $X_e > X_e^{\text{sol}}$, only mixed micelles are left in the third stage. This behavior can be well explained in terms of a simple thermodynamic model if mixed micelles, membranes, and the aqueous solution of detergent are considered thermodynamic pseudophases. This is a good approximation in most cases, although phases in the strict sense are homogeneous and separated macroscopically. Major deviations have been found for charged detergents forming very small micelles, such as bile salts,⁹ where long-range micelle–micelle interactions and the entropy of mixing of micelles in the dispersion give rise to

[†] Research Institute of Molecular Pharmacology FMP.

[‡] Biozentrum der Universität Basel.

(1) Brown, D. A.; Rose, J. K. *Cell* **1992**, *68*, 533–544.
(2) Simons, K.; Ikonen, E. *Nature* **1997**, *387*, 569–572.
(3) Edidin, M. *Annu. Rev. Biophys. Biomol. Struct.* **2003**, *16*, 257–283.
(4) Munro, S. *Cell* **2003**, *115*, 377–388.
(5) Simons, K.; Vaz, W. L. *Annu. Rev. Biophys. Biomol. Struct.* **2004**, *33*, 269–295.

(6) Helenius, A.; Simons, K. *Biochim. Biophys. Acta* **1975**, *415*, 29–79.
(7) Lichtenberg, D.; Opatowski, E.; Kozlov, M. M. *Biochim. Biophys. Acta* **2000**, *1508*, 1–19.
(8) Lichtenberg, D. *Biochim. Biophys. Acta* **1985**, *821*, 470–478.
(9) Hildebrand, A.; Neubert, R.; Garidel, P.; Blume, A. *Langmuir* **2002**, *18*, 2836–2847.

significant contributions to the free energy of the system. A refined model has been established to account for such effects.¹⁰

Selective solubilization and detergent resistance cannot be treated in terms of the three-stage model. Rafts^{2,5} are often assumed to be basically equivalent to liquid-ordered domains forming in certain lipid mixtures.^{11–13} The equivalence of detergent-resistant membranes (DRMs) with rafts has been claimed on the basis that the detergent virtually does not insert into ordered membrane domains. Thus, one is tempted to conclude that the ordered domains are inert against the detergent and the fluid domains behave as predicted by the three-stage model. However, this reasoning neglects that changing one phase in an equilibrium affects the other phases, as well. For example, if a fluid-phase-preferring molecule (the detergent) is added, it should tend to shift the equilibrium in favor of the fluid phase (regardless of where it is localized). In a sophisticated qualitative consideration, London and Brown¹⁴ mentioned other critical issues. For example, DRMs might overestimate the amount of ordered phase because they are usually isolated at low temperature or form by selective solubilization of certain lipids from a homogeneous intermediate state. Experimental data imply that the detergent may promote the formation of ordered domains already before solubilization and suggest nonideal interactions between detergents and order-preferring lipids as a possible driving force for such an effect.^{15,16} Using neutron scattering, Nicolini et al.¹⁷ have detected changes in domain size induced by detergents. Van Rheeën et al.¹⁸ have provided evidence that detergent-induced domain formation as suggested by model studies occurs also in vivo, and that minute amounts of Triton lead to phosphatidylinositol 4,5-bisphosphate (PIP₂) clusters that do not exist in detergent-free cell membranes. On the basis of such findings, a more critical view of the “DRM = raft” hypothesis has been acquired recently,^{3–5} but the problem still suffers from a lack of quantitative understanding.

Our aim is to make a first step toward such a quantitative understanding. We present a model describing the effects of a detergent on membrane domains before and during selective solubilization by extending the classical three-stage model, taking into account a third component and a fourth phase. On this level of complexity, a systematic approach requires starting with the simplest case, which is ideal mixing of the components in all phases. We will show that this basic case provides important insight and yields useful rules for such systems. However, we will also have to accept that this model is not sophisticated enough to account for all key properties of real multicomponent membranes. To illustrate the substantial influence of nonideal mixing, we introduce a single nonideality parameter into our model at the end of the study.

- (10) Roth, Y.; Opatowski, E.; Lichtenberg, D.; Kozlov, M. M. *Langmuir* **2000**, *16*, 2052–2061.
 (11) McMullen, T. P. W.; Lewis, R. N. A. H.; McElhaney, R. N. *Curr. Opin. Colloid Interface Sci.* **2004**, *8*, 459–468.
 (12) Veatch, S. L.; Polozov, I. V.; Gawrisch, K.; Keller, S. L. *Biophys. J.* **2004**, *86*, 2910–2922.
 (13) Ipsen, J. H.; Mouritsen, O. G.; Zuckermann, M. J. *Biophys. J.* **1989**, *56*, 661–667.
 (14) London, E.; Brown, D. A. *Biochim. Biophys. Acta* **2000**, *1508*, 182–195.
 (15) Heerklotz, H. *Biophys. J.* **2002**, *83*, 2693–2701.
 (16) Heerklotz, H.; Szadkowska, H.; Anderson, T.; Seelig, J. *J. Mol. Biol.* **2003**, *329*, 793–799.
 (17) Nicolini, C.; Thiyagarajan, P.; Winter, R. *Phys. Chem. Chem. Phys.* **2004**, *6*, 5531–5534.
 (18) van Rheeën, J.; Achame, E. M.; Janssen, H.; Calafat, J.; Jalink, K. *EMBO J.* **2005**, *24*, 1664–1673.

Theory

The fom Model for Ideal Mixing. The model applies to a thermodynamic equilibrium of two lipids, L1 and L2, and one detergent, D, during “fom” coexistence, that is, forming fluid (f) and ordered (o) membranes, micelles (m), and aqueous solution (aq, only for the detergent). The criterion for a system to be in equilibrium is that no transfer of any molecule from one phase to another can further reduce the Gibbs free energy of the system, meaning that the chemical potential of each component must be equal in all coexisting phases. For the detergent in the fom range, ideal mixing in all phases yields

$$\mu_D^{0,o} + RT \ln X_D^o = \mu_D^{0,f} + RT \ln X_D^f = \mu_D^{0,m} + RT \ln X_D^m = \mu_D^{0,aq} + RT \ln X_D^{aq} \quad (1)$$

The chemical potential comprises a constant standard value, μ_D^0 , and a composition-dependent term, $RT \ln X_D^p$, containing the contribution from the entropy of ideal mixing. R denotes the universal gas constant, T the absolute temperature, and X_D^p the mole fraction of detergent in a phase $p = o, f, m, \text{ or } aq$. We may rewrite eq 1 and the equivalent equations for the lipids, L1 and L2, using partition coefficients of a component C between the phases $p1$ and $p2$, $K_C^{p1/p2}$, as

$$\mu_C^{0,p1} - \mu_C^{0,p2} = -RT \ln \frac{X_C^{p1}}{X_C^{p2}} \equiv -RT \ln K_C^{p1/p2} \quad (2)$$

Writing the mole fractions in terms of molar concentrations, c_C^p , yields six independent equations of the type

$$K_C^{p1/o} = \frac{c_C^{p1}(c_D^o + c_{L1}^o + c_{L2}^o)}{(c_D^{p1} + c_{L1}^{p1} + c_{L2}^{p1})c_C^o} \quad (3)$$

for the components C = L1, L2, or D and phases $p1 = f$ or m and $p2 = o$ (i.e., $K_D^{f/o}$, $K_D^{m/o}$, $K_{L1}^{f/o}$, $K_{L1}^{m/o}$, $K_{L2}^{f/o}$, and $K_{L2}^{m/o}$). For the aqueous detergent solution

$$K_D^{aq/o} = \frac{c_D^{aq}(c_D^o + c_{L1}^o + c_{L2}^o)}{55.5 \text{ M} \times c_D^o} \quad (4)$$

Since these equations still describe mole fraction partition coefficients, the standard states remain hypothetical pure phases ($X_C^p = 1$) rather than 1 M solutions. The ordered phase is chosen as the reference state merely for technical reasons (o is present in many phase ranges) and without restriction of generality. All other $K_C^{p1/p2}$ values depend on the seven o-based partition coefficients given by eqs 3 and 4.

Trivially, the sum of all partial concentrations of a component (all referring to the total volume) must equal the total concentration, yielding another three independent equations, such as

$$c_D = c_D^o + c_D^f + c_D^m + c_D^{aq} \quad (5)$$

for c_D and analogous expressions for c_{L1} and c_{L2} . The system of eqs 3–5 represents the model used here; all 10 equations are given explicitly in the Supporting Information. Selecting appropriate values for the seven $K_C^{p1/p2}$ values and the three total concentrations, c_C , yields 10 equations with 10 unknown variables (c_C^p with C = D, L1, or L2 and $p = f, o, m, \text{ and, for D, also } aq$), so that an unequivocal solution can be determined

numerically using the Solver (Frontline Systems, Incline Village, USA) function in an Excel spreadsheet (Microsoft, Redmond, USA).

The phase model used here implicitly refers to large domains, that is, macroscopically separated phases with a negligible mixing entropy of the different domains and negligible interfacial energies of the borders between the domains. In case of weak line tension between the different domains, the latter become small, thus gaining some additional entropy and making lipid sorting somewhat more favorable.

The Models for the Phase Ranges fo, om, f, m, and fm. If, for the selected set of parameters, the system does not show **fo**m coexistence, at least one of the resulting partial concentrations becomes negative, indicating that the **fo**m model is not appropriate in the respective concentration range. A model for **fo** coexistence (membranes with fluid and ordered domains and detergent monomers, but no micelles) is obtained by omitting the equations for $K_D^{m/o}$, $K_{L1}^{m/o}$, $K_{L2}^{m/o}$, and setting $c_C^m = 0$ for all components, C. The model for **om** coexistence is derived analogously by omitting all equations and concentrations for the **f** phase. For the **f** phase range (only fluid membranes and aqueous detergent monomers), the equilibrium is given by $K_D^{aq/o}/K_D^{f/o}$ (cf. eq 3 with $\mathbf{p1} = \mathbf{f}$, $C = D$, and eq 4), and analogous expressions hold for the **m** range (only micelles and aqueous detergent monomers).

For **fm** (solubilization of fluid membranes in the absence of ordered domains), we have to change the reference state of our K values to **f**, deriving $K_C^{m/f} = K_C^{m/o}/K_C^{f/o}$ and an analogous equation for $K_D^{aq/f}$. The model then simplifies to the classical three-stage case (**f**, **fm**, and **m**) for $c_{L2} = 0$ and $c_C^o = 0$ for all components, C.

Input Parameters. Unfortunately, some of the seven partition coefficients used here are not straightforward to be estimated or measured. We therefore chose another, more illustrative set of input parameters that serves to calculate these seven K values (cf. the Supporting Information for conversion rules).

(1) The critical micellar concentration (CMC) of the detergent determines its partitioning between the micellar and the aqueous phase, $K_D^{m/aq}$, and, with $K_D^{m/o}$ (derived below), also $K_D^{aq/o}$.

(2,3) The effective mole fractions at the onset and completion of solubilization of the fluid-phase-preferring lipid L1, $X_e^{sat-(L1)}$ and $X_e^{sol-(L1)}$, yield $K_D^{m/f}$ and $K_{L1}^{m/f}$ and, with $K_D^{m/o}$ and $K_{L1}^{f/o}$ (derived below), also the basic $K_D^{f/o}$ and $K_{L1}^{m/o}$. As standard values, we chose $X_e^{sat-(L1)} = 0.29$ and $X_e^{sol-(L1)} = 0.63$ as found for Triton X-100/1-palmitoyl-2-oleoyl-*sn*-glycero-3-phosphocholine (POPC) at 37 °C.¹⁶ The somewhat higher values reported for the partitioning of Triton^{19–21} and most other strong detergents into POPC or egg lecithin at room temperature^{22,23} would lead to the same general behavior.

(4,5) Analogously, we select the onset and completion of solubilization of a pure ordered membrane consisting of L2, $X_e^{sat-(L2)}$ and $X_e^{sol-(L2)}$, which yield $K_D^{m/o}$ and $K_{L2}^{m/o}$. These parameters are not straightforward to be measured because

solubilization of ordered phases may implicitly include the formation of disordered phases. We varied these parameters over a broad range to obtain general conclusions without experimental data (cf. Results).

(6) We define the fraction of ordered lipid as

$$\xi^o \equiv \frac{c_{L1}^o + c_{L2}^o}{c_{L1} + c_{L2}} \quad (6)$$

The value of ξ^o depends on lipid composition, temperature, pressure, and detergent content. We select the fraction of ordered lipid in the absence of detergent, $\xi^o(0) \equiv \xi^o(X_e = 0)$ as another input parameter. With increasing temperature, the ordered phase melts, and ξ^o varies from unity to zero. The progress of the thermotropic transition can, for instance, be measured by scanning calorimetry.

(7) One basic partition coefficient, the affinity of L2 to the fluid as compared with the ordered phase, $K_{L2}^{f/o}$, is specified as an input parameter. Without restriction of generality, we assume that L2 prefers the ordered phase, $K_{L2}^{f/o} < 1$. Both $K_{L2}^{f/o}$ and $\xi^o(0)$ serve to calculate $K_{L1}^{f/o}$, and the requirement that $K_{L1}^{f/o} > 0$ limits the range for choosing $K_{L2}^{f/o}$ at a given $\xi^o(0)$.

Using these seven input parameters and the total concentrations, c_{L1} and c_{L2} , we calculate the solutions for increasing c_D , corresponding to a titration of detergent into the lipid dispersion. If the results are, however, plotted as a function of the effective detergent mole fraction in aggregates, defined as

$$X_e \equiv \frac{c_D - c_D^{aq}}{c_D - c_D^{aq} + c_{L1} + c_{L2}} \quad (7)$$

they will agree for all calculations sharing a certain L2-to-L1 molar ratio, c_{L2}/c_{L1} , regardless of the absolute concentrations, c_{L1} and c_{L2} . We chose an equimolar mixture for all cases presented here.

Results

Typical Behavior of Predominantly Ordered Lipid Mixtures. Figure 1 shows the results of a typical model calculation for the input parameters given in the legend. The results for the partial concentrations of the components, C, in the phases, **p**, are plotted as percentages of the total concentration, $\xi_C^p \equiv c_C^p/c_C$. The **fo**m model returns positive solutions for the range of $0.31 \text{ mM} < c_D < 0.73 \text{ mM}$ ($0.15 < X_e < 0.37$). At lower detergent content, the system is in **fo** equilibrium. Over a large concentration range of $0.73 \text{ mM} < c_D < 4.5 \text{ mM}$ ($0.37 < X_e < 0.81$), “resistant” ordered membrane particles coexist with micelles (**om**), and only at very high detergent concentrations of $c_D > 4.5 \text{ mM}$ is the membrane fully solubilized (**m**). The consistency of the solution is illustrated by the fact that the partial concentrations vary continuously at the phase boundaries. For example, for $c_D = 0.31 \text{ mM}$ (**fo|fo**m boundary), the model for **fo** as well as that for **fo**m yield the same result. The data given in Figure 1 are plotted as a function of the absolute detergent concentration, c_D , in Figure S1 in the Supporting Information.

The results show that in the **fo** range, a considerable amount of L1 but also a little L2 is transferred from **o** into **f**, that is, ordered domains or part of them are converted into fluid ones, and the remaining **o** domains are enriched in L2. The ordered domains are further changed upon selective solubilization of

(19) Paternostre, M. T.; Roux, M.; Rigaud, J. L. *Biochemistry* **1988**, *27*, 2668–2677.

(20) Partearroyo, M. A.; Alonso, A.; Goñi, F. M.; Tribout, M.; Paredes, S. J. *Colloid Interface Sci.* **1996**, *178*, 156–159.

(21) Kragh-Hansen, U.; le Maire, M.; Möller, J. V. *Biophys. J.* **1998**, *75*, 2932–2946.

(22) Heerklotz, H.; Seelig, J. *Biophys. J.* **2000**, *78*, 2435–2440.

(23) Heerklotz, H. In *Phospholipids Handbook*, 2nd ed.; Cevc, G., Ed.; Plenum Press: New York, 2005.

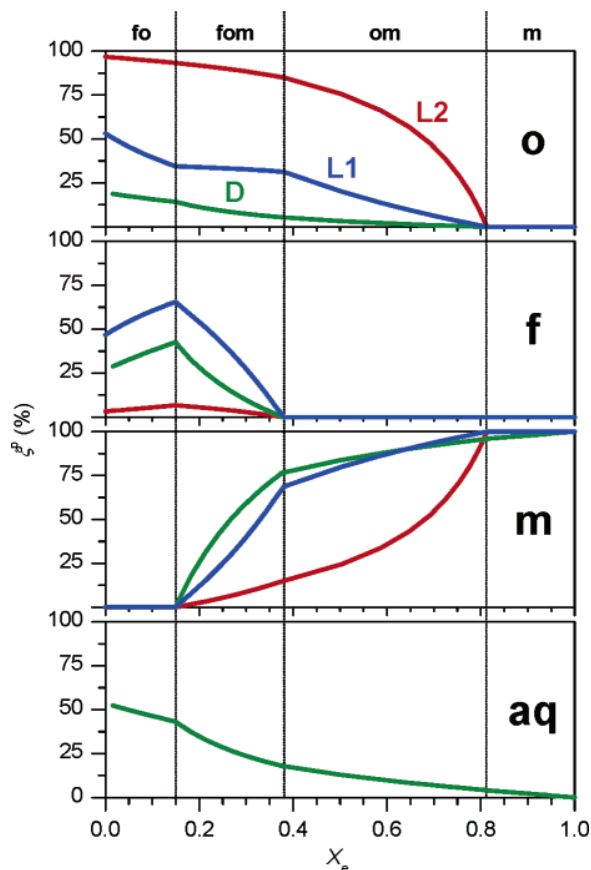


Figure 1. Results of a simulation for fixed lipid concentration ($c_{L1}/c_{L2} = 1$) and increasing detergent concentration given as effective mole fraction, X_e (abscissa). The input parameters are CMC = 0.23 mM, $X_e^{\text{sat}}(\text{L1}) = 0.29$, $X_e^{\text{sol}}(\text{L1}) = 0.63$, $X_e^{\text{sat}}(\text{L2}) = 0.10$, $X_e^{\text{sol}}(\text{L2}) = 0.90$, $\xi^o(0) = 75\%$, and $K_{L2}^{\text{f/o}} = 0.1$. Plotted are the fractions, ξ^p , of the two lipids, L1 and L2, and of the detergent, D, localized in each of the four possible phases (p): ordered (o) and fluid (f) membranes, micelles (m), and aqueous solution (aq). Phase boundaries are recognized by the appearance or disappearance of phases and indicated by dotted lines.

the **f** phase (**fom**). In the **fom** and **om** ranges, the amount of L2 in **o** domains decreases nearly linearly with the total detergent concentration (cf. Figure S1 in the Supporting Information), and the disappearance of fluid membranes at the **fom|om** boundary has only a minor effect on the solubilization of L2. The aqueous detergent concentration, c_D^{aq} , increases continuously with increasing total c_D and approaches the CMC for large c_D . However, the fraction of detergent that is in aqueous solution decreases, so that the effective mole fraction, X_e , approaches the total mole fraction. When it comes to discussing the extraction of DRMs, which is usually done at high concentrations ($c_D \gg \text{CMC}$), we can ignore the aqueous detergent and interpret X_e approximately as the total mole fraction of detergent in the system.

Typical Behavior of Predominantly Fluid Membranes. Figure 2 illustrates a calculation for a system that can be imagined to represent a higher temperature, where most of the ordered domains are “molten”. We assume a relatively small fraction of ordered domains in the detergent-free membrane, $\xi^o(0) = 20\%$, and a strong sorting of L1 into disordered domains, $K_{L2}^{\text{f/o}} = 0.4$. Addition of detergent converts ordered domains progressively into fluid ones until an **fo|f** boundary is reached, beyond which only homogeneous fluid membranes are

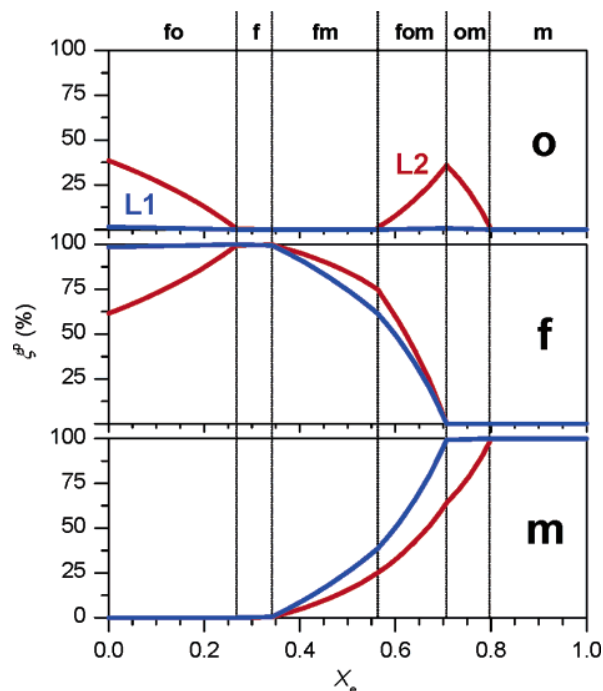


Figure 2. The fractions, ξ^p , of the lipids, L1 and L2, in the ordered (o), fluid (f), and micellar (m) phase, and the phase ranges as a function of the effective mole fraction of detergent in the system, X_e . Ordered domains are disintegrated by addition of detergent to the membrane until **fo|f** but reappear upon selective solubilization of L1 at the **fm|fom** boundary. The input parameters are the same as in Figure 1 with the exception of $\xi^o(0) = 20\%$ and $K_{L2}^{\text{f/o}} = 0.4$. The results for the detergent are not shown.

left. After the appearance of micelles at $X_e(\text{f|fm})$, there is a preferential solubilization of L1 because the order-preferring lipid, L2, has a weaker affinity to micelles. As a consequence, the remaining membranes are enriched in L2, and at a critical L2-to-L1 ratio, ordered domains reappear (**fm|fom** boundary). In the **fom** range, the lipids from fluid domains are sorted into micelles (L1) and ordered domains (L2). At **fom|om**, also the ordered domains start to be solubilized, and this process is completed at virtually the same $X_e(\text{om|m})$ as in Figure 1 describing the solubilization of an originally much more ordered membrane.

General Phase Behavior. Let us, at first, inspect the effect of the preferences of the lipids, L1 and L2, for fluid versus ordered phases on the solubilization behavior. The input parameters describing these properties are $K_{L2}^{\text{f/o}}$ and $\xi^o(0)$. With $\xi^o(0)$ decreasing from unity (all ordered) to zero (all fluid), Figure 3 bears some resemblance to a phase diagram since the **o** phase melts with increasing temperature. The boundaries are distorted because $\xi^o(0)$ is not a linear function of T , and the other input parameters may also depend somewhat on temperature,²³ which is not considered here.

The bottom panel of Figure 3 was obtained for a strong preference of L2 for the **o** phase as quantified by $K_{L2}^{\text{f/o}} = 0.1$. From $\xi^o(0) = 100\%$ (corresponding to low temperature) to $\xi^o(0) \approx 40\%$ (thermotropic transition range), we find the same sequence of phase ranges as illustrated in Figure 1 for $\xi^o(0) = 75\%$, that is, **fo–fom–om–m**. Progressive melting of the ordered domains shifts the onset of micelle formation (**fo|fom**) and, particularly, the complete solubilization of the fluid phase (**fom|om**) to higher detergent contents. This is logical because there is more lipid in the **f** phase to be solubilized in the first

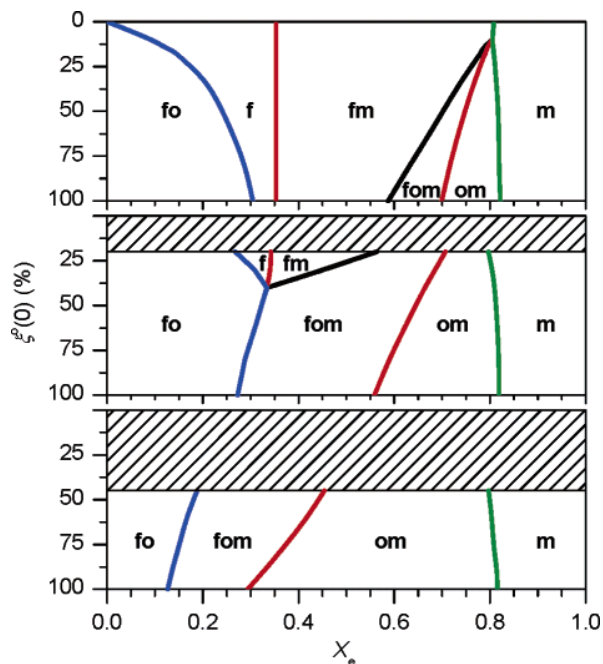


Figure 3. Phase boundaries, X_e , for various degrees of order in the original membrane, $\xi^o(0)$ (ordinates), and partition coefficients of L2: top panel, $K_{L2}^{f/o} = 0.5$; center, 0.4; bottom, 0.1. The other input parameters are the same as in Figure 1. Hatched areas are not accessible because they would correspond to negative $K_{L1}^{f/o}$ values.

place. However, the detergent concentration needed to finally solubilize the “resistant” **o** phase is almost independent of whether the lipid was originally in an **o** or in an **f** phase.

Having more than $\sim 60\%$ of the lipid in the **f** phase is incompatible with a strong preference of L2 for the **o** phase. Systems with less **o** must have higher $K_{L2}^{f/o}$ values; the center panel of Figure 3 uses a value of $K_{L2}^{f/o} = 0.4$. At high initial order ($\xi^o(0) > 50\%$), we obtain the same phase ranges as for $K_{L2}^{f/o} = 0.1$ (bottom panel), but with the phase boundaries shifted to higher detergent contents. At $\xi^o(0) \approx 40\%$, the detergent abolishes all ordered domains already before solubilization starts. Systems with only a few ordered domains already in the absence of detergent ($\xi^o(0) < 20\%$) require even larger values of $K_{L2}^{f/o}$ (top panel). The higher affinity of L2 to the fluid phase shifts the pattern in favor of the fluid phase. Now, intermediate **f** and **fm** phase ranges are obtained already from originally largely ordered membranes (high ξ^o). For $\xi^o(0) < 12\%$, ordered domains cease to reappear. As disorder-preferring detergents cannot promote ordered domains in the case of ideal mixing, the phase behavior must approach that of homogeneous fluid membranes (three-stage model with **f**, **fm**, and **m**) for vanishing ordered domains. The thermodynamic resistance of L2 against solubilization, which is quantified by $X_e(\mathbf{om}|\mathbf{m})$, is virtually independent of $\xi^o(0)$ as well as of $K_{L2}^{f/o}$.

Effects of the Detergent and Fluid Lipid. The interactions of the detergent with the more fluid lipid, L1, are characterized by the CMC, $X_e^{\text{sat}}(\text{L1})$, and $X_e^{\text{sol}}(\text{L1})$. We compared calculations based on parameters typical of POPC/Triton X-100 (TX; CMC = 0.23 mM, $X_e^{\text{sat}}(\text{L1}) = 0.29$, $X_e^{\text{sol}}(\text{L1}) = 0.63$) with those of octyl glucoside (OG; 22 mM, 0.61, 0.76).^{24,25} OG is a weak detergent that usually fails to yield DRMs. The fact that the

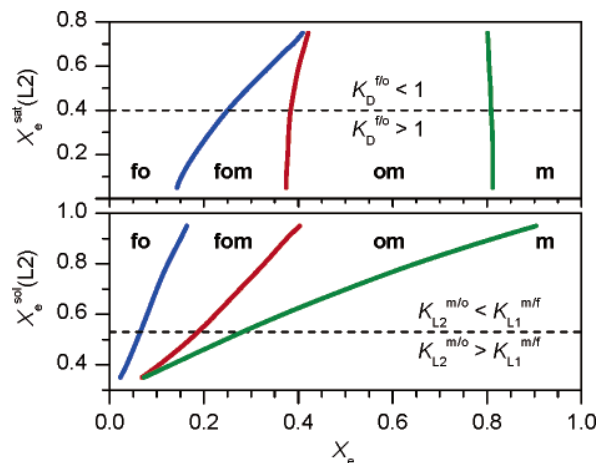


Figure 4. The effect of the onset and completion of solubilization of pure ordered L2, $X_e^{\text{sat}}(\text{L2})$ and $X_e^{\text{sol}}(\text{L2})$, on the phase ranges. For the case of detergents added to detergent-resistant membranes, **f** is more susceptible to solubilization (corresponding to $X_e^{\text{sol}}(\text{L2}) > 0.53$), and the detergent inserts preferably into **f** (corresponding to $X_e^{\text{sat}}(\text{L2}) < 0.40$). All other input parameters are selected as in Figure 1.

CMC of OG is much larger has the consequence that a higher absolute detergent concentration is needed for complete solubilization of the ordered phase, that is, 4.5 mM for TX but 22 mM for OG. However, relative to the CMC, there is more TX needed ($\sim 20 \times \text{CMC}$) than OG ($1 \times \text{CMC}$), so that an isolation procedure using, for example, twice the CMC could yield DRMs with TX but not with OG.

The much higher X_e^{sat} and X_e^{sol} values of OG compared with those of TX also shift the solubilization of the fluid phase in the L1/L2 mixture to higher X_e values: $X_e(\mathbf{fo}|\mathbf{fom})$ from 0.15 (TX) to 0.40 (OG) and $X_e(\mathbf{fom}|\mathbf{om})$ from 0.37 (TX) to 0.57 (OG). The fraction of lipid in the ordered phase, starting at 75% in the calculation, decreases to 59% upon solubilization of the fluid phase at $X_e(\mathbf{fom}|\mathbf{om})$ with TX but to 39% with OG. The enrichment of the **o** phase with L2 ($c_{L2}^o/c_{L1}^o = 1.8$ before addition of detergent) at this point is stronger for OG (5.5) than for TX (2.7). It appears that the effects within **fo** are generally enhanced for OG, which has a much broader **fo** range. Finally, we note that nonideal interactions (cf. below) of weak detergents, such as OG,²² with membranes are expected to be weaker, as well. The “resistance limit”, $X_e(\mathbf{om}|\mathbf{m})$, is independent of the characteristic parameters of the fluid lipid varied here.

Effects of the Solubilization Behavior of L2. Figure 4 illustrates the influence of the solubilization behavior of lipid L2, which is quantified in terms of $X_e^{\text{sat}}(\text{L2})$ and $X_e^{\text{sol}}(\text{L2})$. These two input parameters are used to determine several characteristic partition coefficients, in particular $K_D^{f/o}$, which describes the affinity of the detergent to ordered versus fluid membrane domains, and $K_{L2}^{m/o}$, which indicates the tendency of L2 to become solubilized from ordered domains into micelles.

The top panel of Figure 4 keeps $X_e^{\text{sol}}(\text{L2}) = 0.90$ constant and increases $X_e^{\text{sat}}(\text{L2})$. This corresponds to a decrease of $K_D^{f/o}$ from 8 (at $X_e^{\text{sat}}(\text{L2}) = 0.05$) to 1 (0.40) and 0.6 (0.75). This means that $X_e^{\text{sat}}(\text{L2}) > 0.40$ corresponds to a detergent that prefers insertion into and formation of the ordered compared with the fluid phase, a condition that seems not to be relevant to the isolation of DRMs (but maybe to membrane additives

(24) Paternostre, M.; Meyer, O.; Grabielle-Madellmont, C.; Lesieur, S.; Ghanam, M.; Ollivon, M. *Biophys. J.* **1995**, *69*, 2476–2488.

(25) Keller, M.; Kerth, A.; Blume, A. *Biochim. Biophys. Acta* **1997**, *1326*, 178–192.

other than detergents). If pure L2 requires more detergent for the onset of solubilization, the L1/L2 mixture will do so, as well. The completion of solubilization of the **f** as well as of the **o** phase is, however, essentially unaffected.

Finally, we kept $X_e^{\text{sat}}(\text{L2})$ fixed at 0.10 and increased the detergent content required for the completion of solubilization of pure L2, $X_e^{\text{sol}}(\text{L2})$, from 0.35 to 0.98. Below $X_e^{\text{sol}}(\text{L2}) = 0.53$, $K_{\text{L2}}^{\text{m/o}}$ is larger than $K_{\text{L1}}^{\text{m/f}}$, meaning that the ordered domains will be preferentially solubilized, again a case that is not of interest here. The larger $X_e^{\text{sol}}(\text{L2})$, the more selective is the solubilization of the fluid phase, and the more will the detergent accumulate in the **f** and be repelled from the **o** phase. The consequences are shown in the bottom panel of Figure 4. Growing resistance of pure L2 against solubilization increases the amount of detergent that is needed for the onset of micelle formation in the mixture, $X_e(\text{fo|fom})$, for the complete solubilization of the fluid phase, $X_e(\text{fom|om})$, and, in particular, for the complete solubilization of the ordered phase, $X_e(\text{om|m})$. In fact, this is the only parameter that governs the thermodynamic resistance of the mixture, whereas all other parameters varied so far have virtually no influence on $X_e(\text{om|m})$.

Nonideal Mixing. In general, mixing in the membrane and micelle phases might possibly be nonideal, necessitating additional terms in the expressions for the chemical potentials. Here, we demonstrate the substantial effect of a single nonideality parameter for pairwise interactions between detergent and lipid L2 in the fluid phase. That this interaction is highly nonideal in DRM-forming systems is supported by the finding that the partition coefficient of Triton into largely fluid POPC/egg sphingomyelin (eSM)/cholesterol (1:1:1 mol/mol/mol) vesicles at 37 °C is about 6 times smaller than that into pure POPC.¹⁶ Even though we cannot distinguish whether this nonideality is a consequence of the sphingomyelin or the cholesterol or both of them in a cooperative manner, we chose a moderately unfavorable nonideality parameter, $\rho_{\text{D/L2}}^{\text{f}} = 5$ kJ/mol, to assess the possible consequences of nonideal mixing. The parameter accounts for the excess free energy of the fluid phase as compared with ideal mixing, G_E^{f} , according to

$$G_E^{\text{f}} = \rho_{\text{D/L2}}^{\text{f}} X_{\text{D}}^{\text{f}} X_{\text{L2}}^{\text{f}} \quad (8)$$

The nonideal free energy, G_E^{f} , is much smaller than $\rho_{\text{D/L2}}^{\text{f}}$ because $X_{\text{D}}^{\text{f}}, X_{\text{L2}}^{\text{f}} \ll 1$. All other possible nonideality parameters were neglected.

Figure 5 presents the extreme case of a membrane at the completion of the melting of the ordered domains, so that $\xi^{\text{o}}(0) \approx 0$. Addition of detergent induces the formation of ordered domains, which are growing further beyond the **fo|fom** boundary by selective solubilization of L1. The sample would show >60% of the lipid as thermodynamically resistant, although it was all fluid before the addition of detergent.

Discussion

The Nature of Detergent Resistance. The isolation of a DRM fraction from a membrane sample depends on a number of properties that may be of kinetic, thermodynamic, or technical kind. Our study allows us to discuss DRMs if these are thermodynamically stable. Then, detergent resistance of a lipid means that it remains in a bilayer structure up to very high detergent contents or, in terms of our model, that it has a very high X_e -(**om|m**). It turns out in all calculations that the amount of detergent required for solubilizing the “resistant” **o** domains depends

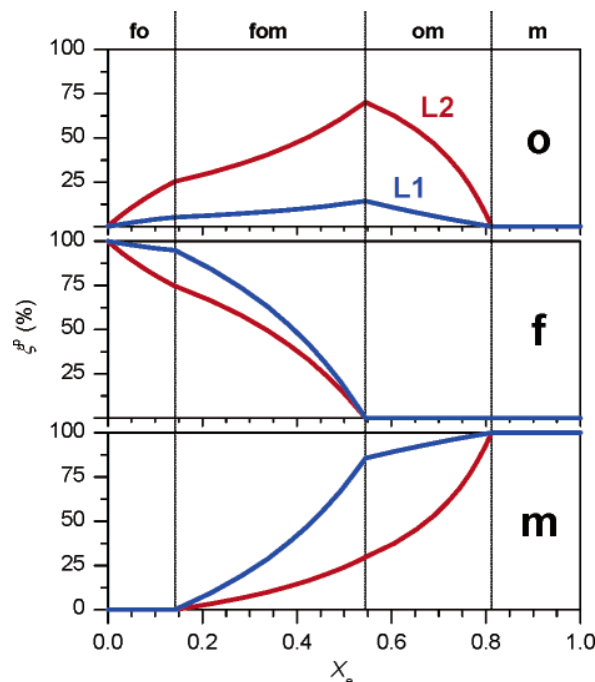


Figure 5. Effect of nonideal mixing between detergent and order-preferring lipid as quantified by a nonideality parameter, $\rho_{\text{D/L2}}^{\text{f}} = 5$ kJ/mol. The fraction of initially ordered membrane is $\xi^{\text{o}}(0) = 0.001$; the other input parameters are as in Figure 1. In the case of unfavorable nonideal mixing between D and L2 and at low initial degree of order, addition of D promotes the ordered phase.

almost exclusively on one input parameter, $X_e^{\text{sol}}(\text{L2})$. For a detailed interpretation of this behavior, it is advantageous to quantify the composition of the system in terms of effective mole ratios, R_e , rather than mole fractions, X_e , using the simple conversion $R_e = X_e/(1 - X_e)$. The D-to-L2 mole ratio in micelles at the disappearance of ordered membrane particles, $R_{\text{D/L2}}^{\text{m}}(\text{om|m})$, is virtually independent of the presence or absence of L1. In pure L2, this ratio is also termed $R_e^{\text{sol}}(\text{L2})$. We may thus write

$$R_{\text{D/L2}}^{\text{m}}(\text{om|m}) = R_e^{\text{sol}}(\text{L2}) = \frac{K_{\text{D}}^{\text{m/o}}(K_{\text{L2}}^{\text{o/m}} - 1)}{K_{\text{D}}^{\text{m/o}} - 1} \xrightarrow{K_{\text{D}}^{\text{m/o}}, K_{\text{L2}}^{\text{o/m}} \gg 1} K_{\text{L2}}^{\text{o/m}} \quad (9)$$

The expression of $R_e^{\text{sol}}(\text{L2})$ in terms of partition coefficients of L2 and D between **o** and **m** is derived in the Supporting Information. The approximation on the right-hand side of eq 9 is valid for large $K_{\text{D}}^{\text{m/o}}$ (detergent prefers **m** strongly over **o**) and large $K_{\text{L2}}^{\text{o/m}}$ (L2 prefers **o** strongly over **m**), which is typically fulfilled by order-preferring lipids. Thus, the resistance of L2 in any mixture with a more readily solubilizable lipid is solely determined by and equal to the preference of the resistant lipid, L2, for **o** over **m**. No property of L1 nor even its mere existence has any influence on the **om|m** phase boundary of the mixture.

A large $K_{\text{L2}}^{\text{o/m}}$ is expected if the transfer of the lipid into the micelle requires not only some change in interfacial curvature but also additional energetically costly transformations, such as chain melting or disordering of almost stretched chains well below the melting temperature. In light of this, all lipids forming gel or ordered phases at a given temperature must be expected to be resistant, both in mixtures with others and alone.

The latter suggestion seems to be in conflict with the finding that pure 1,2-dipalmitoyl-*sn*-glycero-3-phosphocholine (DPPC) or pure sphingomyelin does not necessarily yield DRMs.^{26,27} However, thermodynamic (or maybe kinetic) resistance is only a necessary but not a sufficient criterion for the observation of DRMs. Additionally, the resistant particles must be large enough to be separated by centrifugation. The presence of cholesterol or other lipids may be important for DRMs not primarily by making the domains more resistant but by rendering the resistant particles larger. Furthermore, DRMs might also be thermodynamically unstable nonequilibrium structures that can be isolated because of the slow kinetics of equilibration.¹⁴

Solubilization of Membranes in the Gel Phase. As mentioned in the previous section, pure gel-phase lipids seem to be thermodynamically resistant, but the resistant membrane fragments may be too small to be detected or isolated. Funari et al.²⁸ have described, in fact, “gel-phase micelles”, that is, small bilayer fragments of virtually pure DPPC gel phase surrounded by a hoop of detergent, which represent the thermodynamically resistant but technically soluble systems discussed here. We observed a similar behavior for mixtures of eSM and TX (Heerklotz et al., unpublished); the sample was optically clear below the melting point, T_m , of eSM but “melted” at $T_m = 39$ °C, with approximately the heat expected for pure eSM. The dispersion became turbid above T_m . This supports the hypothesis that most of the lipid is still in an almost detergent-free gel-phase bilayer below T_m (what we call “thermodynamically resistant”), but the bilayer fragments are too small to be detected by turbidity or centrifugation (i.e., “technically soluble”). Upon chain melting, the membrane loses its thermodynamic resistance, and the local detergent concentration at the edges decreases because the detergent distributes over the whole membrane. In turn, the fragments merge to form large membrane particles or vesicles.

These arguments and the analogy of the process to what our model reveals about mixtures also resolves the paradox of enhanced susceptibility to solubilization of membranes slightly below the melting temperature.^{26,27,29} The chains in a gel phase are arranged to form a hexagonal lattice, and clusters of crystal-like packing are separated by line defects. A detergent or any other molecule that does not fit into the lattice is accumulated in the defect domains. This has, for example, long been known for pyrene, which shows an enhanced excimer formation in membranes somewhat below the melting temperature as it segregates into small areas at high local concentration.³⁰ If a detergent is added to a membrane, it will also accumulate in such less tightly packed domains. This preference will give rise to a very high local detergent content in the defect ranges, a growth of the defects, and most likely a splitting or shrinking of the ideally packed gel clusters, rendering them very small. Little detergent is required to let pieces of well-packed gel phase that are too small to make the sample turbid “fall apart” by covering their edges (cf. also London and Brown¹⁴). The same phenomenon may account for the effect of gangliosides,²⁹ if

these, as often assumed, promote ordered phases, and of membrane-perturbing solutes, which may render gel-phase membranes technically soluble even far below the melting point.²⁶

Line Tension and Domain Size: Cholesterol Might Enlarge Resistant Particles. As noted above, the phase equilibrium model used here does not consider the size of the domains, which is determined by the tradeoff between the entropy of mixing (favoring small domains) and the line tension of the domain borders (favoring shorter borders, i.e., larger domains). Hence, molecules reducing the line tension between the domains could abolish detectable DRMs by rendering them too small without affecting the actual equilibrium of the domains as described here. Nicolini et al.¹⁷ have demonstrated by small-angle neutron scattering that Triton may reduce the domain size in model systems. On the contrary, an agent that enhances the line tension may serve to make DRMs large enough to be detectable. Cholesterol seems to be such a line tension modulator. Galla and Sackmann³⁰ have shown that addition of cholesterol to DPPC abolishes the coexistence of gel clusters and defect ranges, so that the segregation of the probe below T_m is eliminated. Hence, more detergent is expected to be required for the disintegration of the membrane, and the particles might be larger. The phase diagram of giant liposomes composed of 1,2-dioleoyl-*sn*-glycero-3-phosphocholine (DOPC)/sphingomyelin/cholesterol established by Kahya et al.³¹ provides crucial insight; domains in the gel–fluid coexistence range are too small to be visualized by confocal fluorescence microscopy and can only be detected by correlation spectroscopy. However, addition of ~20 mol % of cholesterol induces growth of the domains, making them visible in the microscope. In summary, it appears that lipids below their melting temperature may generally be detergent-resistant in the thermodynamic sense, regardless of whether they are mixed with cholesterol or other lipids. Cholesterol may, however, be necessary for rendering the resistant particles large enough to make them visible or separable by centrifugation.

Another possible role of cholesterol is to induce a marked nonideal mixing in the fluid phase. This would not affect the resistance of L2 given by $X_c(\mathbf{om}|\mathbf{m})$, but it could greatly increase the amount of resistant lipid, $\xi^0(\mathbf{om}|\mathbf{m})$, by detergent-induced formation of ordered domains, as illustrated in Figure 5. Very large concentrations of cholesterol can also eliminate visible domains in giant liposomes,^{31,32} but this is often explained by the formation of a continuous liquid-ordered phase.^{11,33}

Are Rafts Equivalent to DRMs? It has often been assumed that functional *in vivo* domains in detergent-free membranes (lipid rafts) and DRMs are both governed by an equilibrium of fluid and ordered lipid domains. Let us, for the sake of the argument, assume that this is so. Then, our model should yield the key properties of rafts at $X_c = 0$ and those of the corresponding DRMs at $X_c(\mathbf{fom}|\mathbf{om})$, where the fluid membrane domains are fully solubilized. The assumption of ideal mixing in all phases implies that only part of the rafts are actually obtained as DRMs at the same temperature ($\xi^0(\mathbf{fom}|\mathbf{om}) < \xi^0(0)$) and that the DRMs are enriched in L2 (c_{L2}/c_{L1} at $\mathbf{fom}|\mathbf{om}$

(26) Patra, S. K.; Alonso, A.; Goñi, F. M. *Biochim. Biophys. Acta* **1998**, *1373*, 112–118.

(27) Alonso, A.; Villena, A.; Goñi, F. M. *FEBS Lett.* **1981**, *123*, 200–204.

(28) Funari, S. S.; Nuscher, B.; Rapp, G.; Beyer, K. *Proc. Natl. Acad. Sci. U.S.A.* **2001**, *98*, 8938–8943.

(29) Sot, J.; Collado, M. I.; Arrondo, J. L. R.; Alonso, A.; Goñi, F. M. *Langmuir* **2002**, *18*, 2828–2835.

(30) Galla, H. J.; Sackmann, E. *Biochim. Biophys. Acta* **1974**, *339*, 103–115.

(31) Kahya, N.; Scherfeld, D.; Bacia, K.; Poolman, B.; Schwille, P. *J. Biol. Chem.* **2003**, *278*, 28109–28115.

(32) Feigenson, G. W.; Buboltz, J. T. *Biophys. J.* **2001**, *80*, 2775–2788.

(33) de Almeida, R. F.; Fedorov, A.; Prieto, M. *Biophys. J.* **2003**, *85*, 2406–2416.

is larger than at $X_e = 0$). Taking into account one nonideality parameter shows, however, that DRMs might also overestimate the amount of lipid in rafts and may, in the extreme case, be induced by the detergent in originally homogeneous fluid membranes.

Thus, the present model suggests that DRMs must be expected to differ markedly from rafts. There may, of course, be special cases where all the detergent effects cancel out each other, so that the ordered domains are, indeed, isolated without major changes. A set of parameters that minimizes the effects of the detergent on the abundance and composition of ordered domains up to the **fom|om** boundary (DRMs) is $\xi^o(0) = 40\%$, $K_{L2}^{f/o} = 0.2$, $X_e^{sol}(L2) = 0.93$, $\rho_{L2D}^f = 2.5$ kJ/mol (other parameters as in Figure 1). The first two parameters describing the detergent-free system correspond to the case of an extremely strong sorting of the lipids between the domains, $K_{L1}^{f/o} = 21$. Consequently, only 3% of all L1 but 77% of all L2 resides in **o** domains (averaging to $\xi^o(0) = 40\%$) in the detergent-free system. This pronounced enrichment of **o** with L2 leaves practically no freedom for the general trend of the detergent to further enrich **o** in L2. The tendency to fluidize the membrane prior to micelle formation by adding fluid phase-preferring detergent (here, $K_D^{f/o} = 4.3$) is balanced by the weak nonideality parameter. $X_e^{sol}(L2)$ is chosen such as to yield an affinity of L2 to micelles, $K_{L2}^{m/o} = 0.1$, that allows neither progressive solubilization (cf. Figure 1) nor formation (cf. Figure 2) of ordered domains within the **fom** range. The results are plotted as Figure S2 in the Supporting Information.

Summarizing, we cannot strictly exclude that a detergent may isolate ordered domains without major changes, but this would be the exception rather than the rule and seems rather unlikely. First, the lipid mixture would need to show favorable properties. Second, the detergent would be required to possess very specific properties with respect to at least two independent parameters. If more membrane components are involved than the two considered here, even more parameters would need to fit in order to eliminate detergent effects. Reports^{3-5,14} on different model systems have claimed both the presence and the absence of marked changes in ordered domains upon addition of certain detergents. Even if there is, by chance, an appropriate detergent for a given membrane and temperature, there remains the problem of its identification. As detergent-induced effects may either enhance or diminish ordered domains, it is not justified

to assume that the detergent yielding the largest DRM fraction is the correct one. In any case, it is obvious that different detergents will yield different DRMs from the same rafts.

Conclusions

Our calculations yield a number of useful rules:

(1) Thermodynamically, resistance of a lipid against solubilization by a detergent depends only on the affinity of this lipid to the micellar phase, which is quantified by the solubilization boundary of the pure lipid, X_e^{sol} . The presence of another, more susceptible lipid plays no role.

(2) Preferential solubilization of a fluid lipid from mixed membranes increases the relative concentration of the order-preferring lipid there, which may give rise to the growth or appearance of ordered domains.

(3) Detergent-induced formation of ordered domains before the onset of solubilization cannot be explained on the basis of ideal mixing but may result from unfavorable interactions between detergent and order-preferring lipid in the fluid domains.

(4) Thermodynamic (or kinetic) resistance against the detergent is a necessary but not a sufficient criterion for obtaining DRMs. Another key parameter is the size of the resistant membrane fragments. Thermodynamically resistant particles may be so small that they are technically soluble. Cholesterol might (among many other effects) increase the size of resistant particles, thus making them extractable by centrifugation.

(5) Anomalously low resistance of lipids somewhat below their melting temperature could be explained by the accumulation of detergent within minor, fluidlike defect structures between crystal-like gel clusters.

Acknowledgment. We are indebted to Profs. Félix Goñi and Erwin London for their important and constructive comments on the manuscript. This work was supported by the European Commission (Grant No. QLK3-CT-2002-01989 to S.K.) and the Swiss National Science Foundation (Grant No. 31-67216 to H.H.).

Supporting Information Available: Additional results and derivations. This material is available free of charge via the Internet at <http://pubs.acs.org>.

JA052764Q

Supporting Information for “A Quantitative Model Describing the Selective Solubilization of Membrane Domains”

Sandro Keller,[†] Alekos Tsamaloukas,[‡] and Heiko Heerklotz^{*,‡}

[†] Research Institute of Molecular Pharmacology FMP, Robert-Rössle-Strasse 10, 13125 Berlin, Germany

[‡] Biozentrum der Universität Basel, Klingelbergstrasse 50/70, 4056 Basel, Switzerland

* heiko.heerklotz@unibas.ch

1.	<i>Additional results</i>	S2
1.1	<i>Plotting the results as a function of the total detergent concentration</i>	S2
1.2	<i>Special case keeping σ largely unchanged upon solubilization of f</i>	S2
2.	<i>Equations and derivations</i>	S3
2.1	<i>Fit equations</i>	S3
2.2	<i>Derivation of basic partition coefficients from input parameters</i>	S4
2.3	<i>Derivation of eq 9</i>	S5

1. ADDITIONAL RESULTS

1.1 Plotting the results as a function of the total detergent concentration

As discussed in the Theory section, it has several advantages to plot the results as a function of X_e . For the interpretation of these figures, it is, however, important to be aware of the fact that the often-observed linear changes of partial concentrations with the total detergent concentration, c_D , as depicted in Figure S1, appear curved using an X_e abscissa (cf. Figure 1). In the X_e plot, the extensive **om** range, which is typical of detergent resistance (where the resistant fraction is hardly changed over a broad range in detergent concentration), is condensed compared with the ranges at lower detergent concentration.

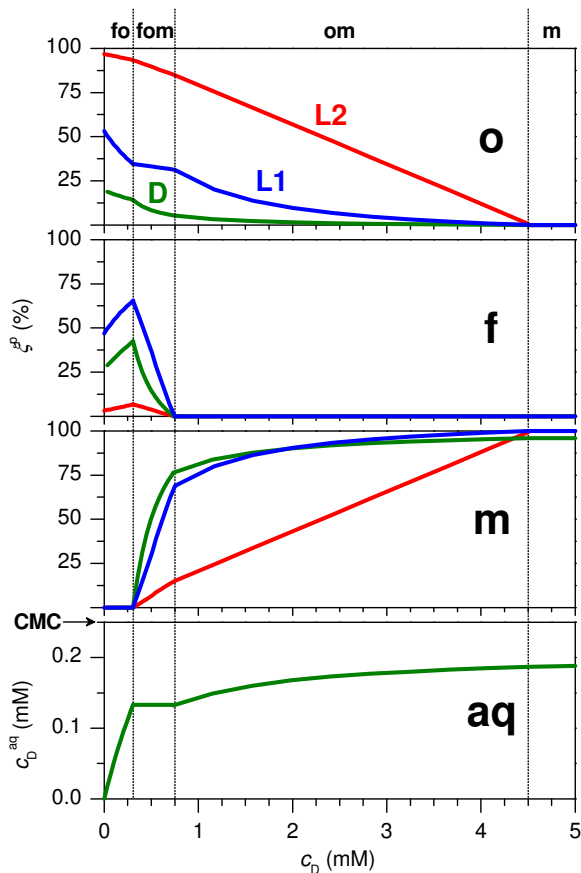


Figure S1. The results shown in Figure 1 plotted as a function of the total detergent concentration, c_D . The input parameters are $c_{L1} = c_{L2} = 0.5$ mM, $CMC = 0.23$ mM, $X_e^{sat}(L1) = 0.29$, $X_e^{sol}(L1) = 0.63$, $X_e^{sat}(L2) = 0.10$, $X_e^{sol}(L2) = 0.90$, $\zeta^{so}(0) = 75\%$, and $K_{L2}^{f/o} = 0.1$. The bottom panel gives the aqueous detergent concentration, c_D^{aq} , rather than the fraction of detergent in the aqueous phase, ζ_D^{aq} .

1.2 Special case keeping **o** largely unchanged upon solubilization of **f**

In the Discussion, we derive a specific combination of input parameters so that the different detergent-induced effects on **o** domains cancel out each other, and the abundance and composition of the **o** phase remain virtually unchanged upon solubilization of the **f** domains. This special case corresponds to the general assumption that DRMs are equivalent to rafts, but there is no strong argument for the conjecture that these very specific conditions are, by chance, fulfilled in a biological membrane sample interacting with a selected detergent. Figure S2 illustrates the resulting plot for this special case.

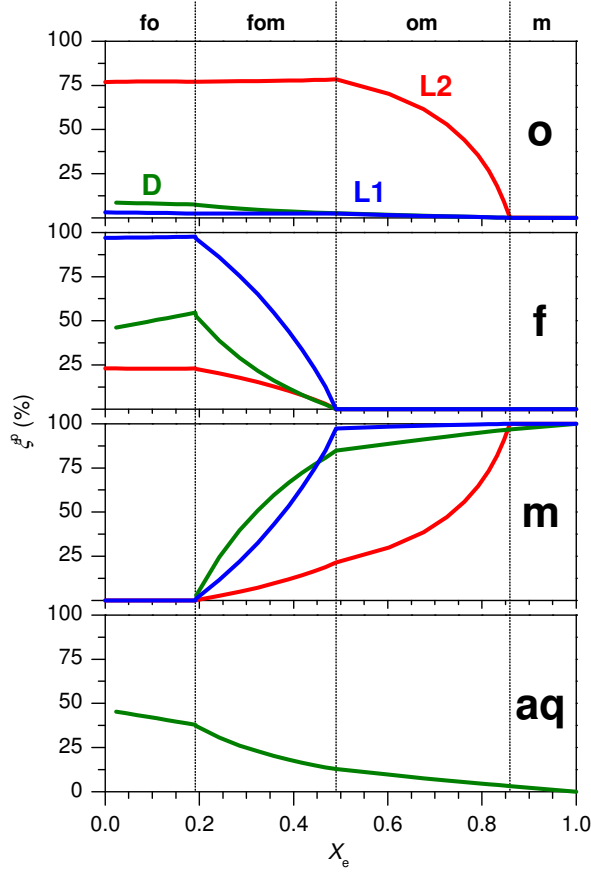


Figure S2. Results calculated for CMC = 0.23 mM, $X_e^{\text{sat}}(\text{L1}) = 0.29$, $X_e^{\text{sol}}(\text{L1}) = 0.63$, $X_e^{\text{sat}}(\text{L2}) = 0.10$, $X_e^{\text{sol}}(\text{L2}) = 0.93$, $\zeta^{\text{fo}}(0) = 40\%$, $K_{\text{L2}}^{\text{f/o}} = 0.2$, and $\rho_{\text{D/L2}}^{\text{f}} = 2.5$ kJ/mol.

2. EQUATIONS AND DERIVATIONS

2.1 Fit equations

In the Theory section, we explain the derivation of the **fom** model. The complete set of equations is given by the partition coefficients,

$$K_{\text{D}}^{\text{aq/o}} = \frac{c_{\text{D}}^{\text{aq}} (c_{\text{D}}^{\text{o}} + c_{\text{L1}}^{\text{o}} + c_{\text{L2}}^{\text{o}})}{55.5 \text{ M} \times c_{\text{D}}^{\text{o}}} \quad (\text{S1}),$$

$$K_{\text{D}}^{\text{m/o}} = \frac{c_{\text{D}}^{\text{m}} (c_{\text{D}}^{\text{o}} + c_{\text{L1}}^{\text{o}} + c_{\text{L2}}^{\text{o}})}{(c_{\text{D}}^{\text{m}} + c_{\text{L1}}^{\text{m}} + c_{\text{L2}}^{\text{m}}) c_{\text{D}}^{\text{o}}} \quad (\text{S2}),$$

$$K_{\text{D}}^{\text{f/o}} = \frac{c_{\text{D}}^{\text{f}} (c_{\text{D}}^{\text{o}} + c_{\text{L1}}^{\text{o}} + c_{\text{L2}}^{\text{o}})}{(c_{\text{D}}^{\text{f}} + c_{\text{L1}}^{\text{f}} + c_{\text{L2}}^{\text{f}}) c_{\text{D}}^{\text{o}}} \quad (\text{S3}),$$

$$K_{L1}^{m/o} = \frac{c_{L1}^m (c_D^o + c_{L1}^o + c_{L2}^o)}{(c_D^m + c_{L1}^m + c_{L2}^m) c_{L1}^o} \quad (S4),$$

$$K_{L1}^{f/o} = \frac{c_{L1}^f (c_D^o + c_{L1}^o + c_{L2}^o)}{(c_D^f + c_{L1}^f + c_{L2}^f) c_{L1}^o} \quad (S5),$$

$$K_{L2}^{m/o} = \frac{c_{L2}^m (c_D^o + c_{L1}^o + c_{L2}^o)}{(c_D^m + c_{L1}^m + c_{L2}^m) c_{L2}^o} \quad (S6),$$

$$K_{L2}^{f/o} = \frac{c_{L2}^f (c_D^o + c_{L1}^o + c_{L2}^o)}{(c_D^f + c_{L1}^f + c_{L2}^f) c_{L2}^o} \quad (S7),$$

and by the equations of mass balance,

$$c_D = c_D^o + c_D^f + c_D^m + c_D^{aq} \quad (S8),$$

$$c_{L1} = c_{L1}^o + c_{L1}^f + c_{L1}^m \quad (S9),$$

$$c_{L2} = c_{L2}^o + c_{L2}^f + c_{L2}^m \quad (S10).$$

2.2 Derivation of basic partition coefficients from input parameters

This section describes how the basic partition coefficients, $K_D^{aq/o}$, $K_D^{f/o}$, $K_D^{m/o}$, $K_{L1}^{f/o}$, $K_{L1}^{m/o}$, and $K_{L2}^{m/o}$, are calculated from the input parameters, CMC, $X_e^{sat}(L1)$, $X_e^{sol}(L1)$, $X_e^{sat}(L2)$, $X_e^{sol}(L2)$, $\zeta^o(0)$, and $K_{L2}^{f/o}$.

(1) The CMC yields the partition coefficient of the detergent between micelles and the aqueous phase, $K_D^{m/aq}$. For pure detergent micelles, $X_D^m = 1$, and the total concentration of a dilute aqueous solution is always 55.5 M, so that

$$K_D^{aq/o} = \frac{K_D^{m/o}}{K_D^{m/aq}} = K_D^{m/o} \frac{CMC}{55.5 \text{ M}} \quad (S11).$$

(2,3) The partition coefficients of the lipids and the detergent between membranes and micelles are related to the onset and completion of solubilization of the pure lipids. During **fm** coexistence in an L1/D system, the detergent mole fractions are $X_D^m = X_e^{sol}(L1)$ in micelles and $X_D^f = X_e^{sat}(L1)$ in membranes, and the corresponding lipid mole fractions are $X_{L1}^m = 1 - X_e^{sol}(L1)$ and $X_{L1}^f = 1 - X_e^{sat}(L1)$, respectively. This gives

$$K_D^{f/o} = \frac{K_D^{m/o}}{K_D^{m/f}} = K_D^{m/o} \frac{X_e^{sat}(L1)}{X_e^{sol}(L1)} \quad (S12),$$

$$K_{L1}^{m/o} = K_{L1}^{f/o} K_{L1}^{m/f} = K_{L1}^{f/o} \frac{1 - X_e^{sol}(L1)}{1 - X_e^{sat}(L1)} \quad (S13).$$

(4,5) By analogy, the solubilization boundaries of pure L2 in a homogeneous ordered phase, $X_D^m = X_e^{sol}(L2)$ and $X_D^o = X_e^{sat}(L2)$, yield

$$K_D^{m/o} = \frac{X_e^{\text{sol}}(\text{L2})}{X_e^{\text{sat}}(\text{L2})} \quad (\text{S14}),$$

$$K_{\text{L2}}^{m/o} = \frac{1 - X_e^{\text{sol}}(\text{L2})}{1 - X_e^{\text{sat}}(\text{L2})} \quad (\text{S15}).$$

(6,7) To quantify the preference of the lipids for the **o** versus the **f** phase in the absence of detergent, $\xi^{\text{o}}(0)$ and $K_{\text{L2}}^{\text{f/o}}$ are selected. Then, $K_{\text{L1}}^{\text{f/o}}$ is calculated according to

$$K_{\text{L1}}^{\text{f/o}} \equiv \frac{X_{\text{L1}}^{\text{f}}}{X_{\text{L1}}^{\text{o}}} = \frac{\xi^{\text{o}} c_{\text{L}} - K_{\text{L2}}^{\text{f/o}} c_{\text{L2}}^{\text{o}}}{\xi^{\text{o}} c_{\text{L}} - c_{\text{L2}}^{\text{o}}} \quad (\text{S16}).$$

2.3 Derivation of eq 9

We consider the three-stage model of solubilization of a single lipid. If L2 forms an **o** membrane and is solubilized in a phase sequence of **o**, **om**, and **m**, eqs S14 and S15 yield $X_e^{\text{sat}}(\text{L2})$ and $X_e^{\text{sol}}(\text{L2})$ as

$$X_e^{\text{sat}}(\text{L2}) = \frac{1 - K_{\text{L2}}^{\text{o/m}}}{1 - K_{\text{L2}}^{\text{o/m}} K_D^{\text{m/o}}} \quad (\text{S17}),$$

$$X_e^{\text{sol}}(\text{L2}) = \frac{K_D^{\text{m/o}} (1 - K_{\text{L2}}^{\text{o/m}})}{1 - K_{\text{L2}}^{\text{o/m}} K_D^{\text{m/o}}} \quad (\text{S18}).$$

We may now convert the mole fraction, X_e^{sol} , into the mole ratio, R_e^{sol} , according to

$$R_e^{\text{sol}}(\text{L2}) \equiv \frac{c_{\text{D}}^{\text{m}}(\text{om|m})}{c_{\text{L2}}^{\text{m}}(\text{om|m})} = \frac{X_e^{\text{sol}}(\text{L2})}{1 - X_e^{\text{sol}}(\text{L2})} = \frac{K_D^{\text{m/o}} (K_{\text{L2}}^{\text{o/m}} - 1)}{K_D^{\text{m/o}} - 1} \quad (\text{S19}),$$

which corresponds to eq 9 in the Discussion.

Nonideal mixing in multicomponent lipid/detergent systems

Alekos Tsamaloukas¹, Halina Szadkowska, and Heiko Heerklotz

¹ Biozentrum of the University of Basel, Division of Biophysical Chemistry, Klingelbergstrasse 70, CH-4056 Basel, Switzerland

E-mail: alekos.tsamaloukas@unibas.ch

Abstract. A detailed understanding of the mixing properties of membranes to which detergents are added is mandatory to improve the application and interpretation of detergent based protein or lipid extraction assays. For Triton X-100 (TX-100), a nonionic detergent frequently used in the process of solubilizing and purifying membrane proteins and lipids, we present here a detailed study of the mixing properties of binary and ternary lipid mixtures by means of high-sensitivity isothermal titration calorimetry (ITC). To this end the partitioning thermodynamics of TX-100 molecules from the aqueous phase to lipid bilayers composed of various mixtures of 1-palmitoyl-2-oleoyl-*sn*-glycero-3-phosphocholine (POPC), egg-sphingomyelin (SM), and cholesterol (cho) are characterized. Composition dependent partition coefficients K are analyzed within the frame of a thermodynamic model developed to describe nonideal mixing in multicomponent lipid/detergent systems. The results imply that POPC, fluid SM, and TX-100 mix almost ideally (nonideality parameters $|\rho_{\alpha/\beta}| < RT$). However, favourable SM/cho ($\rho_{\text{SM}/\text{cho}} \leq -6 RT$) and unfavourable PC/cho interactions ($\rho_{\text{PC}/\text{cho}} = 2 RT$) may under certain conditions cause POPC/TX-100 enriched domains to segregate from SM/cho-enriched ones. TX-100/cho contacts are unfavourable ($\rho_{\text{cho}/\text{TX}} = 4 RT$) so that the system tends to avoid them. That means, addition of TX-100 promotes the separation of SM/cho- from PC/TX-100-rich domains. It appears that cho/detergent interactions are a crucial parameter governing the abundance and composition of detergent-resistant membrane patches.

PACS numbers: 87.16.Dg

Submitted to: *J. Phys.: Condens. Matter*

1. Introduction

The use of detergents is common practice in membrane research to study integral membrane proteins and lipids [1, 2, 3]. Selective solubilization techniques, that extract certain lipids and proteins but leave others in unsolubilized membrane patches have a great potential. First, they allow one to optimize the isolation of a membrane component. Second, they may provide insight into preferential interactions between different membrane constituents, such as lipids and proteins, in the original membrane. More than 30 years ago Steck and co-workers demonstrated in two careful experimental studies [4, 5] that the application of different reagents to isolated human erythrocyte membranes (also termed ghost membranes) can be used to selectively solubilize different proteins from this membrane. In their studies they found a “reciprocal solubilization profile”: Protein perturbants like sodium hydroxide and others extracted mainly polar (hydrophilic) polypeptides from the membrane. In contrast, nonionic detergents like Triton X-100 (TX-100) mainly solubilized glycerolipid and glycoprotein, while in parallel yielding sphingolipid/cholesterol enriched aggregates containing other classes of proteins as unsolubilized residues. With great caution concerning their experimental findings these authors noted that it is however speculative “whether these aggregates arise by demixing following detergent action or exist in some form in the original ghost.”

Over the last ~ 10 years a vast body of literature has evolved that is essentially based on the assumption that so-called lipid raft domains [6, 7, 8, 9] can be isolated as detergent-resistant membrane (DRMs) patches. However, it should be taken into account that the action of a detergent on a membrane system will interfere with it and probably alter it as well (see, e.g., [7, 10, 11] for a discussion of the DRM=raft hypothesis). Studies employing model membrane systems have clearly demonstrated the ability of TX-100 to promote the formation of domains [12, 13] in a previously homogenous membrane. Furthermore, only recently it was shown by van Rheenen et al. [14] that detergent treatment leads to a clustering of the phospholipid phosphatidylinositol 4,5-bisphosphate (PIP₂) *in vivo*.

The complexity of the issue as well as its great practical potential are illustrated by the finding that different detergents can give rise to compositionally different DRMs from the same membrane [15, 16, 17]. If lipid/detergent (and in turn protein/detergent) interactions and their effects on fractions upon selective solubilization can be understood in a quantitative manner it may eventually become possible to rationally predict the optimum detergent for a given protein of interest. As a step in this direction Keller et al. [18] have recently established a simple thermodynamic model describing the selective solubilization of membrane domains. These calculations suggest that nonideal mixing effects are necessary to explain the induction of ordered domains by a detergent before the onset of membrane solubilization. However, to date very few experimental data dealing with nonideal mixing in membranes to which detergents are added have been published. There is a clear need for such data in order to extend the model further.

Binary mixtures of detergents (D) and unsaturated PC were treated in [19, 20, 21, 22, 23] and suggested only slightly nonideal mixing with nonideality parameters (for pairwise interactions) of typically $\rho_{PC/D} \sim -0.7 RT$. A key for a better understanding of selective solubilization are detergent/cholesterol interactions, but these cannot be studied in binary systems because pure cholesterol forms no membranes. Here we overcome this problem by establishing a formalism suitable to derive nonideality parameters in ternary and quaternary systems. As such, at the example of TX-100 that is used frequently in model system studies [24, 25, 26, 27] as well as in the protein extraction procedure from biological membranes [28, 29], we study here in detail the mixing properties of TX-100 additive membranes by means of isothermal titration calorimetry (ITC). The interaction parameters we collect from the modeling of our data provide a quantitative basis for the ability of a detergent to alter or induce domains in a membrane. Of course, great care must be taken when discussing the outcome of biochemical protocols in terms of fundamental physical parameters established in model systems. Nevertheless, biophysical model studies are valuable for recognizing problems, designing experiments, and understanding results obtained *in vivo*.

2. Materials and Methods

2.1. Substances and sample preparation

The lipids 1-palmitoyl-2-oleoyl-*sn*-glycero-3-phosphocholine (POPC) and egg-sphingomyelin (eSM) were purchased from Avanti Polar Lipids, Alabaster, AL. Cholesterol (cho) and polyethylene glycol tert-octylphenyl ether (Triton X-100, TX-100) were from Fluka, Buchs, Switzerland. Mixtures of POPC and cho were prepared by addition of cho to the dry lipid powder, resuspension in chloroform/methanol, and consecutive drying under a gentle stream of nitrogen. Similarly, mixtures of POPC and eSM were prepared by adding appropriate amounts of eSM to the dry POPC lipid powder. All samples were held under vacuum for at least 12 hours for further drying. The composition of the samples was checked by weighing the dry material before and after an addition. The dry lipid mixtures used for the uptake assays were suspended in 100 mM NaCl, 10 mM Tris buffer at pH 7.4 by gentle vortexing to reach a lipid concentration of 15 mM, i.e., $c_{PC} = 15$ mM for cho- and $c_{PC} + c_{SM} = 15$ mM for SM-containing mixtures. In case of the samples used in the release as well as in the Rowe assay [30], the dry lipid film was suspended in a 1.5 mM TX-100 stock solution (or 0.25 mM, 2.5 mM, and 4 mM for experiments with pure POPC vesicles) to yield a lipid concentration (as defined above) of 15 mM. The values for the mole fraction of bound TX-100 in the membrane, X_{TX}^b , thus achieved are calculated afterwards based on the results obtained for the respective partition coefficient. After five consecutive freeze-thaw cycles, large unilamellar vesicles (LUVs) were prepared by ten extrusion runs through two stacked Nuclepore polycarbonate filters with a pore diameter of approximately 100 nm in a Lipex extruder (Northern Lipids Inc., Vancouver, Canada).

Extrusion was performed at 50°C for samples containing eSM due to its chain melting temperature of $T_m \sim 39^\circ\text{C}$ [13] and at room temperature for those containing POPC and cho.

2.2. ITC and DSC measurements

Isothermal titration calorimetry (ITC) experiments were performed on a VP ITC calorimeter from MicroCal, Inc. (Northampton, MA) [31, 32]. A total of 300 μL of lipid suspension is injected in aliquots of a few μL (typical injection protocol: $1 \times 1 \mu\text{L}$, $3 \times 5 \mu\text{L}$, and $28 \times 10 \mu\text{L}$) into a 1.4 mL cell containing either a TX-100 solution at concentration $c_{\text{TX}}^{\text{ini}} = 50 - 150 \mu\text{M}$ (uptake assay) or buffer (release assay) [33]. All partitioning experiments were conducted at 37°C (see below for explanation). Data are displayed as normalized heats, $Q_{\text{obs}}(c_L)$, with normalization to the total number of moles of material (including cho) injected. Blank experiments, i.e., titration of lipid vesicles into buffer showed small and constant heats of dilution so that instead of subtracting the $Q_{\text{obs}}(c_L)$ -values obtained in these experiments, a constant heat of dilution is introduced as a third parameter into the model outlined below. In addition to uptake and release experiments we have applied the Rowe protocol [30] as another independent way to determine the partition coefficient and enthalpy. Here the same LUVs as used in the release assay are titrated into solutions of different TX-100 concentration, $c_{\text{TX}}^{\text{cell}}$, loaded into the cell. The heat released or consumed upon the first 10 μL injection (the first 1 μL injection is not considered in the data evaluation) is plotted as a function of $c_{\text{TX}}^{\text{cell}}$. From the intercept with the $c_{\text{TX}}^{\text{cell}}$ -axis (total TX-100 concentration in the cell matches the free detergent concentration in the syringe) the partition coefficient can be calculated and the enthalpy is available from the slope of the curve (see the supporting information for details).

The differential scanning calorimetry (DSC) measurements were performed on a VP DSC calorimeter from MicroCal, Inc. (Northampton, MA) [34]. The sample cell of 0.5 mL was filled with a suspension of LUVs composed of mixtures of POPC and eSM with or without the above-mentioned TX-100 content in the membrane at a lipid concentration of 15 mM. For each sample a series of five consecutive scans with scan rates of 60, 30 and 10 K/h was performed and the instrument was operated in the high-gain mode. All traces shown were corrected by the results obtained in blank experiments, i.e., scans where both calorimeter cells are filled with buffer. Data are presented as apparent isobaric heat capacity c_p as a function of temperature T normalized to the SM concentration in the membrane.

2.3. Data analysis and curve fitting

Analysis of the raw ITC traces was performed using Origin for ITC provided with the instrument and the DSC traces were correspondingly analyzed using Origin for DSC. The normalized differential heats obtained from an integration of the power peaks resulting after each injection in an ITC experiment were exported to a Microsoft Excel

spreadsheet and analyzed therein similarly to what is detailed in [35]. For each SM- and cho-content in the membrane one release experiment was fitted globally against one uptake experiment. This procedure was repeated with (usually five) uptake experiments recorded at different $c_{\text{TX}}^{\text{ini}}$ as specified above. The partition coefficients and molar transfer enthalpies listed are accordingly mean values with estimated maximal errors of: $\delta(K) = 15\%$, and $\Delta(\Delta H) = \pm 2 \text{ kJ/mol}$, respectively.

3. Theory

3.1. Partitioning models

The partitioning of water-soluble substances into membranes (or their release from them) is described by different models [36]. Here we will use a model defined via:

$$X_{\text{TX}}^{\text{b}} \equiv \frac{c_{\text{TX}}^{\text{b}}}{c_{\text{L}} + c_{\text{TX}}^{\text{b}}} = K c_{\text{TX}}^{\text{w}}, \quad (1)$$

where the concentration of membrane bound TX-100, c_{TX}^{b} , is related to the amount of aqueous TX-100, c_{TX}^{w} , via the partition coefficient K . The total concentration of lipid (PC+cho, and PC+SM, respectively) quantified by the term c_{L} is assumed to be exclusively in the bilayer state, i.e., the aqueous concentration of lipid is assumed to be zero. We have omitted the constant factor $c_{\text{W}} = 55.5 \text{ M}$ in (1) describing the concentration of water in a dilute aqueous solution resulting from the general definition of the mole fraction partition coefficient: $K_{\text{X}} \equiv X_{\text{TX}}^{\text{b}}/X_{\text{TX}}^{\text{w}}$. Therefore the partition coefficients listed have the dimension: $[K] = (\text{mM})^{-1}$. For small concentrations of bound detergent, i.e., $c_{\text{TX}}^{\text{b}} \ll c_{\text{L}}$ the partition coefficient K defined by (1) approaches the mole-ratio partition coefficient defined as: $K \equiv c_{\text{TX}}^{\text{b}}/(c_{\text{L}}c_{\text{TX}}^{\text{w}})$ [36].

The mass conservation principle prescribes for the total TX-100 concentration within the calorimeter cell: $c_{\text{TX}}^{\text{tot}} = c_{\text{TX}}^{\text{w}} + c_{\text{TX}}^{\text{b}}$. Insertion into (1) yields a second-order polynomial in c_{TX}^{b} . The heat released or consumed upon an injection in an ITC experiment is linearly related to a change in the amount of bound detergent, $\Delta c_{\text{TX}}^{\text{b}}$, multiplied by the corresponding transfer enthalpy, ΔH . Normalizing the heats of each injection with respect to the amount of lipid injected into the cell during this particular injection, one obtains normalized differential heats, $Q_{\text{obs}}(c_{\text{L}})$. These can be modeled according to the general expression (see [35] for further details):

$$Q_{\text{obs}}(c_{\text{L}}) = \frac{\Delta c_{\text{TX}}^{\text{b}}}{\Delta c_{\text{L}}} \Delta H + Q_{\text{dil}}, \quad (2)$$

where the term Q_{dil} denotes a small (usually less than 5% of ΔH), constant heat of dilution arising in any ITC experiment from effects other than partitioning or specific binding. The three-parameter model as detailed in (2) is based on the assumption that both the partition coefficient and enthalpy are constant during the course of an experiment. This need not be fulfilled in the most general situation, see for instance [19] and [21] for the case of a composition dependent partition coefficient in binary mixtures. An extension to the case studied here, i.e., ternary mixtures is given below.

3.2. Composition-dependent K for a ternary mixture

We consider a lipid bilayer composed of POPC (the host fluid phase lipid), a second lipid denoted L_1 (either SM or cho), and study the uptake/release of TX-100 by this system. The following equation for K as a function of membrane-bound TX-100, X_{TX}^{b} , can be derived (see the appendix for further details):

$$K(X_{\text{TX}}^{\text{b}}, \zeta_{\text{L}}) = K_{\text{PC}}(X_{\text{TX}}^{\text{b}}) \exp \left\{ - \frac{(1 - X_{\text{TX}}^{\text{b}})^2 \zeta_{\text{L}}}{RT(1 + \zeta_{\text{L}})} \left[\rho_{L_1/\text{TX}} - \rho_{\text{PC}/\text{TX}} - \frac{\rho_{\text{PC}/L_1}}{1 + \zeta_{\text{L}}} \right] \right\}, \quad (3)$$

where $\zeta_{\text{L}} = X_{L_1}/X_{\text{PC}} = n_{L_1}/n_{\text{PC}}$ denotes the mole ratio of the two lipids in the membrane, and $K_{\text{PC}}(X_{\text{TX}}^{\text{b}})$ stands for the partition coefficient of TX-100 into a POPC membrane. The nonideality parameters (given as multiples of RT ; R being the universal gas constant and T the absolute temperature) for pairwise interactions are denoted by $\rho_{\alpha/\beta}$ and are in general temperature dependent. They have the general form [37]:

$$\rho_{\alpha/\beta} = \frac{N_{\text{A}}}{RT} z \left(\epsilon_{\alpha/\beta} - \frac{\epsilon_{\alpha/\alpha} + \epsilon_{\beta/\beta}}{2} \right), \quad (\alpha, \beta) \hat{=} \text{PC}, L_1, \text{TX}, \quad (4)$$

where, e.g., $\epsilon_{\alpha/\beta}$ denotes the energy of interaction of component α with component β (in kJ), N_{A} is Avogadro's number, and z a coordination number (the number of lipid or detergent nearest neighbours).

In principle it is possible to insert (3) via the K -dependent value of c_{TX}^{b} into the model function (2) used to fit the ITC traces (solving (1) under the above-mentioned constraint for $c_{\text{TX}}^{\text{tot}}$ yields a functional relation: $c_{\text{TX}}^{\text{b}} = f(K, c_{\text{L}}, c_{\text{TX}}^{\text{tot}})$). However, this remains an implicit equation since the partition coefficient K depends on c_{TX}^{b} via (3) [21]. The differentiation with respect to c_{L} necessary in (2) can in principle be carried out using standard procedures for differentiating implicit functions [38] as performed for example in [21]. Following similar reasoning as put forward in [35] we have decided to refrain from fitting the data with a composition-dependent K and to afterwards analyze the trends observed in a series of experiments at different concentrations according to (3).

4. Results

4.1. DSC

To avoid dealing with a membrane consisting of two coexisting phases, we checked the thermotropic behaviour of the POPC/SM-mixtures by means of DSC prior to performing the ITC experiments. Representative results for the mixtures used in the uptake as well as those in the release protocols are shown in figure 1 recorded at a scan rate of 30 K/h. As suggested by pure POPC melting at $T_{\text{m}} \sim -2^{\circ}\text{C}$ [39] and eSM melting at $T_{\text{m}} \sim 39^{\circ}\text{C}$ [13], we observe predominantly the high-temperature flank of the chain melting peak of the investigated binary lipid mixtures. The temperature where the transition is completed increases with increasing SM-content. In the case of the sample with $X_{\text{SM}} = 0.2$, the shoulder shifts from $T_{\text{s}} \sim 10^{\circ}\text{C}$ up to $T_{\text{s}} \sim 14^{\circ}\text{C}$ upon TX-100

inclusion ($X_{\text{TX}}^{\text{b}} \sim 0.08$ as calculated with the mean value of the partition coefficient K given below) in the membrane. DSC traces have virtually returned to the baseline at 37°C . Therefore we point out that possible detrimental effects of a chain melting transition on both thermodynamic parameters accessible by ITC, i.e., the partition coefficient K and transfer enthalpy ΔH , can be ruled out for the samples studied here.

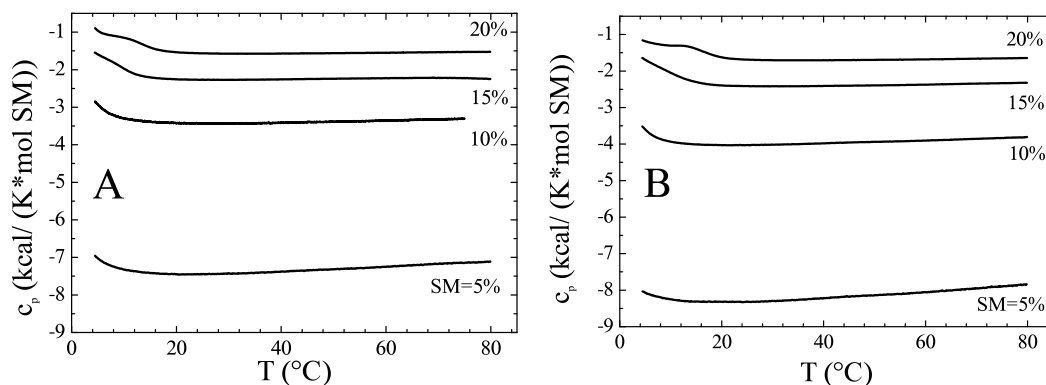


Figure 1. The apparent isobaric heat capacity c_p for mixtures of POPC and eSM with the eSM mole fraction, X_{SM} , as depicted in the plot. Panel A: Experiments with 15 mM LUVs without TX-100 bound to the membrane, and Panel B for samples including TX-100 with a mole fraction of bound detergent of $X_{\text{TX}}^{\text{b}} \sim 0.08$.

4.2. ITC

4.2.1. POPC/TX-100 interaction Figure 2 shows representative raw ITC data as well as the global analysis of one uptake and release experiment with POPC vesicles at 37°C . For the release assay, LUVs were prepared in a 1.5 mM TX-100 solution. Based on the mean value for the partition coefficient as obtained in the global fits, this corresponds to a membrane with a mole fraction of bound TX-100 of $X_{\text{TX}}^{\text{b}} \sim 0.08$. For the uptake experiment, the literature value for POPC/TX-100 interaction from [13] was used to decide upon the $c_{\text{TX}}^{\text{ini}}$ -value. This experiment was consequently conducted at $c_{\text{TX}}^{\text{ini}} = 75 \mu\text{M}$ in order to achieve an initial TX-100 content in the membrane close to that of the release sample. Additionally figure 2 shows the raw data obtained with the Rowe protocol injecting the same vesicles as used for the release assays into solutions with different TX-100 concentration, $c_{\text{TX}}^{\text{cell}}$, loaded into the cell. In panel E of figure 2 the heats resulting from an integration of the power peaks displayed in D are plotted as a function of $c_{\text{TX}}^{\text{cell}}$. The intercept with the $c_{\text{TX}}^{\text{cell}}$ -axis corresponds to the free TX-100 concentration present in the syringe and can be directly used to calculate K . Based on the partitioning models explained in the theory section, the slope of the linear regressions shown in panel E of figure 2 can be used to determine the transfer enthalpy, ΔH (see the supporting information for details). The dependence of the partition coefficient and transfer enthalpy on the mole fraction of membrane-bound TX-100, X_{TX}^{b} ,

is summarized in figure 3. Within the estimated accuracy of the two model parameters, the three different experimental assays utilized in this work yield consistent results. The resulting mean values are: $K = (1.2 \pm 0.2) \text{ (mM)}^{-1}$ for the partition coefficient, and $\Delta H = (12 \pm 2) \text{ kJ/mol}$ for the transfer enthalpy in agreement with the literature [13], respectively.

The small deviations that are observed in figure 3 do not allow us to speculate about asymmetric TX-100 incorporation into the membrane, slow detergent flip-flop, and other possible effects conceivable to explain deviations between uptake and release assay [33]. Given the restriction to small X_{TX}^{b} and the experimental uncertainty of K , the constancy of the mole fraction partition coefficient does not rule out that the system is equally well described by a constant mole-ratio partition coefficient (data not shown). Uptake experiments have to be carried out well below the critical micelle concentration (CMC) of TX-100 at 37°C (CMC \sim 230 μM , data not shown) but above $c_{\text{TX}}^{\text{ini}} \sim 50 \mu\text{M}$ to achieve a satisfactory heat signal. Release experiments have to be performed well below the onset of membrane solubilization at $(X_{\text{TX}}^{\text{b}})_{\text{sat}} = 0.29$ given in [13]. For membranes with $X_{\text{TX}}^{\text{b}} \leq 0.05$ the heat signals obtained in a release assay are rather small, so that we have instead applied the Rowe protocol [30] in the small X_{TX}^{b} -regime.

4.2.2. POPC/SM/TX-100 interaction Figure 4 shows the buffer/membrane partition coefficient for TX-100 and the corresponding molar transfer enthalpy as a function of the mole fraction of SM in the membrane, X_{SM} . The TX-100 content in the membrane was $X_{\text{TX}}^{\text{b}} \sim 0.08$ as calculated with the value for the partition coefficient obtained from the global analysis of the data shown in figure 4. Within the assumed accuracy of the parameters, both parameters are independent of the SM mole fraction in the membrane. Mean values for the two parameters are: $K = (1.2 \pm 0.2) \text{ (mM)}^{-1}$ and $\Delta H = (12 \pm 2) \text{ kJ/mol}$, respectively.

4.2.3. POPC/cho/TX-100 interaction In figure 5 the buffer/membrane partition coefficient for TX-100 and the corresponding molar transfer enthalpy are shown as a function of the mole fraction of cho in the membrane, X_{Cho} . Based on the values collected for the partition coefficients for the various membranes investigated, the mole fraction of TX-100 in the membrane varies between $X_{\text{TX}}^{\text{b}} \sim 0.06$ and $X_{\text{TX}}^{\text{b}} \sim 0.10$. While the partition coefficient decreases within the studied X_{Cho} -interval from $K = (1.2 \pm 0.2) \text{ (mM)}^{-1}$ at $X_{\text{Cho}} = 0$ to $K = (0.5 \pm 0.1) \text{ (mM)}^{-1}$ at $X_{\text{Cho}} = 0.33$, a concomitant increase ($\sim 2.2\times$) of the transfer enthalpy is observed.

5. Discussion

5.1. Pair interaction parameters for PC/SM/cho/TX-100

Our main goal is to provide a complete set of 6 nonideality parameters describing the mixing properties of PC/SM/cho membranes in the absence and presence of TX-100.

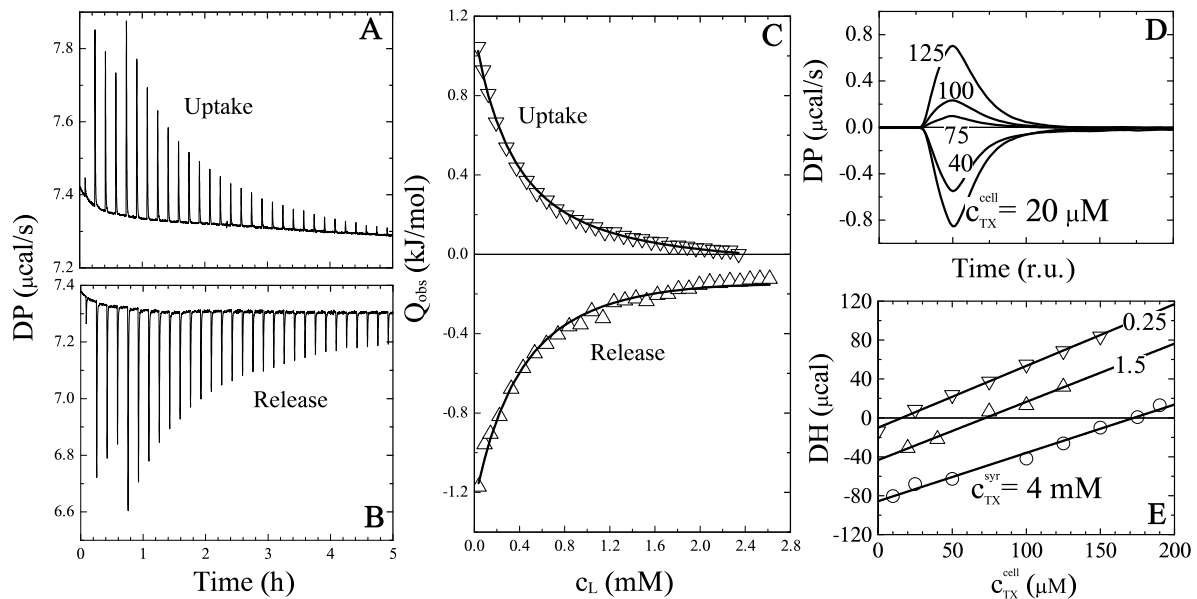


Figure 2. Experimental data of TX-100 interacting with POPC vesicles at $T = 37^\circ\text{C}$. Panels A,B: Compensation heat power, DP, versus time for a typical injection protocol of: $1 \times 1 \mu\text{L}$, $3 \times 5 \mu\text{L}$, and $26 \times 10 \mu\text{L}$. C: Global analysis of the integrated, normalized heats of ITC uptake (∇) and release (Δ) assay. Data fitting (solid lines) according to a X_{TX}^b -based partitioning model for a mole fraction of membrane-bound TX-100: $X_{\text{TX}}^b \sim 0.08$. Panel D: Raw experimental data of the Rowe protocol injecting $10 \mu\text{L}$ POPC vesicles incubated with $c_{\text{TX}}^{\text{syr}} = 1.5 \text{ mM}$ (total TX-100 concentration in the syringe) into solutions with different TX-100 concentration, $c_{\text{TX}}^{\text{cell}}$, loaded into the cell (all peaks are shifted such that the peak maximum coincides with time point $t = 0$; therefore the x-axis is scaled in r.u.). Panel E: Plot of the heats resulting from an integration of the power peaks as shown in D for vesicles incubated with: 0.25 mM (∇), 1.5 mM (Δ), and 4 mM (\circ) TX-100 solutions. Solid lines in E correspond to linear regressions to the data.

We will therefore discuss the observed composition-dependent variations of K within the framework of the thermodynamic model outlined in the theory section. The dependence of K on X_{L_1} will be investigated. Since the mole fractions of the species present in the membrane add up to unity, we can transform (3) into:

$$K(X_{L_1}) = K_{\text{PC}}(X_{\text{TX}}^b) \times \exp \left\{ - \frac{(1 - X_{\text{TX}}^b)(1 - X_{\text{TX}}^b - X_{L_1}) X_{L_1}}{RT} \left[\frac{\rho_{L_1/\text{TX}} - \rho_{\text{PC}/\text{TX}}}{1 - X_{\text{TX}}^b - X_{L_1}} - \frac{\rho_{\text{PC}/L_1}}{1 - X_{\text{TX}}^b} \right] \right\}. \quad (5)$$

For the two ternary mixtures we will use $X_{\text{TX}}^b = 0.08$ as the mole fraction of bound TX-100 present in our experiments to transform (5) into a simple, analytical function of one variable: X_{L_1} , i.e., either X_{SM} or X_{Cho} .

The thermodynamic parameters characterizing the system PC/SM/TX-100 show no significant deviations (within the studied X_{SM} -interval) from the values obtained for

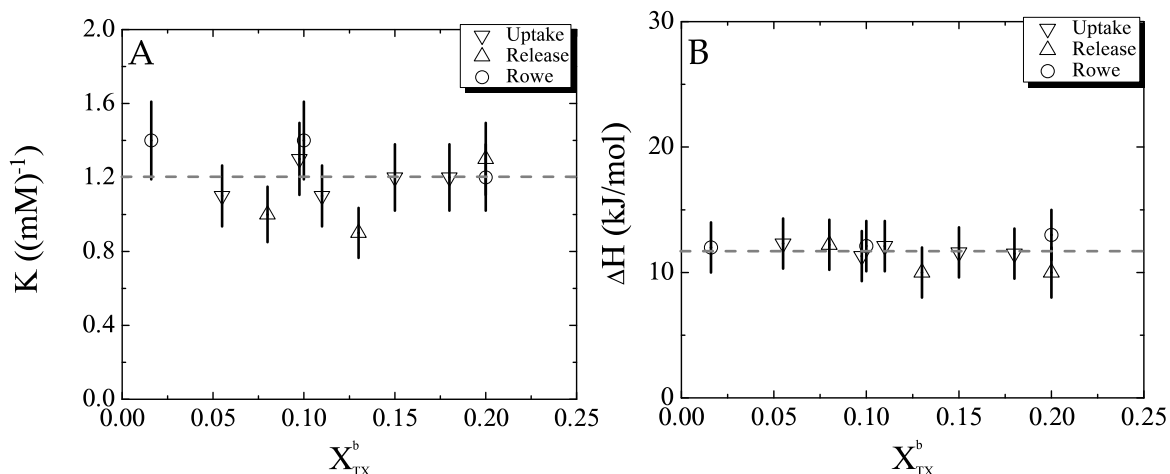


Figure 3. Plot of the buffer/membrane partition coefficient K (Panel A) and partition enthalpy ΔH (Panel B) as a function of the mole fraction of bound TX-100 in the membrane, X_{TX}^{b} , determined at $T = 37^\circ\text{C}$ for POPC LUVs. Results obtained with the three different assays are shown: fit parameters collected for uptake (∇), release (Δ), and Rowe (\circ) protocol. Dashed lines correspond to the mean values for K and ΔH obtained from global fits to the uptake and release data with errors as given in the main text.

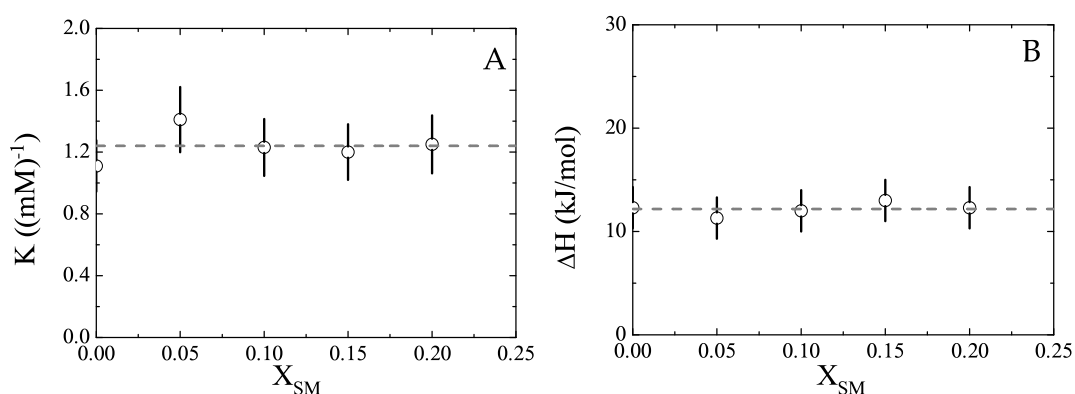


Figure 4. Panel A: The buffer/membrane partition coefficient for TX-100, K , and the molar enthalpy change of transfer, ΔH (Panel B), as a function of the mole fraction of SM, X_{SM} , in the membrane measured at $T = 37^\circ\text{C}$ with a mole fraction of bound TX-100, $X_{\text{TX}}^{\text{b}} \sim 0.08$. Data points correspond to the values obtained in global fits to uptake/release data (see text). Dashed lines correspond to the apparent mean value of K and ΔH , respectively.

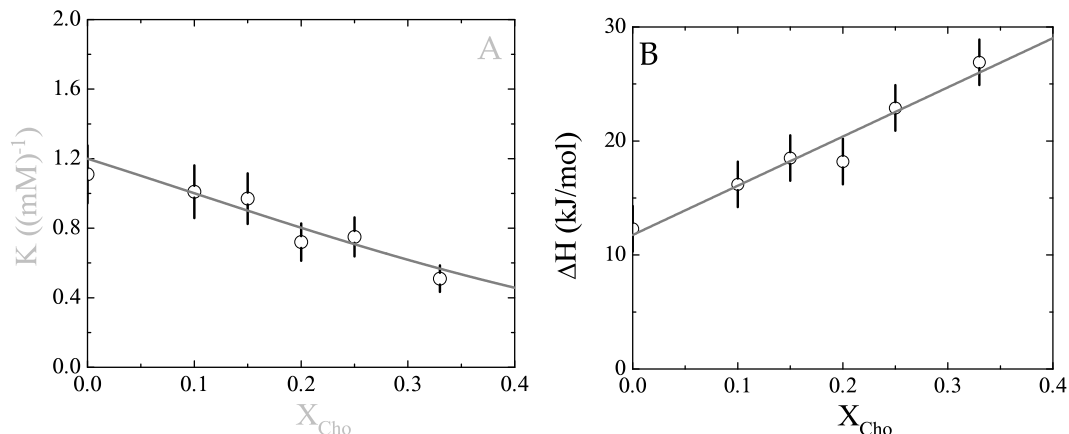


Figure 5. The buffer/membrane partition coefficient for TX-100, K (Panel A), and the molar enthalpy change of transfer, ΔH (Panel B), as a function of the mole fraction of cho, X_{cho} , in the membrane measured at $T = 37^\circ\text{C}$ with a mole fraction of bound TX-100, $X_{\text{TX}}^{\text{b}} \sim 0.08$. Data points correspond to the values obtained in global fits to uptake/release data (see text). Panel B: One-parameter fit of K as a function of X_{cho} according to (5) using fixed values of $K_{\text{PC}} = 1.2 (\text{mM})^{-1}$, $\rho_{\text{PC}/\text{cho}} = 2 RT$ [35], $\rho_{\text{PC}/\text{TX}} = 0$, $X_{\text{TX}}^{\text{b}} = 0.08$, resulting in $\rho_{\text{cho}/\text{TX}} = 4 RT$. The straight line in Panel B is included as a *guide to the eye* and is not based on any model calculation.

the binary mixture PC/TX-100. For a binary system, a constant K and/or ΔH would immediately allow one to conclude that the two species mix in an ideal way. Because the first factor in the exponential function in (5) (the term outside the square brackets in (5)) does not vanish within reasonable intervals for both X_{TX}^{b} , i.e., $X_{\text{TX}}^{\text{b}} \in [0, 0.25]$, and X_{SM} , i.e., $X_{\text{SM}} \in [0, 0.3]$ the term in square brackets must become zero. Using the estimate $\rho_{\text{PC}/\text{TX}} = (0 \pm 1) RT$ describing the PC/TX-100 interaction that results from figure 3 we can conclude that $\rho_{\text{PC}/\text{SM}}$ and $\rho_{\text{SM}/\text{TX}}$ have to be zero as well. As such the addition of TX-100 to a membrane consisting of a mixture of a unsaturated lipid (PC) and a fluid, saturated lipid (SM, at the temperature of our experiments and within the X_{SM} -interval chosen) is very unlikely to induce the formation of domains.

The nonideal mixing behavior in the system PC/cho/TX-100 is apparent upon inspection of figure 5. We have modeled the dependence of K on X_{cho} with (5) using the following parameter assignments in a one-parameter fit: $\rho_{\text{PC}/\text{cho}} = (2 \pm 1) RT$ as given in [35], $\rho_{\text{PC}/\text{TX}} = (0 \pm 1) RT$ as resulting from this study, and $K_{\text{PC}} = 1.2 (\text{mM})^{-1}$. The resulting value for the nonideality parameter describing cho/TX-100 interaction is: $\rho_{\text{cho}/\text{TX}} = (4 \pm 1) RT$. This result is insensitive to the value we assign to X_{TX}^{b} . For example, a variation of X_{TX}^{b} within the interval $X_{\text{TX}}^{\text{b}} \in [0.06, 0.10]$ leads to values for $\rho_{\text{cho}/\text{TX}}$ that stay well within the given error interval of this parameter. Furthermore it is worth noting that in a two parameter fit (the experimental data shown in figure 5 allow for at maximum two adjustable parameters) using both $\rho_{\text{PC}/\text{TX}}$ and

$\rho_{\text{cho}/\text{TX}}$, the former parameter stayed well within the interval given above. A slightly smaller positive detergent/cho nonideality parameter is implied by the data of Wenk et al. in their studies of POPC/octyl- β -D-glucopyranoside (OG) [22] and POPC/octyl- β -thioglucopyranoside (OTG) [23] interaction. Their observation of constant mole ratio partition coefficients suggests small, negative PC/detergent nonideality parameters of $\rho_{\text{PC}/\text{OG}} = \rho_{\text{PC}/\text{OTG}} \sim -0.7 RT$. Analysis of their data in the framework of our model yields for the detergent/cho nonideality parameters: $\rho_{\text{cho}/\text{OG}} = (3 \pm 1) RT$, and $\rho_{\text{cho}/\text{OTG}} = (3 \pm 1) RT$, respectively. These experiments were conducted at $T = 28^\circ\text{C}$ so that it can be expected that the nonideality parameters would be even smaller at $T = 37^\circ\text{C}$.

POPC/detergent interactions at room temperature were found to be only slightly nonideal with respect to the Gibbs free energy ($\rho_{\text{PC}/\text{D}} \sim -0.7 RT$), but this is often a result of a compensation of rather strongly unfavourable enthalpic and favourable entropic effects [20]. This behaviour can be explained with detergent-induced disordering of the membrane which perturbs intermolecular interactions ($\Delta H > 0$) but increases motional and conformational freedom ($\Delta S > 0$). This nonideality increases with increasing spontaneous curvature of the detergent and decreases with increasing temperature [20]. The lack of a detectable composition dependence of ΔH found here (figure 3B) could be explained with the relatively high temperature and the very limited accessible range in X_{TX}^{b} . It is also intriguing that there seems to be no significant difference between the ΔH of transfer into POPC and fluid SM, and the ΔH of transfer into POPC alone. It appears that the specific behaviour of SM in domain-forming membranes requires the existence of an ordered (liquid ordered or gel) phase [26, 40] induced by low temperature, high SM content and/or high cholesterol concentration.

5.2. The “canonical lipid raft mixture”

Let us consider the relationship between pair interactions studied in binary and ternary systems with the behaviour of a quaternary system. The partition coefficient K of TX-100 into POPC membranes is $1.2 (\text{mM})^{-1}$, addition of fluid SM has no effect on K , and addition of 33 mole-% of cho reduces it to $0.5 (\text{mM})^{-1}$. However, a membrane containing a equimolar mixture of PC, SM, and cho (the so-called *canonical lipid raft mixture*) has an even lower $K = (0.2 \pm 0.1) (\text{mM})^{-1}$ [13]. The quaternary mixture differs from the ternary ones (PC/cho/TX-100 and PC/SM/TX-100) by the additional existence of SM/cho contacts some of which are broken by added TX-100 and replaced by TX/cho and TX/SM contacts. The fact that SM/cho interactions oppose TX-100 incorporation (reducing K) implies that they must be favourable ($\rho_{\text{SM}/\text{cho}} < 0$). That means, there is a tendency (opposed by the entropy of mixing) to form more than the random number of SM/cho contacts in a mixture. If such a tendency dominates the free energy of a system, the molecules may form superlattices [41, 42] or complexes [43, 44]. A quantitative estimate is possible using an expression for K in a homogeneously mixed,

four-component system as given in the supporting information. Simulation of K on the basis of the parameters derived above and variable $\rho_{\text{SM}/\text{cho}}$ reveals that a value of $\rho_{\text{SM}/\text{cho}} = -(6 \pm 3) RT$ accounts for the experimental value of $K = (0.2 \pm 0.1) (\text{mM})^{-1}$ assuming virtually random mixing.

For a membrane containing PC, SM, and cho, the parameters in figure 6 imply a tendency to demix into a PC rich phase (thus reducing unfavourable PC/cho contacts) and a SM/cho-rich phase (to avoid replacing favourable SM/cho contacts are by PC/SM and PC/cho contacts). Such a demixing is indeed occurring in the PC/SM/cho system at lower temperature [12]. It should be noted that the existence or induction of few residual ordered domains at 37°C would, e.g., avoid some TX/cho contacts so that K into a hypothetical random mixture of PC/SM/cho would be even smaller than $0.2 (\text{mM})^{-1}$. Taking this into account, the determination of the nonideality parameter assuming random mixing yields an upper limit, $\rho_{\text{SM}/\text{cho}} \leq -6 RT$.

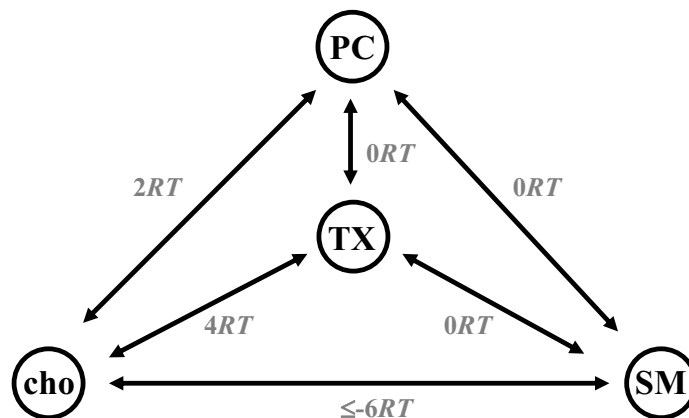


Figure 6. Free energy nonideality parameters $\rho_{\alpha/\beta}$ at $T = 37^\circ\text{C}$ describing the mixing properties in the quaternary mixture POPC/eSM/cho/TX-100. Errors for the $\rho_{\alpha/\beta}$ determined for the two ternary mixtures (left-side and right-side triangle) in this study are of the order $\pm 1RT$. The value for $\rho_{\text{SM}/\text{cho}}$ was estimated with the help of the literature value for the partition coefficient of TX-100 given in [13] (see text).

5.3. Selective solubilization and detergent resistance

The nonideality parameters collected in figure 6 suggest that Triton added to a homogeneously mixed PC/SM/cho membrane has two unfavourable effects: it interacts unfavourably with cho and it interrupts favourable SM/cho contacts. Both these effects can be avoided (on the expense of mixing entropy) if TX-100 is (along with most PC) separated from much of the SM and cho into different domains. That means, in the extreme case, addition of TX-100 could promote domain formation in a previously homogeneous membrane as suggested experimentally [12]. If there are preexisting domains, added TX-100 would partition preferentially into PC-rich domains and tend to enhance the sorting of the lipids as discussed in [18]. The fact that the local cho content

is reduced in the environment of TX-100 (rendering ΔH smaller) and the Triton-induced transfer of cho from PC-rich into SM-rich domains (an accompanying, exothermic effect) might also explain why TX-100 partitioning into PC/SM/cho membranes (1:1:1, mole) at 37°C is less endothermic, $\Delta H = 18$ kJ/mol [13], than into PC/cho (2:1, mole), $\Delta H = 26$ kJ/mol. The above discussion implies that the nonideality parameter of a detergent interacting with cho, $\rho_{\text{cho/D}}$, may belong to the key parameters governing the abundance and composition of the detergent-resistant membrane fraction. The latter differ greatly between different detergents [16, 17]. For octyl glucoside (OG), $\rho_{\text{cho/OG}}$, is most likely smaller than for TX-100 (see above) so that the balance between the general disordering effect of a detergent and the specific, ordered domain-promoting effect [18] arising from $\rho_{\text{cho/D}}$ is altered in favour of disorder and solubilization. Indeed, OG has been found to yield a smaller DRM fraction than TX-100 from Madin-Darby Canine Kidney (MDCK) epithelial cells which was less enriched in cho and SM [15]. A detailed understanding of nonideal interactions of different detergents with different lipids may in the future allow for an optimization of selective solubilization procedures for different classes of membrane proteins. It will also shed light on the issue what selective solubilization of a protein along with certain lipids reveals about protein-lipid interactions *in vivo*.

Acknowledgments

Financial support from the Swiss National Science Foundation (grant 31-67216.01) is gratefully acknowledged. We thank Sandro Keller (FMP Berlin) for important comments on this manuscript.

Derivation of Equation (3)

For a general ternary mixture we can write for the mole-fractions in the membrane:

$$X_{\text{PC}} + X_{\text{L}_1} + X_{\text{TX}}^{\text{b}} = 1, \quad (\text{A.1})$$

and for the mole ratio of the two lipid components in the membrane:

$$\zeta_{\text{L}} = \frac{X_{\text{L}_1}}{X_{\text{PC}}} = \frac{n_{\text{L}_1}}{n_{\text{PC}}}, \quad (\text{A.2})$$

which is, in contrast to the lipid mole fractions, conserved upon addition of TX-100. The expressions n_{α} in (A.2) are in general used for the mole number of component α .

The interaction terms in the molar excess free energy G_{E} (in kJ/mol) are given by:

$$G_{\text{E}} = \rho_{\text{PC/L}_1} X_{\text{PC}} X_{\text{L}_1} + \rho_{\text{PC/TX}} X_{\text{PC}} X_{\text{TX}}^{\text{b}} + \rho_{\text{L}_1/\text{TX}} X_{\text{L}_1} X_{\text{TX}}^{\text{b}}. \quad (\text{A.3})$$

Equation (A.3) is readily transformed with (A.1) and (A.2) into:

$$G_{\text{E}} = \left(\frac{1 - X_{\text{TX}}^{\text{b}}}{1 + \zeta_{\text{L}}} \right) \left[\rho_{\text{PC/L}_1} \zeta_{\text{L}} \left(\frac{1 - X_{\text{TX}}^{\text{b}}}{1 + \zeta_{\text{L}}} \right) + \rho_{\text{PC/TX}} X_{\text{TX}}^{\text{b}} + \rho_{\text{L}_1/\text{TX}} \zeta_{\text{L}} X_{\text{TX}}^{\text{b}} \right]. \quad (\text{A.4})$$

We can then write for a composition dependent partition coefficient in case of nonideal mixing [19] (the constant factor c_W omitted in our definition of K in (1) has to be included now to render the argument of the logarithm dimensionless):

$$-RT \ln \left(K (X_{\text{TX}}^b, \zeta_L) \right) = \Delta\mu^0 + G_E + (1 - X_{\text{TX}}^b) \frac{\partial}{\partial X_{\text{TX}}^b} G_E, \quad (\text{A.5})$$

so that we obtain:

$$K (X_{\text{TX}}^b, \zeta_L) = \exp \left(-\frac{\Delta\mu^0}{RT} \right) \times \exp \left\{ -\frac{(1 - X_{\text{TX}}^b)^2}{RT(1 + \zeta_L)} \left[-\frac{\rho_{\text{PC/L}_1} \zeta_L}{1 + \zeta_L} + \rho_{\text{PC/TX}} + \rho_{\text{L}_1/\text{TX}} \zeta_L \right] \right\}. \quad (\text{A.6})$$

The term $\Delta\mu^0 = \mu_{\text{TX}}^0(\text{bilayer}) - \mu_{\text{TX}}^0(\text{water})$ describes the change in standard chemical potential of TX-100 when partitioning from the aqueous phase into a hypothetical, pure TX-100 bilayer. Inserting $\zeta_L = 0$ into (A.6), i.e., considering the case where TX-100 inserts into a POPC membrane, yields:

$$K_{\text{PC}} (X_{\text{TX}}^b) = \exp \left(-\frac{\Delta\mu^0}{RT} \right) \exp \left(-\rho_{\text{PC/TX}} \frac{(1 - X_{\text{TX}}^b)^2}{RT} \right), \quad (\text{A.7})$$

so that after simple rearrangements, (A.6) can be converted into (3).

References

- [1] M. le Maire, S. Kwee, J.P. Andersen, and J.V. Møller. Mode of interaction of polyoxyethyleneglycol detergents with membrane proteins. *Eur. J. Biochem.*, 129:525–532, 1983.
- [2] M. le Maire, P. Champeil, and J.V. Møller. Interaction of membrane proteins and lipids with solubilizing detergents. *Biochim. Biophys. Acta*, 1508:86–111, 2000.
- [3] R.M. Garavito and S. Ferguson-Miller. Detergents as tools in membrane biochemistry. *J. Biol. Chem.*, 276:32403–32406, 2001.
- [4] T.L. Steck and J. Yu. Selective solubilization of proteins from red blood cell membranes by protein perturbants. *J. Supramol. Struct.*, 1:220–232, 1973.
- [5] J. Yu, D.A. Fischman, and T.L. Steck. Selective solubilization of proteins and phospholipids from red blood cell membranes by nonionic detergents. *J. Supramol. Struct.*, 1:233–247, 1973.
- [6] K. Simons and E. Ikonen. Functional rafts in cell membranes. *Nature*, 387:569–572, 1997.
- [7] E. London and D.A. Brown. Insolubility of lipids in TX-100: physical origin and relationship to sphingolipid/cholesterol membrane domains (rafts). *Biochim. Biophys. Acta*, 1508:182–195, 2000.
- [8] K. Simons and R. Ehehalt. Cholesterol, lipid rafts, and disease. *The Journal of Clinical Investigation*, 110(5):597–603, 2002.
- [9] K. Simons and W.L.C. Vaz. Model Systems, Lipid Rafts, And Cell Membranes. *Annu. Rev. Biophys. Biomol. Struct.*, 33:269–296, 2004.
- [10] S. Munro. Lipid rafts: Elusive or Illusive? *Cell*, 115:377–388, 2003.
- [11] D. Lichtenberg, F.M. Goñi, and H. Heerklotz. Detergent-resistant membranes should not be identified with membrane rafts. *Trends in Biochemical Sciences*, 30:430–436, 2005.
- [12] H. Heerklotz. Triton promotes domain formation in lipid raft mixtures. *Biophys. J.*, 83:2693–2701, 2002.

- [13] H. Heerklotz, H. Szadkowska, T. Anderson, and J. Seelig. The sensitivity of lipid domains to small perturbations demonstrated by the effect of Triton. *J. Mol. Biol.*, 329:793–799, 2003.
- [14] J. van Rheenen, E.M. Achame, H. Janssen, J. Calafat, and K. Jalink. PIP₂ signaling in lipid domains: a critical re-evaluation. *The EMBO Journal*, 24:1664–1673, 2005.
- [15] K. A. Melkonian, T. Chu, L. B. Tortorella, and D. A. Brown. Characterization of proteins in detergent-resistant membrane complexes from Madin-Darby Canine Kidney epithelial cells. *Biochemistry*, 34:16161–16170, 1995.
- [16] N. Madore, K.L. Smith, C.H. Graham, A. Jen, K. Brady, S. Hall, and R. Morris. Functionally different GPI proteins are organized in different domains on the neuronal surface. *EMBO J.*, 18:6917–6926, 1999.
- [17] S. Schuck, M. Honscho, K. Ekroos, A. Shevchenko, and K. Simons. Resistance of cell membranes to different detergents. *Proc. Natl. Acad. Sci. USA*, 100:5795–5800, 2003.
- [18] S. Keller, A. Tsamaloukas, and H. Heerklotz. A quantitative model describing the selective solubilization of membrane domains. *J. Am. Chem. Soc.*, 127:11469–11476, 2005.
- [19] H. Heerklotz, H. Binder, G. Lantzsch, and G. Klose. Membrane/water partition of oligo(ethylene oxide) dodecyl ethers and its relevance for solubilization. *Biochim. Biophys. Acta*, 1196:114–122, 1994.
- [20] H. Heerklotz, H. Binder, G. Lantzsch, G. Klose, and A. Blume. Lipid/Detergent interaction thermodynamics as a function of molecular shape. *J. Phys. Chem. B*, 101:639–645, 1997.
- [21] M. Keller, A. Kerth, and A. Blume. Thermodynamics of interaction of octyl glucoside with phosphatidylcholine vesicles: partitioning and solubilization as studied by high sensitivity titration calorimetry. *Biochim. Biophys. Acta*, 1326:178–192, 1997.
- [22] M. R. Wenk, T. Alt, A. Seelig, and J. Seelig. Octyl- β -D-glucopyranoside partitioning into lipid bilayers: Thermodynamics of binding and structural changes of the bilayer. *Biophys. J.*, 72:1719–1731, 1997.
- [23] M. R. Wenk and J. Seelig. Interaction of octyl- β -thioglucopyranoside with lipid membranes. *Biophys. J.*, 73:2565–2574, 1997.
- [24] F.M. Goñi, M-A. Urbaneja, J.L.R. Arrondo, A. Alonso, A.A. Durrani, and D. Chapman. The interaction of phosphatidylcholine bilayers with Triton X-100. *Eur. J. Biochem.*, 160:659–665, 1986.
- [25] M.A. Partearroyo, M.A. Urbaneja, and F.M. Goñi. Effective detergent/lipid ratios in the solubilization of phosphatidylcholine vesicles by Triton X-100. *FEBS Lett.*, 302:138–140, 1992.
- [26] T. Nyholm and J. P. Slotte. Comparison of Triton X-100 penetration into phosphatidylcholine and sphingomyelin mono- and bilayers. *Langmuir*, 17:4724–4730, 2001.
- [27] E. Schnitzer, D. Lichtenberg, and M.M. Kozlov. Temperature-dependence of the solubilization of dipalmitoylphosphatidylcholine (DPPC) by the non-ionic surfactant Triton X-100, kinetic and structural aspects. *Chem. Phys. Lipids*, 126:55–76, 2003.
- [28] D.A. Berthold, G.T. Babcock, and C.A. Yocum. A highly resolved, oxygen-evolving Photosystem II preparation from spinach thylakoid membranes. *FEBS Letters*, 134:231–234, 1981.
- [29] H. Schiller and H. Dau. Preparation protocols for high-activity Photosystem II membrane particles of green algae and higher plants, pH dependence of oxygen evolution and comparison of S₂-state multiline signal by X-band EPR. *J. Photochem. Photobiol. B*, 55:138–144, 2000.
- [30] F. Zhang and E. S. Rowe. Titration calorimetric and differential scanning calorimetric studies of the interactions of *n*-butanol with several phases of dipalmitoylphosphatidylcholine. *Biochemistry*, 31:2005–2011, 1992.
- [31] T. Wiseman, S. Williston, J.F. Brandts, and L.N. Lin. Rapid measurement of binding constants and heats of binding using a new titration calorimeter. *Anal. Biochem.*, 179:131–137, 1989.
- [32] M. Chellani. Isothermal titration calorimetry: biological applications. *Am. Biotechnol. Lab*, 17:14–18, 1999.
- [33] H. Heerklotz. Microcalorimetry of lipid membranes. *Journal of Physics: Condensed Matter*, 16:441–467, 2004.

- [34] V.V. Plotnikov, J.M. Brandts, L.N. Lin, and J.F. Brandts. A new ultrasensitive scanning calorimeter. *Anal. Biochem.*, 250:237–244, 1997.
- [35] A. Tsamaloukas, H. Szadkowska, J. P. Slotte, and H. Heerklotz. Interactions of cholesterol with lipid membranes and cyclodextrin characterized by calorimetry. *Biophys. J.*, 89:1109–1119, 2005.
- [36] H. Heerklotz and J. Seelig. Titration calorimetry of surfactant–membrane partitioning and membrane solubilization. *Biochim. Biophys. Acta*, 1508:69–85, 2000.
- [37] G. Cevc and D. Marsh. *Phospholipid bilayers: Physical principles and models*, volume 5. John Wiley & Sons, Inc., New York, 1 edition, 1987.
- [38] H.G. Zachmann. *Mathematik für Chemiker*. VCH Verlagsgesellschaft mbH, Weinheim, 5 edition, 1994.
- [39] R. Koynova and M. Caffrey. Phases and phase transitions of the phosphatidylcholines. *Biochim. Biophys. Acta*, 1376:91–145, 1998.
- [40] F. Ollila and J.P. Slotte. Partitioning of Triton X-100, deoxycholate and C₁₀EO₈ into bilayers composed of native and hydrogenated egg yolk sphingomyelin. *Biochim. Biophys. Acta*, 1564:281–288, 2002.
- [41] J. Huang. Exploration of molecular interactions in cholesterol superlattices: effect of multibody interactions. *Biophys. J.*, 83:1014–1025, 2002.
- [42] B. Cannon, G. Heath, J. Huang, J.A. Somerharju, J.A. Virtanen, and K.H. Cheng. Time-resolved fluorescence and Fourier transform infrared spectroscopic investigations of lateral packing defects and superlattice domains in compositionally uniform cholesterol/phosphatidylcholine bilayers. *Biophys. J.*, 84:3777–3791, 2003.
- [43] A. Radhakrishnan and H. M. McConnell. Condensed complexes of cholesterol and phospholipids. *Biophys. J.*, 77:1507–1517, 1999.
- [44] A. Radhakrishnan, T. G. Anderson, and H. M. McConnell. Condensed complexes, rafts and the chemical activity of cholesterol in membranes. *Proc. Natl. Acad. Sci. USA*, 97:12422–12427, 2000.

Supporting Information for: Nonideal mixing in multicomponent lipid/detergent systems

Alekos Tsamaloukas¹, Halina Szadkowska, and Heiko Heerklotz

¹ Biozentrum of the University of Basel, Division of Biophysical Chemistry, Klingelbergstrasse 70, CH-4056 Basel, Switzerland

E-mail: alekos.tsamaloukas@unibas.ch

Estimation of $\rho_{\text{SM}/\text{cho}}$

Similar to the procedure for a ternary mixture a quaternary system may be described with the relation:

$$X_{\text{PC}} + X_{\text{L}_1} + X_{\text{L}_2} + X_{\text{TX}}^{\text{b}} = 1, \quad (1)$$

where:

$$\zeta_{\text{L}_1} = \frac{X_{\text{L}_1}}{X_{\text{PC}}} = \frac{n_{\text{L}_1}}{n_{\text{PC}}}, \quad (2)$$

and:

$$\zeta_{\text{L}_2} = \frac{X_{\text{L}_2}}{X_{\text{PC}}} = \frac{n_{\text{L}_2}}{n_{\text{PC}}} \quad (3)$$

Within the framework of pairwise nonideal interactions between components α and β we have for the molar excess free energy G_{E} :

$$G_{\text{E}} = \sum_{\alpha \neq \beta} \rho_{\alpha/\beta} X_{\alpha} X_{\beta}, \quad (4)$$

with, e.g., X_{α} denoting the mole fraction of component α in the membrane, the nonideality parameters denoted $\rho_{\alpha/\beta}$, and the summation running over α and β . Using (1), (2), and (3) we can express G_{E} as a function $G_{\text{E}} = f(\zeta_{\text{L}_1}, \zeta_{\text{L}_2}, X_{\text{TX}}^{\text{b}}, \rho_{\alpha/\beta})$. The resulting expression is:

$$G_{\text{E}} = -\frac{1}{(1 + \zeta_{\text{L}_1} + \zeta_{\text{L}_2})^2} \times \left\{ A\rho_{\text{PC}/\text{L}_1} + B\rho_{\text{PC}/\text{L}_2} + C\rho_{\text{L}_1/\text{L}_2} + D\rho_{\text{PC}/\text{TX}} + E\rho_{\text{L}_1/\text{TX}} + F\rho_{\text{L}_2/\text{TX}} \right\}, \quad (5)$$

where:

$$\begin{aligned} A &= -X_{\text{PC}} (1 - X_{\text{TX}}^{\text{b}}) \left[\zeta_{\text{L}_1} (\zeta_{\text{L}_1} + \zeta_{\text{L}_2} + 1) \right] \\ B &= -X_{\text{PC}} (1 - X_{\text{TX}}^{\text{b}}) \left[\zeta_{\text{L}_2} (\zeta_{\text{L}_1} + \zeta_{\text{L}_2} + 1) \right] \\ C &= -\zeta_{\text{L}_1} \zeta_{\text{L}_2} (1 - X_{\text{TX}}^{\text{b}})^2 \\ D &= -X_{\text{PC}} X_{\text{TX}}^{\text{b}} \left[1 + 2(\zeta_{\text{L}_1} + \zeta_{\text{L}_2} + \zeta_{\text{L}_1} \zeta_{\text{L}_2}) + \zeta_{\text{L}_1}^2 + \zeta_{\text{L}_2}^2 \right] \end{aligned} \quad (6)$$

$$\begin{aligned}
E &= -X_{\text{TX}}^{\text{b}} (1 - X_{\text{TX}}^{\text{b}}) \left[\zeta_{\text{L}_1} (\zeta_{\text{L}_1} + \zeta_{\text{L}_2} + 1) \right] \\
F &= -X_{\text{TX}}^{\text{b}} (1 - X_{\text{TX}}^{\text{b}}) \left[\zeta_{\text{L}_2} (\zeta_{\text{L}_1} + \zeta_{\text{L}_2} + 1) \right] \\
X_{\text{PC}} &= \frac{1 - X_{\text{TX}}^{\text{b}}}{1 + \zeta_{\text{L}_1} + \zeta_{\text{L}_2}}
\end{aligned} \tag{7}$$

For the partition coefficient we get using (A.5) of the main text:

$$K(\zeta_{\text{L}_1}, \zeta_{\text{L}_2}, X_{\text{TX}}^{\text{b}}, \rho_{\alpha/\beta}) = \exp\left(-\frac{\Delta\mu^0}{RT}\right) \times \exp\left(-\frac{1}{RT} \left[G_{\text{E}} + (1 - X_{\text{TX}}^{\text{b}}) \frac{\partial}{\partial X_{\text{TX}}^{\text{b}}} G_{\text{E}} \right]\right). \tag{8}$$

The case of TX-100 inserting into a POPC membrane, i.e., $\zeta_{\text{L}_1} = \zeta_{\text{L}_2} = 0$, yields the expression $K_{\text{PC}} = \exp\left(-\frac{\Delta\mu^0}{RT}\right)$ when setting $\rho_{\text{PC}/\text{TX}} = 0$ (see (A.7) of the main text). We have evaluated (8) numerically for $\zeta_{\text{L}_1} = \zeta_{\text{L}_2} = 1$, $X_{\text{TX}}^{\text{b}} = 0.08$, and the nonideality parameters $\rho_{\alpha/\beta}$ for the two ternary mixtures as given in the main text. Upon insertion of the partition coefficient $K = (0.2 \pm 0.1) \text{ (mM)}^{-1}$ determined for the so-called canonical raft mixture PC/SM/cho (1:1:1, mole) into (8), we can thus make an estimate for the nonideality parameter $\rho_{\text{SM}/\text{cho}}$.

Determination of ΔH with the Rowe assay

The transfer enthalpy ΔH is a model independent quantity that can be determined by ITC. A linear dependence of the measured differential heat (resulting from the first 10 μL injection), DH , on the concentration of TX-100 loaded into the cell, $c_{\text{TX}}^{\text{cell}}$, results when employing a mole ratio based partitioning model. For the X_{TX}^{b} -interval we could investigate in our study, both partitioning models are equally well suited. The mole fraction ratio based model yields a nonlinear relation of DH on $c_{\text{TX}}^{\text{cell}}$. However, for small X_{TX}^{b} the expression degenerates into the linear relation given here, and we start our derivation with the simpler model based on the mole ratio. We have the general relation:

$$DH = \Delta n_{\text{TX}}^{\text{b}} \Delta H, \tag{9}$$

where we need to express the change in the amount of membrane-bound TX-100, $\Delta n_{\text{TX}}^{\text{b}}$, upon injection of a small aliquot ΔV from the syringe into the cell with volume V^{cell} . We have:

$$\begin{aligned}
\Delta n_{\text{TX}}^{\text{b}} &= (n_{\text{TX}}^{\text{b}})^{\text{cell}} - (n_{\text{TX}}^{\text{b}})^{\text{syr}} \\
&= V^{\text{cell}} (c_{\text{TX}}^{\text{b}})^{\text{cell}} - \Delta V \cdot (c_{\text{TX}}^{\text{b}})^{\text{syr}} \\
&= V^{\text{cell}} \frac{K c_{\text{L}}^{\text{cell}} c_{\text{TX}}^{\text{cell}}}{1 + K c_{\text{L}}^{\text{cell}}} - \Delta V \frac{K c_{\text{L}}^{\text{syr}} c_{\text{TX}}^{\text{syr}}}{1 + K c_{\text{L}}^{\text{syr}}},
\end{aligned} \tag{10}$$

where the concentration of membrane-bound TX-100 (both in the syringe and in the cell) is expressed on the basis of the mole ratio partition coefficient given as (see theory section of the main text):

$$c_{\text{TX}}^{\text{b}} = \frac{K c_{\text{L}} c_{\text{TX}}}{1 + K c_{\text{L}}} . \quad (11)$$

Insertion of (10) into (9) yields the desired linear relation:

$$DH = m c_{\text{TX}}^{\text{cell}} + b , \quad (12)$$

with:

$$m = \Delta H \frac{K c_{\text{L}}^{\text{cell}} V^{\text{cell}}}{1 + K c_{\text{L}}^{\text{cell}}} \quad (13)$$

$$b = - \Delta H \frac{K c_{\text{L}}^{\text{syrt}} c_{\text{TX}}^{\text{syrt}} \Delta V}{1 + K c_{\text{L}}^{\text{syrt}}} . \quad (14)$$

With the partition coefficient K determined directly from the intercept with the $c_{\text{TX}}^{\text{cell}}$ -axis, the slope m can be used to determine ΔH .

Thermodynamic comparison of the interactions of cholesterol with unsaturated phospholipid and sphingomyelins

Alekos Tsamaloukas, Halina Szadkowska, and Heiko Heerklotz*

26th December 2005

*Corresponding author. Address: Biozentrum of the University of Basel, Division of Biophysical Chemistry, Basel, Switzerland. E-mail: heiko.heerklotz@unibas.ch

Abstract:

A comparative analysis of the interaction of cholesterol (cho) with palmitoyl-oleoyl-phosphatidylcholine (POPC) and sphingomyelins (SM) was performed in largely homogeneous, fluid phase membranes at 50°C. To this end three independent assays for isothermal titration calorimetry (ITC) were applied to POPC/SM/cho-mixtures. Cholesterol is solubilized by randomly methylated- β -cyclodextrin (cyd) and the uptake of cho into (or release from) large unilamellar vesicles is measured. The affinity of cho to a POPC/SM (1:1) membrane with 30 mol-% cho is about $2\times$ higher than to POPC alone; extrapolation to pure SM yields an affinity ratio of $R_K \sim 5$. Bringing cho in contact with SM is highly exothermic (-7 kJ/mol for POPC/SM (1:1), and -13 kJ/mol extrapolated to pure SM, both compared to POPC). No pronounced differences were observed between egg, bovine brain, and palmitoyl SM. With decreasing cho content, R_K increases and ΔH becomes more exothermic, suggesting a trend towards superlattice formation. That SM/cho-interactions are enthalpically favourable implies that the preference of cho for SM increases upon cooling and can induce domain formation below a certain temperature. The enthalpy gain is partially compensated by a loss in entropy in accordance with the concept of cho-induced chain ordering, which improves intermolecular interactions (van der Waals, H-bond) but reduces conformational and motional freedom. The ability of cyd to extract sphingomyelin from membranes is twofold weaker than for POPC.

Introduction

The organization of the plasma membrane of cells is a topic of considerable interest in contemporary membrane biology. In particular, the question whether membrane lipids form a homogenous matrix for membrane proteins to dissolve in or whether the lipids themselves show tendencies to form domains constitutes a yet open question. Biochemical assays based on detergent treatment of cell membranes led to the concept of so called “detergent resistant membranes” (DRMs) (1), membrane patches insoluble in (cold, nonionic) detergents and being enriched in cholesterol (cho) and sphingolipids. These DRMs have been assumed to represent pre-existing domains in the membrane, giving rise to the concept of so called “lipid rafts” (2, 3). However, in recent years both model system studies (4–7) and studies with biological specimen (8–10) have put the “DRM=raft”-hypothesis into question (for reviews see, e.g., (11–14)) so that insight into detergent-free membranes is urgently needed.

Cholesterol, amongst its diverse functions in biological membranes, is believed to be of considerable importance for the formation of domains. Preferential interactions of cho with different lipids could account for the uneven distribution among intracellular membranes (15) and cholesterol-induced domain formation. To quantify these, various experimental assays have been described in the literature. For example, Lange et al. (16) studied the exchange of cho between erythrocyte ghost membranes and phospholipid vesicles whereas Yeagle and Young (17) monitored cho exchange between vesicles of different size. In order to overcome the problem caused by slow equilibration processes observed in these type of experiments, only recently the use of cyclodextrins (cyd) was established (18–22). Niu and Litman (23) measured differential affinities of cho for different lipids using binary cyd-lipid vesicle systems. Relating partition coefficients of cho between cyd and differently composed lipid vesicles, they were able (by employing a thermodynamic cycle) to quantify differential affinities of cho for different lipids.

Following a similar rationale, we have recently established two convenient assays for isothermal titration calorimetry (ITC) (24), measuring either the uptake of or the release of cho by lipid vesicles. One important advantage of the calorimetric approach is that not only affinities but also enthalpic and entropic contributions to the partitioning process can be quantified (25). Unfortunately, it was impossible to apply the techniques introduced for POPC simply to vesicles of SM since their equilibration kinetics are much too slow. We have resolved this problem by two strategies. First, we have studied the effect of varying amounts of SM added to POPC vesicles. Second, we have developed an alternative assay similar to the partitioning protocol of Zhang and Rowe (26). These authors studied the interaction of *n*-butanol with various phases of dipalmitoylphosphatidylcholine (DMPC). Their protocol is based on a “null-experiment” injecting lipid-alcohol mixed vesicles into solutions of different alcohol concentration. They searched for the situation where the observable heat effects change from endothermic to exothermic with the point of vanishing heat signal yielding the partition coefficient (free alcohol concentration in the syringe matches the one present in the calorimeter cell). Similar reasoning can be applied to the partitioning of cho and will be illustrated herein for the first time.

We apply the three aforementioned assays to study the interaction of cho with lipid mixtures composed of 1-palmitoyl-2-oleoyl-*sn*-glycero-3-phosphocholine (POPC) and sphingomyelin (SM) of different origin. A major issue for these experiments is the fact that sphingomyelins have high chain melting temperatures ranging between $T_m \sim 37\text{--}53^\circ\text{C}$ (27–29) and that gel phase membranes are rather poor acceptors of cholesterol (17). In order to

avoid misleading conclusions arising from nonhomogenous membranes and also in line with other experimental studies like fluorescence (30, 31), NMR (32, 33), ESR (34), and x-ray diffraction (28, 35) working (partially) at elevated temperatures, we have conducted our partitioning experiments at $T=50^{\circ}\text{C}$. Taking this precaution, we seek to minimize the effect a domain containing membrane has on the thermodynamic parameters accessible by ITC, i.e., the partition coefficient, K_X , and enthalpy, ΔH . On the basis of the results we discuss also the behaviour expected at lower temperature.

Theory

The partitioning process of cholesterol from cyd/cho-complexes into a membrane (or the release from a membrane into cyd/cho-complexes) can be analyzed within the framework of our recently established model (24). Briefly, a cyd/membrane partition coefficient may be defined via:

$$K_X = \frac{c_{\text{cho}}^{\text{b}} c_{\text{cyd}}^2}{(c_{\text{L}} + c_{\text{cho}}^{\text{b}}) c_{\text{cho}}^{\text{cyd}}}, \quad (1)$$

where $c_{\text{cho}}^{\text{b}}$ denotes the concentration of membrane-bound and $c_{\text{cho}}^{\text{cyd}}$ the concentration of cyd-complexed cholesterol, c_{L} stands for the lipid concentration, and c_{cyd} for the concentration of free cyclodextrin. The term c_{cyd} is squared since the predominant cho/cyd-binding stoichiometry was shown to be 1:2 (24). Upon inserting $c_{\text{cho}}^{\text{cyd}} = c_{\text{cho}} - c_{\text{cho}}^{\text{b}}$ into Eq. 1, a second order polynomial in $c_{\text{cho}}^{\text{b}}$ results with the physically meaningful solution given by (the term c_{cho} denotes the total cho concentration):

$$c_{\text{cho}}^{\text{b}} = \frac{c_{\text{L}} - c_{\text{cho}} + c_{\text{cyd}}^2/K_X}{2} \left[\sqrt{1 + 4 \frac{c_{\text{L}} c_{\text{cho}}}{(c_{\text{L}} - c_{\text{cho}} + c_{\text{cyd}}^2/K_X)^2}} - 1 \right]. \quad (2)$$

Materials and Methods

Substances and sample preparation

The lipids 1-palmitoyl-2-oleoyl-*sn*-glycero-3-phosphocholine (POPC), egg (eSM) and bovine brain (bSM) sphingomyelin were purchased from Avanti Polar Lipids (Alabaster, AL). *N*-palmitoyl-sphingomyelin (pSM) was a kind gift of Peter J. Slotte (Åbo Akademi University, Turku, Finland). Cholesterol (cho) and randomly methylated- β -cyclodextrin (cyd) were from Fluka (Buchs, Switzerland). Mixtures of POPC, cho and sphingomyelin were prepared as described (5, 36). The dry lipid mixtures were suspended in 100 mM NaCl, 10 mM Tris buffer at pH 7.4 by gentle vortexing to reach a total lipid concentration (without including the amount of cho) of $c_{\text{PC}} + c_{\text{SM}} = 10$ mM for the uptake and release experiments. The Rowe assays (26) were performed exclusively with $c_{\text{PC}} + c_{\text{SM}} = 15$ mM and a mole fraction of bound cho, $X_{\text{cho}} = 0.2$. Large unilamellar vesicles (LUVs) were prepared by 10 extrusion runs through a Nucleopore polycarbonate filter at 50°C in a Lipex extruder (Northern Lipids, Vancouver, Canada).

ITC measurements

All ITC experiments were performed at $T = 50^\circ\text{C}$ on a VP ITC calorimeter from MicroCal (Northampton, MA, USA) (37, 38) as described in detail elsewhere (24). Briefly, in case of the release assay mixed POPC/SM LUVs with a well defined amount of membrane-bound cho, $X_{\text{cho}} = 0.2$ or $X_{\text{cho}} = 0.3$, were titrated into a solution with $c_{\text{cyd}} = 5\text{ mM}$ and the release of cho from the membrane into cyd/cho-complexes was measured. For the uptake assay, cho-free LUVs were titrated into cyd-solutions of $c_{\text{cyd}} = 5\text{ mM}$ including varying amounts of cho, $c_{\text{cho}} = 0\text{--}110\ \mu\text{M}$. The heats obtained by an integration of the power peaks resulting after an injection are corrected by the values obtained in blank experiments, i.e., titration of the same LUVs into buffer (release assay), and titration into a cyd solution with $c_{\text{cyd}} = 5\text{ mM}$ (uptake assay), respectively. Data are displayed as normalized heats, Q_{obs} , with normalization to the amount of lipidic material (excluding cho) injected.

In order to overcome the issue of very slow partitioning kinetics, we have additionally applied a strategy similar to the Rowe protocol (26) for samples with large mol fractions of SM. This protocol works as follows: Lipid vesicles with a fixed amount of membrane bound cho, X_{cho} (in our case only mixed POPC/eSM vesicles with $X_{\text{cho}} = 0.2$ were studied utilizing this assay), are loaded into the injection syringe and the heat resulting from injecting an aliquot of $10\ \mu\text{L}$ into the calorimeter cell was measured. The cell was filled with solutions of fixed cyd-concentration, $c_{\text{cyd}} = 5\text{ mM}$, but variable cho-concentration, $c_{\text{cho}}^{\text{cell}} = 0\text{--}100\ \mu\text{M}$. The heat, DH (given in μcal), obtained from each experiment conducted at different $c_{\text{cho}}^{\text{cell}}$ was corrected by the value obtained in a blank experiment, i.e., titration of the same vesicles into buffer. From a plot of the corrected DH -values as a function of $c_{\text{cho}}^{\text{cell}}$, both the partition coefficient and enthalpy can be obtained (see below). Even if the precise determination of the titration heat is impaired severely by slow equilibration kinetics, it remains still straightforward to identify the case of vanishing heat signal, i.e., the case where the $DH(c_{\text{cho}}^{\text{cell}})$ -curve intercepts with the $c_{\text{cho}}^{\text{cell}}$ -axis. Thus a determination of the partition coefficient was always possible, whereas the enthalpy for partitioning could not be determined in case of samples with $X_{\text{SM}} > 0.7$.

Data analysis

ITC uptake and release traces were modeled in a Microsoft Excel spreadsheet according to the equation (see (24) for further details):

$$Q_{\text{obs}}(c_L) = \frac{\Delta c_{\text{cho}}^{\text{b}}}{\Delta c_L} \Delta H + Q_{\text{dil}}, \quad (3)$$

with the molar enthalpy of transfer ΔH (always given for uptake of cho by the membrane), and the dilution heat Q_{dil} . The latter is introduced into our model function Eq. 3 to account for any constant heat effects that are not covered by the subtraction of the heats obtained in blank experiments (24).

In case of the Rowe assay, the heat consumed (or released) upon the first $10\ \mu\text{L}$ -injection (denoted by ΔV_2), DH , is plotted as a function of the cho-concentration loaded into the cell, $c_{\text{cho}}^{\text{cell}}$. The first injection of $1\ \mu\text{L}$ is not considered for the data evaluation as it is subject to larger errors (39). However, the material injected into (or replaced from) the cell by this injection has to be considered for a correct determination of K_X and ΔH , respectively. From the intercept with the $c_{\text{cho}}^{\text{cell}}$ -axis, $c_{\text{cho}}^{\text{cell},0}$, the partition coefficient K_X can be calculated using Eq. 1 and equating $c_{\text{cho}}^{\text{cell},0} = c_{\text{cho}}^{\text{cyd}}$. Here both parameters, i.e., K_X and

ΔH , were obtained by fitting the following relation (used in an Excel spreadsheet) to the experimental data:

$$\begin{aligned} DH &= \Delta c_{\text{cho}}^{\text{b}} \Delta H V_0 \\ &= \left\{ c_{\text{cho}}^{\text{b}}(2) \left(1 + \frac{\Delta V_2}{2V_0} \right) + c_{\text{cho}}^{\text{b}}(1) \left(\frac{\Delta V_2}{2V_0} - 1 \right) - \frac{\Delta V_2}{V_0} c_{\text{cho}}^{\text{syrr}} \right\} \Delta H V_0, \end{aligned} \quad (4)$$

where $\Delta c_{\text{cho}}^{\text{b}}$ stands for the change in concentration of membrane-bound cho occurring upon the second injection, V_0 is the cell volume of 1.4 mL, and $c_{\text{cho}}^{\text{syrr}}$ is the bound (=total) cho concentration present in the injection syringe. The expressions $c_{\text{cho}}^{\text{b}}(i)$ are calculated on the basis of Eq. 2 using corrected concentrations as explained in (24).

Generally, K_X and ΔH values obtained in the modeling of the data are listed with estimated maximal errors of $\delta(K_X) = 20\%$, and $\Delta(\Delta H) = \pm 2 \text{ kJ/mol}$ for $c_{\text{SM}}/(c_{\text{SM}} + c_{\text{PC}}) < 0.5$, and $\delta(K_X) = 40\%$ and $\Delta(\Delta H) = \pm 4 \text{ kJ/mol}$ above this ratio, respectively.

Results

Uptake and Release assay

Fig. 1 shows representative experimental raw data as well as the global analysis of cho uptake and release data. For the release experiment, 10 mM LUVs with mole-fractions of pSM, $X_{\text{pSM}} = 0.25$, and cho, $X_{\text{cho}} = 0.2$ were titrated into a solution with $c_{\text{cyd}} = 5 \text{ mM}$. In case of the uptake experiment, 10 mM LUVs with $X_{\text{pSM}} = 0.25$ were titrated into a solution with $c_{\text{cyd}} = 5 \text{ mM}$, and $c_{\text{cho}} = 70 \text{ }\mu\text{M}$, respectively. For both experiments conducted at 50°C the injection protocol consisted of $1 \times 1 \text{ }\mu\text{L}$, $3 \times 5 \text{ }\mu\text{L}$, and $26 \times 10 \text{ }\mu\text{L}$ injections to better resolve the steep part of the curve at the beginning.

Independent analysis of the uptake trace yields for the model parameters entering into Eq. 3: $K_X = 101 \text{ mM}$, $\Delta H = -10 \text{ kJ/mol}$, and $Q_{\text{dil}}^{\text{up}} = -0.001 \text{ kJ/mol}$. The release data set is best modeled with: $K_X = 72 \text{ mM}$, $\Delta H = -13 \text{ kJ/mol}$, and $Q_{\text{dil}}^{\text{rel}} = -0.1 \text{ kJ/mol}$, while the global fit results in: $K_X = (79 \pm 16) \text{ mM}$, $\Delta H = -(13 \pm 2) \text{ kJ/mol}$, $Q_{\text{dil}}^{\text{up}} = 0.1 \text{ kJ/mol}$, and $Q_{\text{dil}}^{\text{rel}} = -0.1 \text{ kJ/mol}$, respectively.

Rowe assay

As pointed out already, uptake/release partitioning assays become impractical due to extremely slow re-equilibration after an injection for vesicles containing large amounts of SM. A solution to this problem is a modified Rowe assay (26). Fig. 2 shows raw experimental data as well as the modeling of the data according to Eq. 4. LUVs composed of 50 mol-% eSM, 20 mol-% cho, and 30 mol-% POPC at a total lipid concentration: $c_{\text{PC}} + c_{\text{SM}} = 15 \text{ mM}$ were titrated into cyd-solutions ($c_{\text{cyd}} = 5 \text{ mM}$) including different concentrations of cho: $c_{\text{cho}}^{\text{cell}} = 0\text{--}60 \text{ }\mu\text{M}$. Analysis of the data shown in panel B according to Eq. 4 yields: $K_X = (147 \pm 59) \text{ mM}$, and $\Delta H = -(20 \pm 4) \text{ kJ/mol}$, respectively.

Summary of the cho partitioning experiments

An overview of the experimental results obtained with both uptake/release- and Rowe assay is provided with Fig. 3. Displayed are the partition coefficient, K_X , and molar enthalpy change, ΔH , as a function of membrane composition given as the mole fraction

of SM among the phospholipids: $x \equiv c_{\text{SM}}/(c_{\text{SM}} + c_{\text{PC}})$ (excluding the variable cho concentration, merely for practical reasons). The origin ($x = 0$) corresponds to the case of cho partitioning into a POPC membrane (with the respective values taken from (24)) and the point $x = 1$ accordingly to the partitioning into a SM membrane. Solid symbols represent results for eSM with $X_{\text{cho}} = 0.3$, which were obtained by global fits (\bullet) and, at high SM content, individual uptake curves (\blacktriangle). The partition coefficient, K_X , increases with increasing amount of SM in the vesicles, and the partitioning enthalpy, ΔH , becomes increasingly exothermic. In general, the latter shown in panel B of Fig. 3 was included only up to mixtures with $x < 0.9$, as its assignment (independently of the assay used) above this value was not considered to be reliable (see also below). Release experiments were impossible to be performed above $x = 0.8$. As such, the error bars given for these points are significantly larger (see: Materials and Methods) than those given for values obtained in global analysis of uptake/release data sets at small c_{SM} .

We have evaluated $K_X(x)$ and $\Delta H(x)$ according to a model based on pairwise nonideality parameters for POPC/SM, POPC/cho, and, SM/cho, analogously to the procedure described in (40) (data not shown). The resulting fits were virtually linear but a precise determination of the nonideality parameters is impossible without accurate additional information. Therefore, we excluded the model here and refer to quasi-empirical, linear fits of the data (solid and dashed lines in Fig. 3). Results for K_X and ΔH at $x = 0$ (taken from (24)), $x = 0.5$, and linearly extrapolated to $x = 1$ are given in Tab. 1. Open symbols (\diamond), (∇), and (\circ) in Fig. 3 specify parameters obtained with eSM-vesicles incorporating 20 mol-% cho. Results obtained by global data analysis of uptake/release assay with pSM-vesicles, $X_{\text{cho}} = 0.2$, are depicted by (\times) in Fig. 3. Generally, up to $x = 0.5$, no pronounced deviation from the behaviour of eSM-vesicles is observed. A spot check experiment (uptake assay) with bSM-vesicles, $X_{\text{cho}} \sim 0.3$, is similarly described by parameters that agree within error with those collected for the other sphingomyelins used in this study ($(+)$ in Fig. 3).

In summary, we find no significant deviations between the results of different assays (uptake, release, Rowe) and between different sphingomyelins (eSM, pSM, bSM). For both, K_X and ΔH , a larger scatter appears for $x > 0.5$. Differential scanning calorimetry experiments (data not shown), suggest that for samples with $X_{\text{SM}} > 0.5$ and $X_{\text{cho}} = 0.2$ or 0.3 the main transition of the lipids is not fully completed at 50°C . Therefore, the deviations we observe may be due to residual gel phase domains in an otherwise already fluid phase membrane.

Lipid extraction assay

Employing the protocol established by Anderson et al. (41), the dissolution of pure eSM vesicles by cyd at 50°C was measured as shown in Fig. 4. LUVs with $c_{\text{L}} = 5, 8, \text{ and } 10 \text{ mM}$ were titrated in $5 \mu\text{L}$ aliquots into the calorimeter cell containing cyd-solutions with $c_{\text{cyd}} = 20\text{--}60 \text{ mM}$. Data shown in panel B of Fig. 4 are normalized with respect to the amount of lipid injected but not blank corrected. The appropriate blank titration, i.e., injection of buffer into a cyd solution at the respective concentration yields constant heat values (data not shown). Using the model given in (41) to describe the formation of a cyd/lipid inclusion complex, the breakpoints of the experimental traces shown in Fig. 4 can be used to estimate the (equilibrium) complex formation constant K_Φ . These breakpoints correspond to the case where first intact vesicles begin to coexist with cyd/lipid inclusion complexes in the calorimeter cell, i.e., when vesicles coming from the injection syringe are no longer completely dissolved by cyd. Assuming that the inclusion complex has the same stoichiometry as shown for POPC in (41), i.e., 1 lipid per 4 cyclodextrins, we can calculate

K_{Φ} via:

$$K_{\Phi} = \frac{1}{c_{\text{cyd}}^3} \frac{R_{\text{SM/cyd}}}{(1 - 4R_{\text{SM/cyd}})^4}, \quad (5)$$

where $R_{\text{SM/cyd}}$ is the molar ratio of SM and cyd in the calorimeter cell at the position of the breakpoint. We obtain as mean value from the traces shown in Fig. 4: $K_{\Phi}(\text{eSM}) = (295 \pm 60) (\text{M})^{-3}$. This value is smaller than the one for POPC resulting by interpolation of the data given in (41) to 50°C : $K_{\Phi}(\text{POPC}) = (531 \pm 106) (\text{M})^{-3}$.

Discussion

PC→SM transfer of cho

Analogously to the thermodynamic cycle used by Niu and Litman (23), we can discuss differences between cho interactions with membranes of different SM content, x , independently of cyclodextrin, by comparing different points on the linear regressions to the $K_X(x)$ and $\Delta H(x)$ data shown in Fig. 3. The ratio $R_K \equiv K_X(x)/K_X(0)$ is, again, a partition coefficient: that for cho between SM-containing membranes and pure POPC membranes. Similarly, the enthalpy difference $\Delta(\Delta H) \equiv \Delta H(x) - \Delta H(0)$ corresponds to the enthalpy of transfer of cho from a POPC membrane into a SM-containing membrane. The values of R_K given in Tab. 1 imply that cho would accumulate to about five- to twelvefold concentration in a hypothetical pure SM domain coexisting with a pure PC domain. The transfer to SM would yield an enthalpy gain of $\Delta(\Delta H) \sim -(13-23) \text{ kJ/mol}$. Equivalently, intermolecular interactions of cho would contribute favourably by $\Delta(\Delta\mu^0) \sim -5 \text{ kJ/mol}$ ($X_{\text{cho}} = 0.3$, see Tab. 1) to the standard free energy change of demixing of a membrane into PC and SM domains. Demixing is, of course, opposed by the entropy of mixing and would therefore, if it occurs at all, not lead to pure PC and SM but only to PC-rich and SM-rich domains.

The effect of the cho concentration

Comparing the data at $X_{\text{cho}} = 0.3$ (solid symbols) with those at smaller cho concentration, $X_{\text{cho}} = 0.2$ (open symbols), we find a significant increase in K_X and R_K and more exothermic enthalpy changes, ΔH and $\Delta(\Delta H)$, at the lower cholesterol content (see Tab. 1). It is intriguing that X_{cho} has opposite effects on K_X and ΔH of POPC and SM as indicated by the solid and dashed lines in Fig. 3 crossing each other. Whereas K_X of POPC increases slightly with increasing cholesterol content (24), it decreases markedly for SM. This has important implications for the mixing behaviour of SM/cho membranes, since it causes a tendency to avoid cho/cho contacts and to arrange molecules in a non-random fashion to increase the number of mixed, SM/cho contacts. Such behaviour is the basis for the formation of superlattices which have indeed been found for SM/cho systems under certain conditions (42, 43). An explanation for such a behaviour was given in terms of the ‘‘umbrella model’’ (44).

Thermodynamics of SM/cho interactions

The knowledge of ΔH yields also the entropic contribution to SM/cho compared to POPC/cho interactions. Since the enthalpy of cho transfer from POPC to SM measured here, $\Delta(\Delta H)$, should approximately agree with the enthalpy under standard conditions, $\Delta(\Delta H^0)$, we may

apply $\Delta(\Delta\mu^0) = \Delta(\Delta H^0) - T\Delta(\Delta S^0)$ to derive the entropic contribution to SM/cho interactions. We find that SM/cho interactions are accompanied by a strong, unfavourable loss in entropy that is contributing $-T\Delta(\Delta S^0) \sim +(8-15)$ kJ/mol to the standard free energy (Tab. 1). This behaviour is in accord with the concept of cho-induced ordering of SM chains. This improves molecular packing (van der Waals interactions), conformational enthalpy, and may include formation of H-bonds ($\Delta(\Delta H) < 0$) but reduces conformational and motional freedom ($\Delta(\Delta S^0) < 0$). We emphasize that ΔH per mol of cho becoming surrounded by SM agrees with $\sim 0.5-0.75\times$ the enthalpy per mol of SM undergoing the fluid→gel transition (~ -30 kJ/mol, (5, 28, 29)). The linear $\Delta(\Delta H(x))$ suggests, that at least at 50°C, cho is not “freezing” one or two neighbouring chains (which might happen in a specific complex (45, 46)) but gradually ordering all chains in its environment. We should note that the specific interaction between cho and SM involves a considerable enthalpy and is expected to induce major structural changes to the molecules. However, because this enthalpy is largely compensated by entropy, it does not give rise to a significant deviation of the molecules from a non-random arrangement. It can, therefore, not be detected by fluorescence energy transfer measurements like those performed in (47).

Temperature dependence

Another advantage of knowing ΔH is that it gives an estimate for the temperature dependence of the differential affinities. This is important since principal and technical problems hindered us to determine K_X at lower temperatures. Le Chatelier’s principle requires that every exothermic process (such as bringing more cho in contact with SM) is promoted by lower temperature. That means the preference of cho for SM and its activity to induce demixing increase upon cooling so that domain formation may proceed below a certain temperature. Quantitative estimates can be obtained using a modified van’t Hoff equation, $d(\ln(R_K)) = dT \Delta(\Delta H)/(RT^2)$. Assuming that $\Delta(\Delta H)$ is not strongly temperature dependent, we may estimate values for R_K at lower temperatures as given for 37°C in Tab. 1.

Comparison with literature data

Let us compare these values with those given in the literature. Our calculated value of $R_K(37^\circ\text{C}) = 5.5$ ($X_{\text{cho}} = 0.3$) for pure SM agrees with the value of 6.8 extrapolated by Niu and Litman (23) for POPC/pSM, and our prediction for POPC/eSM (1:1) is consistent with the result of Leventis and Silvius (21) who obtained $R_K(37^\circ\text{C}) = 2.6$ for SOPC/bSM (1:1). Other authors have obtained smaller values for R_K . For instance, the data of Lange et al. (16), who monitored cho exchange between ghost membranes and SUVs at 46°C can be used to calculate the following values. Cho exchange between egg PC and bSM is described by a value of $R_K = 2.0$, and exchange between egg PC and pSM by $R_K = 1.9$, respectively. Yeagle and Young (17) refrained from deriving $R_K(45^\circ\text{C})$ from similar, vesicle/vesicle transfer experiments because of too little net transfer of cho.

A qualitatively different behaviour was described recently by Veatch et al. (33) who provided detailed information on the system DOPC/DPPC/cho. The preference of cho for the ordered, DPPC-rich phase compared to the fluid, DOPC-rich phase is very weak with $R_K \sim 1.2-1.9$. Furthermore, R_K increases from 1.2 at 20°C to 1.8 at 30°C (DOPC/DPPC, 1:2) suggesting an endothermic transfer of cho from fluid to ordered domains with an enthalpy change of the order of +25 kJ/mol. That means that domain formation in this system is not significantly promoted by preferential interactions of cho with the saturated lipid and that the disappearance of ordered domains at high temperature seems to be opposed

by increasing preferential interactions of cholesterol. A possible explanation is that DOPC is a twofold unsaturated lipid so that its structural preferences differ more from DPPC than those for POPC from SM (see also (7, 48) for a discussion of the behaviour of monounsaturated vs. polyunsaturated lipid species). Hence, demixing in the DOPC/DPPC/cho system may be governed almost exclusively by unfavorable DOPC/DPPC interactions, whereas that in POPC/SM is substantially promoted by cho.

Lipid vs. cho extraction

An important issue for the application of cyd to manipulate the cho content of both model and cell membrane systems (20, 49) is the question what cyd concentrations are allowed to be used in order to leave the membrane intact. We have investigated the extraction of fluid phase SM by cyd as shown in Fig. 4 utilizing the protocol established by Anderson et al. (41). Based on the values obtained for the complex formation constant, K_{Φ} , it appears that at least at 50°C the affinity of SM for the inclusion complex with cyd is about half as large as the one of POPC. This observation reflects that either cyd/SM interactions are less favourable than cyd/POPC interactions or that SM/SM interactions within the membrane are more attractive than PC/PC interactions. The latter is in line with the respective hydrogen bonding properties (50).

In a previous study (24), we have shown that even for a POPC membrane, the cyd concentration window where cho is selectively extracted without removing also phospholipid and thus solubilizing the membrane as such is rather narrow. For example, a cyd concentration of 15 mM added to a POPC/cho vesicle suspension of 0.7 mM POPC and 0.3 mM cho extracts about 10% of the POPC but 90% of the cho (calculated for $T = 50^{\circ}\text{C}$). The data collected here imply that the problem is even more serious in the presence of SM. Although SM itself is less extracted than POPC, the presence of SM opposes the extraction of cho due to favourable SM/cho-interactions in the membrane. In our example (15 mM cyd, 0.7 mM phospholipid, 0.3 mM cho), 90% of cho would be extracted from a POPC membrane but only 75% from a POPC/SM (1:1) membrane. At lower temperature, extraction of cho is suggested to be even weaker from a membrane containing SM. Apart from the simplifying assumptions made in the calculation of the retention of lipid and cho in the membrane, we conclude that the application of cyd to a biological membrane is not straightforward. It requires very careful monitoring of the efficacy of cho extraction and, at the same time, the lack of extraction of other membrane constituents. Effects of cyd application to cells might be due to the dissolution of “lipid rafts” but also a consequence of extracting other molecules or of losing other important functions of cholesterol independently of its effect on lipid domains (13).

Conclusions

1. The affinity of cho to eSM is about 5- to 12-fold larger compared to POPC. The preference becomes stronger with decreasing temperature and decreasing cho concentration.
2. There are no pronounced differences in SM/cho-interactions (affinity, ΔH) between egg, brain, and palmitoyl SM.
3. The transfer of cho from POPC to SM is highly exothermic ($\Delta(\Delta H) \sim -(13-23)$ kJ/mol) but the gain in enthalpy is largely compensated by a loss in entropy.

4. The equilibrium constant for the extraction of SM from membranes by cyd is about twofold smaller than for POPC. However, the presence of SM impedes the extraction of cho.

Acknowledgments

Financial support from the Swiss National Science Foundation (grant 31-67216.01) is gratefully acknowledged. We thank Peter J. Slotte (Åbo Akademi University, Turku, Finland) for providing us with the pSM used in this study.

References

1. Brown, D. A., and J. K. Rose. 1992. Sorting of GPI-anchored proteins to glycolipid-enriched membrane subdomains during transport to the apical cell surface. *Cell* 68:533–544.
2. Simons, K., and E. Ikonen. 1997. Functional rafts in cell membranes. *Nature* 387:569–572.
3. Brown, D. A., and E. London. 2000. Structure and function of sphingolipid- and cholesterol-rich membrane rafts. *J. Biol. Chem.* 275:17221–17224.
4. London, E., and D. A. Brown. 2000. Insolubility of lipids in TX-100: physical origin and relationship to sphingolipid/cholesterol membrane domains (rafts). *Biochim. Biophys. Acta* 1508:182–195.
5. Heerklotz, H. 2002. Triton promotes domain formation in lipid raft mixtures. *Biophys. J.* 83:2693–2701.
6. Silvius, J. R. 2003. Role of cholesterol in lipid raft formation: lessons from lipid model systems. *Biochim. Biophys. Acta* 1610:174–183.
7. McMullen, T. P. W., R. N. A. H. Lewis, and R. N. McElhaney. 2004. Cholesterol-phospholipid interactions, the liquid-ordered phase and lipid rafts in model and biological membranes. *Current Opinion in Colloid and Interface Science* 8:459–468.
8. Melkonian, K. A., T. Chu, L. B. Tortorella, and D. A. Brown. 1995. Characterization of proteins in detergent-resistant membrane complexes from Madin-Darby Canine Kidney epithelial cells. *Biochemistry* 34:16161–16170.
9. Schuck, S., M. Honsho, K. Ekroos, A. Shevchenko, and K. Simons. 2003. Resistance of cell membranes to different detergents. *Proc. Natl. Acad. Sci. USA* 100:5795–5800.
10. van Rheenen, J., E. M. Achame, H. Janssen, J. Calafat, and K. Jalink. 2005. PIP₂ signaling in lipid domains: a critical re-evaluation. *The EMBO Journal* 24:1664–1673.
11. Munro, S. 2003. Lipid rafts: Elusive or Illusive? *Cell* 115:377–388.
12. Edidin, M. 2003. The state of lipid rafts: From model membranes to cells. *Annu. Rev. Biophys. Biomol. Struct.* 32:257–283.
13. Simons, K., and W. L. C. Vaz. 2004. Model Systems, Lipid Rafts, And Cell Membranes. *Annu. Rev. Biophys. Biomol. Struct.* 33:269–296.

14. Lichtenberg, D., F. M. Goñi, and H. Heerklotz. 2005. Detergent-resistant membranes should not be identified with membrane rafts. *Trends in Biochemical Sciences* 30:430–436.
15. Wattenberg, B. W., and D. F. Silbert. 1983. Sterol partitioning among intracellular membranes. *J. Biol. Chem.* 258:2284–2289.
16. Lange, Y., J. S. D’Alessandro, and D. M. Small. 1979. The affinity of cholesterol for phosphatidylcholine and sphingomyelin. *Biochim. Biophys. Acta* 556:388–398.
17. Yeagle, P. L., and J. E. Young. 1986. Factors contributing to the distribution of cholesterol among phospholipid vesicles. *J. Biol. Chem.* 261:8175–8181.
18. Slotte, J. P., and S. Illman. 1996. Desorption of fatty acids from monolayers to cyclodextrins in the subphase. *Langmuir* 12:5664–5668.
19. Yancey, P. G., W. V. Rodriguez, E. P. C. Kilsdonk, G. W. Stoudt, W. J. Johnson, M. C. Phillips, and G. H. Rothblat. 1996. Cellular cholesterol efflux mediated by cyclodextrins. *J. Biol. Chem.* 271:16026–16034.
20. Christian, A. E., M. P. Haynes, M. C. Phillips, and G. H. Rothblat. 1997. Use of cyclodextrins for manipulating cellular cholesterol content. *J. Lip. Res.* 38:2264–2272.
21. Leventis, R., and J. R. Silvius. 2001. Use of cyclodextrins to monitor transbilayer movement and differential lipid affinities of cholesterol. *Biophys. J.* 81:2257–2267.
22. Steck, T. L., J. Ye, and Y. Lange. 2002. Probing red cell membrane cholesterol movement with cyclodextrin. *Biophys. J.* 83:2118–2125.
23. Niu, S.-L., and B. J. Litman. 2002. Determination of membrane cholesterol partition coefficient using a lipid vesicle–cyclodextrin binary system: Effect of Phospholipid Acyl chain unsaturation and headgroup composition. *Biophys. J.* 83:3408–3415.
24. Tsamaloukas, A., H. Szadkowska, J. P. Slotte, and H. Heerklotz. 2005. Interactions of cholesterol with lipid membranes and cyclodextrin characterized by calorimetry. *Biophys. J.* 89:1109–1119.
25. Heerklotz, H. 2004. Microcalorimetry of lipid membranes. *Journal of Physics: Condensed Matter* 16:441–467.
26. Zhang, F., and E. S. Rowe. 1992. Titration calorimetric and differential scanning calorimetric studies of the interactions of *n*-butanol with several phases of dipalmitoylphosphatidylcholine. *Biochemistry* 31:2005–2011.
27. Barenholz, Y., J. Suurkuusk, D. Mountcastle, T. E. Thompson, and R. L. Biltonen. 1976. A calorimetric study of the thermotropic behavior of aqueous dispersions of natural and synthetic sphingomyelins. *Biochemistry* 15:2441–2447.
28. Calhoun, W. I., and G. G. Shipley. 1979. Sphingomyelin–Lecithin bilayers and their interaction with cholesterol. *Biochemistry* 18:1717–1722.
29. Maulik, P. R., and G. G. Shipley. 1996. *N*-Palmitoyl sphingomyelin bilayers: Structure and interaction with cholesterol and dipalmitoylphosphatidylcholine. *Biochemistry* 35:8025–8034.

30. Frank, A., Y. Barenholz, D. Lichtenberg, and T. E. Thompson. 1983. Spontaneous transfer of sphingomyelin between phospholipid bilayers. *Biochemistry* 22:5647–5651.
31. Xu, X., and E. London. 2000. The effect of sterol structure on membrane lipid domains reveals how cholesterol can induce lipid domain formation. *Biochemistry* 39:843–849.
32. Guo, W., V. Kurze, T. Huber, N. H. Afdhal, K. Beyer, and J. Hamilton. 2002. A solid-state NMR study of phospholipid–cholesterol interactions: Sphingomyelin–cholesterol binary systems. *Biophys. J.* 83:1465–1478.
33. Veatch, S. L., I. V. Polozov, K. Gawrisch, and S. L. Keller. 2004. Liquid domains in vesicles investigated by NMR and fluorescence microscopy. *Biophys. J.* 86:2910–2922.
34. Sankaram, M. B., and T. E. Thompson. 1990. Interaction of cholesterol with various glycerolipids and sphingomyelin. *Biochemistry* 29:10670–10675.
35. Maulik, P. R., and G. G. Shipley. 1996. Interactions of *N*-stearoyl sphingomyelin with cholesterol and dipalmitoylphosphatidylcholine in bilayer membranes. *Biophys. J.* 70:2256–2265.
36. Heerklotz, H., H. Szadkowska, T. Anderson, and J. Seelig. 2003. The sensitivity of lipid domains to small perturbations demonstrated by the effect of Triton. *J. Mol. Biol.* 329:793–799.
37. Wiseman, T., S. Williston, J. F. Brandts, and L. N. Lin. 1989. Rapid measurement of binding constants and heats of binding using a new titration calorimeter. *Anal. Biochem.* 179:131–137.
38. Chellani, M. 1999. Isothermal titration calorimetry: biological applications. *Am. Biotechnol. Lab* 17:14–18.
39. Heerklotz, H., and J. Seelig. 2000. Titration calorimetry of surfactant–membrane partitioning and membrane solubilization. *Biochim. Biophys. Acta* 1508:69–85.
40. Tsamaloukas, A., H. Szadkowska, and H. Heerklotz. 2005. Nonideal mixing in multi-component lipid/detergent systems. *submitted to J. Phys.: Condens. Matter* .
41. Anderson, T. G., A. Tan, P. Ganz, and J. Seelig. 2004. Calorimetric measurement of phospholipid interaction with methyl- β -cyclodextrin. *Biochemistry* 43:2251–2261.
42. Huang, J. 2002. Exploration of molecular interactions in cholesterol superlattices: effect of multibody interactions. *Biophys. J.* 83:1014–1025.
43. Cannon, B., G. Heath, J. Huang, J. A. Somerharju, J. A. Virtanen, and K. H. Cheng. 2003. Time-resolved fluorescence and Fourier transform infrared spectroscopic investigations of lateral packing defects and superlattice domains in compositionally uniform cholesterol/phosphatidylcholine bilayers. *Biophys. J.* 84:3777–3791.
44. Huang, J., and G. W. Feigenson. 1999. A microscopic model of maximum solubility of cholesterol in lipid bilayers. *Biophys. J.* 76:2142–2157.
45. Radhakrishnan, A., and H. M. McConnell. 1999. Condensed complexes of cholesterol and phospholipids. *Biophys. J.* 77:1507–1517.

46. Radhakrishnan, A., T. G. Anderson, and H. M. McConnell. 2000. Condensed complexes, rafts and the chemical activity of cholesterol in membranes. *Proc. Natl. Acad. Sci. USA* 97:12422–12427.
47. Holopainen, J. M., A. J. Metso, J.-P. Mattila, J. Arimatti, and P. K. J. Kinnunen. 2004. Evidence for the lack of a specific interaction between Cholesterol and Sphingomyelin. *Biophys. J.* 86:1510–1520.
48. Wang, T.-Y., R. Leventis, and J. R. Silvius. 2000. Fluorescence based evaluation of the partitioning of lipids and lipidated peptides into liquid-ordered lipid microdomains: A model for molecular partitioning into “lipid rafts”. *Biophys. J.* 79:919–933.
49. Niu, S.-L., and B. J. Litman. 2002. Manipulation of cholesterol levels in rod disk membranes by methyl- β -cyclodextrin. *J. Biol. Chem.* 277:20139–20145.
50. Ramstedt, B., and J. P. Slotte. 2002. Membrane properties of sphingomyelins. *FEBS Letters* 531:33–37.

List of Tables

- 1 Results obtained with the data fitting in Fig. 3 and derived quantities. K_X denotes the cyclodextrin/membrane partition coefficient, R_K is the ratio between K_X for a SM-containing membrane and K_X for pure POPC as determined in (24). $\Delta(\Delta\mu^0)$ is the standard chemical potential difference of cho insertion (compared to POPC), $\Delta(\Delta\mu^0) = -RT \ln(R_K(50^\circ\text{C}))$, ΔH is the enthalpy of transfer of cho from cyd into the membrane, $\Delta(\Delta H)$ is the enthalpy of cho transfer from POPC into the membrane of interest assumed to be equal to the enthalpy change under standard conditions, $\Delta(\Delta H^0)$. The standard entropy change of cho transfer from POPC into another membrane is obtained as: $-T\Delta S^0 = \Delta(\Delta\mu^0) - \Delta(\Delta H)$. Values of $R_K(37^\circ\text{C})$ were estimated from $R_K(50^\circ\text{C})$ and $\Delta(\Delta H)$ using a modified van't Hoff equation: $d(\ln(R_K)) = dT \Delta(\Delta H)/(RT^2)$, assuming $\Delta(\Delta H)$ to be constant. Errors for the parameters are as detailed under Materials and Methods.

TABLES

Membrane	X_{cho}	K_X	$R_K(50^\circ\text{C})$	$R_K(37^\circ\text{C})$	$\Delta(\Delta\mu^0)$	ΔH	$\Delta(\Delta H)$	$-T\Delta(\Delta S^0)$
	%	mM				kJ/mol		
PC	20	30	1.0	1.0	0	-5	0	0
PC/SM (1:1)	20	108	3.6	4.3	-4	-17	-12	8
SM	20	360	12	17	-8	-28	-23	15
PC	30	35	1.0	1.0	0	-5	0	0
PC/SM (1:1)	30	73	2.1	2.3	-2	-12	-7	5
SM	30	158	4.5	5.5	-5	-18	-13	8

Table 1

List of Figures

- 1 Experimental raw data of cho uptake and release assay conducted at 50°C. For the release assay 10 mM lipid vesicles with a mol fraction of pSM, $X_{\text{pSM}} = 0.25$ and a mol fraction of cho, $X_{\text{cho}} = 0.2$, were titrated into a 5 mM cyd solution. In case of the uptake assay vesicles with $X_{\text{pSM}} = 0.25$ without cho were titrated into a 5 mM cyd + 70 μM cho solution. For both raw data sets shown in Panel A the injection protocol was: $1 \times 1 \mu\text{L}$, $3 \times 5 \mu\text{L}$, and $26 \times 10 \mu\text{L}$. Panel B: Global fit (solid lines) to the normalized heats, Q_{obs} , of uptake (\circ) and release (\square) assay resulting after integration of the power peaks shown in Panel A. Data are corrected for the heats obtained in a blank experiment injecting the same vesicles into buffer.
- 2 Panel A: Detail of the experimental raw data obtained with the Rowe protocol at 50°C. An aliquot of $\Delta V_2 = 10 \mu\text{L}$ of vesicles with $X_{\text{eSM}} = 0.5$, $X_{\text{cho}} = 0.2$, and $X_{\text{PC}} = 0.3$ was injected into a 5 mM cyd-solution with varying cho concentration, $c_{\text{cho}}^{\text{cell}}$, as depicted in the plot. Panel B: Heats ΔH resulting from an integration of the power peaks shown in A (after blank correction) as a function of $c_{\text{cho}}^{\text{cell}}$. The partition coefficient K_X can be calculated from the intercept with the $c_{\text{cho}}^{\text{cell}}$ -axis and the molar transfer enthalpy, ΔH , can be obtained using Eq. 4.
- 3 The cyclodextrin-membrane partition coefficient, K_X (Panel A), and the molar transfer enthalpy, ΔH (Panel B), of cholesterol measured for various POPC/SM-mixtures at $T = 50^\circ\text{C}$. For both panels symbols used correspond to: global analysis of ITC uptake/release data sets of POPC/eSM vesicles with $X_{\text{cho}} \sim 0.3$ (\bullet), POPC/pSM vesicles with $X_{\text{cho}} \sim 0.2$ (\times), Rowe protocol for POPC/eSM vesicles with $X_{\text{cho}} = 0.2$ (\diamond), uptake experiments with POPC/eSM (\blacktriangle) and POPC/bSM vesicles ($+$), and release experiment (∇) with POPC/eSM vesicles with $X_{\text{cho}} = 0.2$. Solid lines in both panels correspond to linear fits to the POPC/eSM-data with $X_{\text{cho}} = 0.3$ (\bullet), and dashed lines to POPC/eSM-data with $X_{\text{cho}} = 0.2$ (\diamond). For both data sets, the point at $c_{\text{SM}}/(c_{\text{SM}} + c_{\text{PC}}) = 0$ was taken from (24).
- 4 Titration of eSM vesicles into cyd-solutions at $T = 50^\circ\text{C}$. Panel A presents the titration of 8 mM eSM LUVs into a 40 mM cyd solution using $1 \times 1 \mu\text{L}$ (see text) and $56 \times 5 \mu\text{L}$ -aliquots. Panel B: Normalized heats, Q_{obs} , resulting after integration of the power peaks shown in A for titrations of a 20 mM cyd (\circ), 40 mM cyd (Δ), and 60 mM cyd solution (∇) with 5, 8, and 10 mM eSM LUVs, respectively. Data shown in B are not corrected for the heats obtained in titrations of the respective cyd-solutions with buffer (see text).

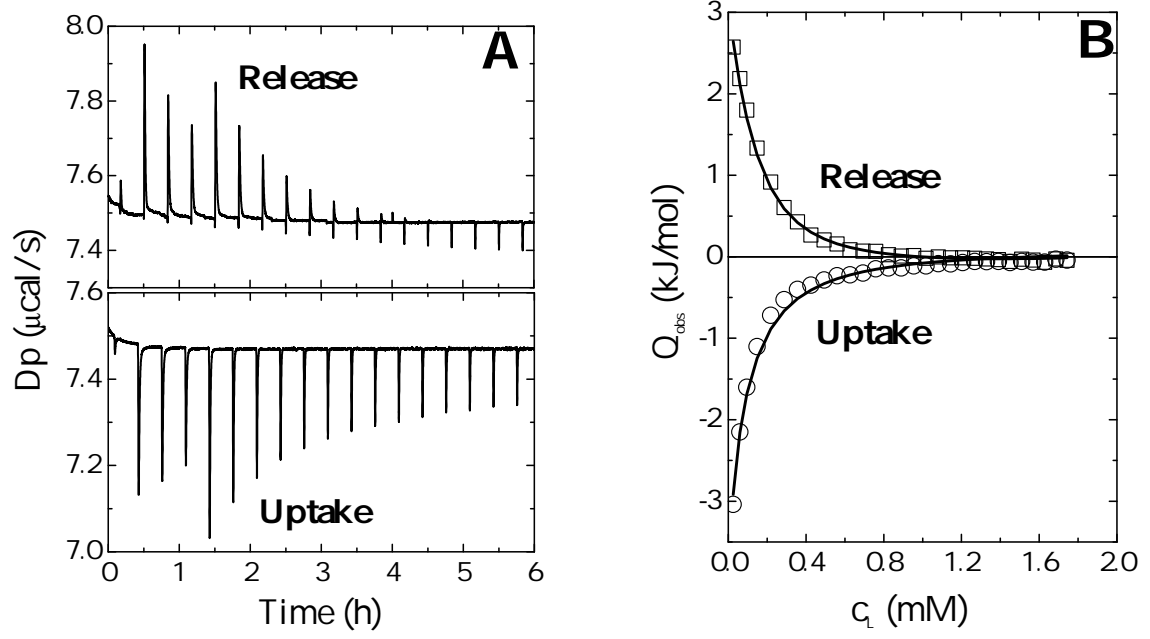


Figure 1

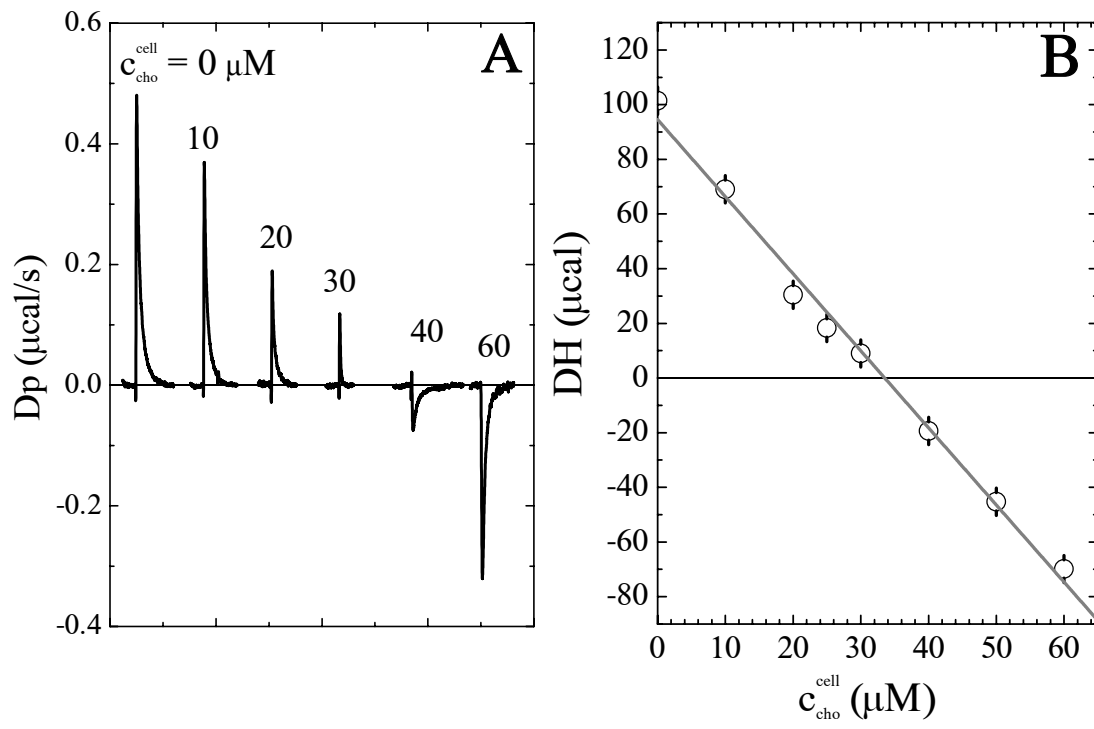


Figure 2

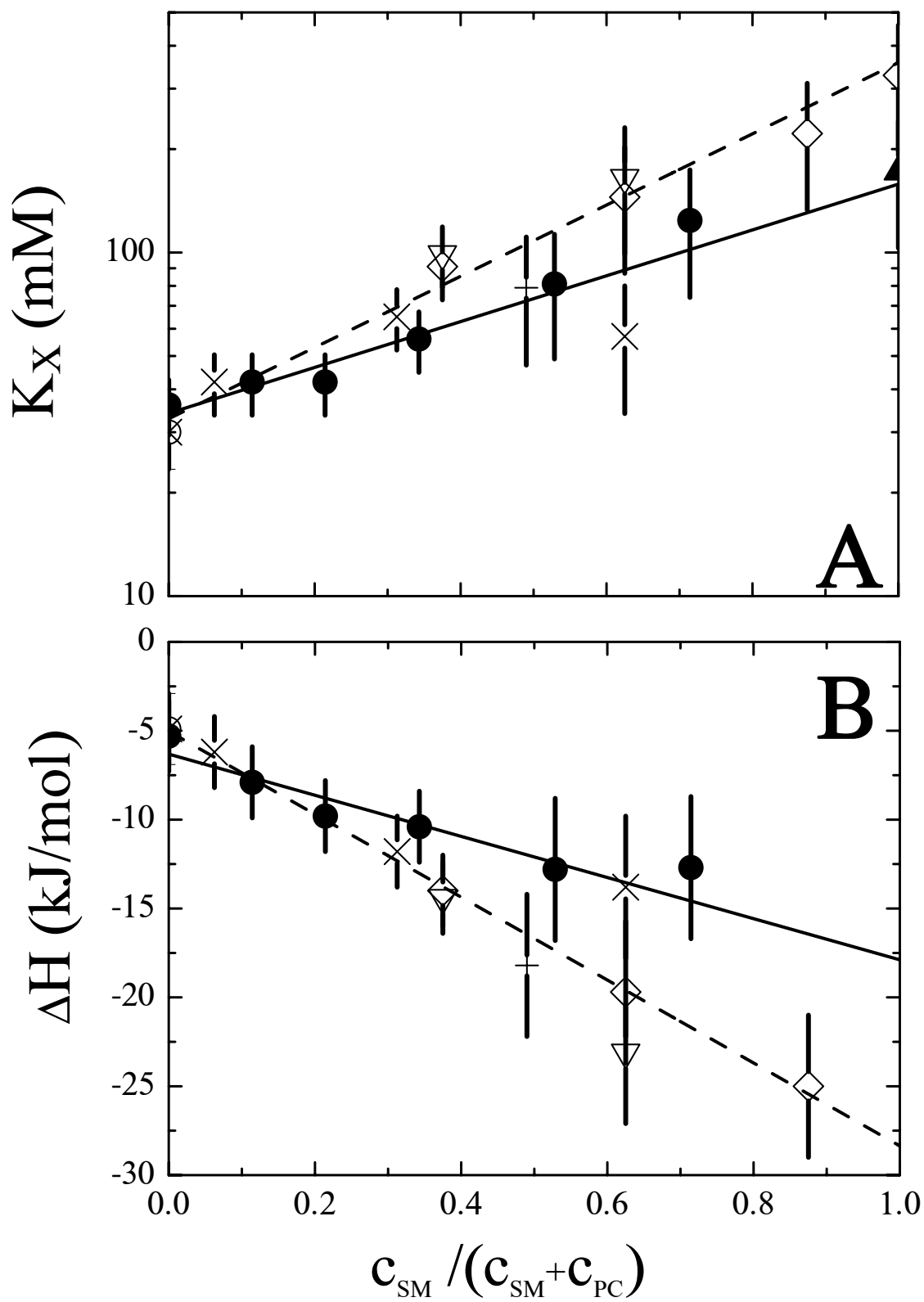


Figure 3

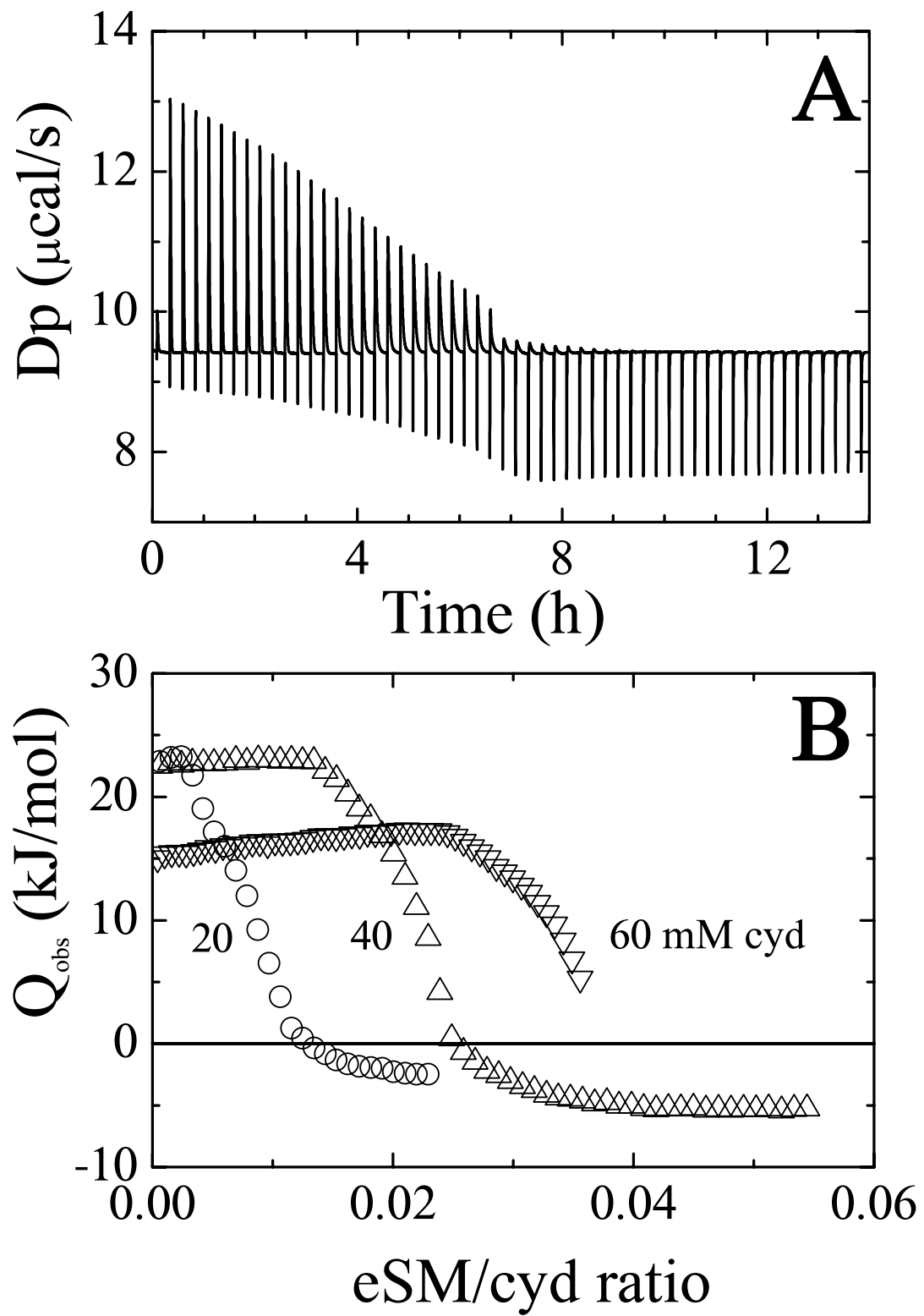


Figure 4

Gradual change or phase transition - characterizing fluid lipid-cholesterol membranes on the basis of thermal volume changes

Heiko Heerklotz* and Alekos Tsamaloukas

Biozentrum der Universität Basel, Div. of Biophysical Chemistry, Klingelbergstr. 70, CH-4056 Basel, Switzerland.

* Corresponding author, Tel. +41-61-267 2180, Fax +41-61-267 2189, Email: heiko.heerklotz@unibas.ch

Cholesterol has been reported to govern biomembrane permeability, elasticity, and the formation of lipid rafts. There has been a controversy whether binary lipid-cholesterol membranes should better be described in terms of a phase separation (liquid ordered and liquid disordered phases) or of gradual changes in largely homogeneous membranes. We present a new approach for detecting and characterizing phase equilibria in colloidal dispersions using pressure perturbation calorimetry (PPC). We apply this to the study of the thermal expansivity of mixtures of 1-palmitoyl 2-oleoyl *sn*-glycero-3-phosphatidylcholine (POPC) and cholesterol as a function of composition and temperature. We show for the first time that cholesterol can condense lipids not only laterally (with respect to interfacial area) but also in volume. A quantitative comparison with expansivity curves simulated assuming either phase separation or random mixing within one phase reveals that the real system shows an intermediate behavior due to sub-microscopic de-mixing effects. However, both models yield consistent system parameters and are thus found to be useful for describing the systems to a similar approximation. Accordingly, one cholesterol may condense 3 ± 1 POPC molecules by $\sim -(1.4 \pm 0.5)$ vol-% at 2°C; both absolute values decrease with increasing temperature.

INTRODUCTION

Cholesterol plays a key role in biological membrane function including the regulation of membrane elasticity and permeability and has been considered essential for the formation of lipid rafts. These phenomena are of utmost biological, medical and pharmaceutical interest. However, details of the interactions of cholesterol with lipid membranes are still a matter of controversy, in spite of enormous efforts dedicated to the issue over several decades (to specify only a few reviews, see (1-4)).

It is widely accepted that cholesterol can induce a liquid ordered (ℓ_o) state in lipid membranes, which has intermediate properties between a gel phase (ordered acyl chains) and a liquid disordered (ℓ_d), fluid phase (high lateral mobility, no crystalline arrangement) (5,6). A macroscopic separation of two liquid (ℓ_o and ℓ_d) phases has been observed for ternary mixtures of, e.g., DOPC, DPPC, and cholesterol, whereas binary lipid-cholesterol mixtures were found to exhibit, at the most, submicroscopic domain formation (7,8). There is, however, an ongoing debate whether also binary mixtures are best described assuming ℓ_o - ℓ_d coexistence in a certain composition and temperature range (see, e.g., (3,4,9)), and the literature is particularly controversial for the POPC-cholesterol system. Phase diagrams including a liquid-liquid (ℓ_o - ℓ_d) coexistence have been established for lipids with saturated chains such as DPPC and sphingomyelin (10,11) but also for unsaturated lipids such as PPEtPC (6) and POPC (12,13). However, NMR studies on POPC-cholesterol did not provide unequivocal evidence for a ℓ_o - ℓ_d two-phase range (9,14). The mechanical properties of POPC-cholesterol membranes studied by micropipette aspiration and vesicle fluctuation analysis revealed no indication of a phase separation as well (9). Results of molecular dynamics simulations of cholesterol-induced ordering and lateral area compression of DPPC could also be well discussed in terms of a continuous change in membrane properties (15).

When it comes to discuss whether lipid mixtures are best described by a phase coexistence, one should recall that thermodynamic phases in the strict sense are macroscopically separate, so that micro- or nanoscopic domains in membranes can only approximately be treated as phases. Nanoscopic domains show additional phenomena such as an entropy of mixing with other domains, an edge energy related to the line tension between the domains, a limited lifetime, and an exchange of molecules between domains. Hence, the question whether a microheterogeneous system qualifies approximately as a phase coexistence or not cannot be answered on the basis of the existence and size of domains alone. Therefore, we pursued the strategy to characterize whether the macroscopic system as a whole behaves like a two-phase or a one-phase system. We selected POPC-cholesterol since this is particularly ambiguous. We show that the thermal volume expansion provides an excellent criterion for assessing whether the composition- and temperature-dependent behavior of the mixture resembles that of a two-phase system or not. We discuss the data in terms of one- and two-phase models in parallel, thus allowing for a direct comparison.

It should be noted that the results provide important new insight also apart from the phase issue. So far, very little has been known about cholesterol-induced changes in the (temperature dependent) partial volume of phospholipids. What has long been clear is that cholesterol may increase the order of saturated acyl chains of neighboring lipids, which results in their effective stretching, an increase in membrane thickness, and a lateral condensation of membrane area (1,2). The volume of the lipid has been assumed to be virtually conserved upon this change in chain order and membrane geometry (e.g., Ref. (15)) since no excess volume of these mixtures arising from cholesterol-induced lipid volume condensation could be measured. This may be surprising taking into account the variety of precise methods to measure densities or partial volumes of lipids (16-18). It was, in fact, shown that the density of membranes increases upon addition of cholesterol (16) but the problem is to distinguish between the intrinsic volume of cholesterol and the excess volume that is due to cholesterol-induced lipid ordering, since there is no pure cholesterol membrane which could serve as a reference state. Another approach is to determine the volume change accompanying lipid melting, which is reduced by cholesterol from 2 % for pure POPC to 1.7 % (cholesterol mole fraction $X = 0.05$), 1.5 % (0.1) and 1.0 % (0.2), suggesting a more densely packed fluid phase and/or less dense gel phase in the presence of cholesterol (19). However, cholesterol effects on the gel and the fluid phase cannot be distinguished this way. Tauc et al. (12) showed that the "effective" phase boundaries in the cholesterol-POPC system are substantially shifted in favor of the ℓ_o phase by high pressure, which implies that the partial volume of the molecules in the ℓ_o state is significantly lower. For example at 25°C, the coexistence range was shifted from cholesterol mole fractions $X \sim 0.10 - 0.40$ at 1 bar to \sim

0.03 – 0.24 at 600 bar. This X-shift of the boundaries corresponds to a shift in the transition temperature of the order of 12 K/kbar, which is comparable with the pressure dependence of melting a POPC gel phase, ~ 20 K/kbar (20). A direct quantification of the volume change of the order-disorder transition at ambient pressure is, however, not straightforward and was not attempted by these authors.

We use a novel method, pressure perturbation calorimetry (PPC) (21), which measures not the volume per se but the heat response of a sample to a small pressure perturbation. This is directly related to the thermal volume expansion at constant pressure. The advantage of measuring not a parameter representing packing (area, order, volume) but its derivative is that the latter exhibits a sudden jump at a phase boundary, where the integral parameters show only a change in slope. The results are compared with model curves derived for a two-phase system and for cholesterol-induced condensation of POPC in a randomly mixed, one-phase membrane. The approach presented here helps resolving the apparent inconsistencies between the models used in the literature and may be important for deriving a more precise, more complex model explicitly considering the micro-heterogeneity of the membranes.

EXPERIMENTAL

Materials

1-Palmitoyl-2-oleoyl-*sn*-glycero-3-phosphocholine (POPC) was purchased from Avanti Polar Lipids (Alabaster, AL, USA) and cholesterol was from Fluka (Buchs, Switzerland). Mixtures of POPC and cholesterol were prepared by dissolution of appropriate amounts of the dry substances in chloroform/methanol. Multilamellar vesicles (MLVs) were prepared by a standard method involving drying of the mixed lipids and re-suspension in pure water as described elsewhere (22). Cholesterol concentrations larger than 50 mol-% were avoided, they would require another preparation technique (23). PPC experiments were performed at a constant POPC concentration of 15 mM including various amounts of cholesterol as specified.

Pressure perturbation calorimetry (PPC)

PPC measurements were carried out in a VP DSC calorimeter from MicroCal (Northampton, MA, USA), equipped with a PPC accessory from the same manufacturer. The sample cell (0.5 mL) was filled with the lipid suspension and the reference cell with water. The technique is explained elsewhere (21,24). Briefly, the sample and reference cell are subject to small pressure jumps of $\Delta p \sim 5$ bar and the system measures the heat required to compensate that induced by the pressure jump (thus keeping the temperature, T , constant). Blank measurements with both cells filled with water are conducted to correct for technical imperfections. The procedure is repeated automatically at many temperatures. Hence, the technique measures the heat response of the lipid to a very small pressure change at constant temperature, approximately corresponding to the differential $\partial Q/\partial p|_T$. This differential heat is related to the the isobaric, thermal volume expansion, $\partial V/\partial T|_p$, which can be seen by inserting the equation for the heat of a reversible process, $dS=dQ/T$, into the Maxwell relation for the isothermal entropy change with pressure, $\partial S/\partial p|_T$:

$$\left. \frac{\partial S}{\partial p} \right|_T = - \left. \frac{\partial V}{\partial T} \right|_p \quad (1).$$

The results can be expressed as the coefficient of thermal expansion, $\alpha = \partial V/(V\partial T)|_p$, or as the change in partial molar volume with temperature, $V' = \partial V/\partial T|_p$, at constant pressure. A good estimate for the partial molar volume of the mixed membrane, V , as a function of the mole fraction of cholesterol, X , is obtained using $V \sim XV_{\text{cho}}^0 + (1-X)V_{\text{PC}}^0$ using partial volumes of $V_{\text{cho}}^0 \sim 325$ mL/mol (15) and $V_{\text{PC}}^0 \sim 760$ mL/mol (17). The small excess volume can be neglected.

THEORY

Composition-dependent expansivity in general

For curve fitting, it is advantageous to use molar expansivities, $V' = \partial V/\partial T$ (given in mL/(mol K)) since contributions to V' from different components or moieties are additive. For obtaining an expression for V' as a function the mole fraction of cholesterol, X , we may write the partial molar volume of the membrane, V , as a combination of the partial molar volumes of disordered PC and cholesterol (V_{PCd} and V_{cho} , respectively, which are assumed to mix ideally) and a contribution from

cholesterol-induced condensation of PC which is quantified by the volume change, $\Delta V = V_{PCo} - V_{PCd}$, and the degree of ordering of PC, $\xi_{PC} = [PC_o]/[PC]$:

$$V = X V_{cho} + (1 - X) \cdot [V_{PCd} + \xi_{PC} \Delta V] \quad (2).$$

Like the degree of a reaction, ξ_{PC} changes from 0 for a fully disordered to 1 for a fully ordered membrane. This model assumes implicitly that the excess volume of cholesterol-induced ordering is largely a property of the PC whereas cholesterol requires a similar intrinsic volume in an ordered or disordered environment. Differentiation yields the model equation for V' :

$$V' = X V'_{cho} + (1 - X) [V'_{PCd} + \xi'_{PC} \Delta V + \xi_{PC} \Delta V'] \quad (3).$$

The different models of the mixed membrane to be compared here provide different expressions for ξ_{PC} and $\xi'_{PC} = d\xi_{PC}/dT$ as outlined in the following.

Phase model

The phase model describes the system in terms of three phase ranges with phase boundaries at X_d and X_o as illustrated by Fig. 1 (top). These are the liquid disordered (ℓ_d) range at $X < X_d$, the $\ell_d + \ell_o$ coexistence range ($X_d < X < X_o$, dotted area in Fig. 1), and the liquid ordered (ℓ_o) range ($X_o < X$).

In the ℓ_d range, no PC is ordered ($\xi_{PC} = 0$) and no PC becomes ordered ($\xi'_{PC} = 0$) so that Eq. (3) becomes:

$$V' = X V'_{cho} + (1 - X) V'_{PCd} \quad (4).$$

In the ℓ_o range, $\xi_{PC} = 1$ and $\xi'_{PC} = 0$ so that we obtain with $V_{PCo}' = V_{PCd}' + \Delta V'$:

$$V' = X V'_{cho} + (1 - X) [V'_{PCd} + \Delta V'] \quad (5).$$

Note that both Eqs. (4) and (5) are linear in X as illustrated by the bold solid lines in Fig. 1, bottom. Note that the expansivity of cholesterol is assumed to be largely independent of the phase state, $V_{cho} = V_{cho,d} = V_{cho,o}$. The value of V_{cho} cannot directly be measured since cholesterol alone forms no membranes; the limit for cholesterol mixing with the membrane is $X = 0.66$ (23) (we are not aware of information regarding the temperature dependence of this limit). The fact that Fig. 1 is based on $V_{PCd}' < V_{PCo}'$ corresponds to $\Delta V' > 0$ so that the more dense phase, ℓ_o , expands “faster” with increasing T than ℓ_d and its partial molar volume “catches up” with that of ℓ_d . At a critical point, the differences between the phases vanish and $V_{PCo} = V_{PCd}$.

In the $\ell_d + \ell_o$ coexistence range, we obtain (see appendix 1):

$$V' = X V'_{cho} + (1 - X) V'_{PCd} + \xi (1 - X_o) \Delta V' + \Delta V [(1 + \xi) a X_d' + \xi (a - 1) X_o'] \quad (6)$$

with the constant a :

$$a \equiv -\frac{1 - X_o}{X_o - X_d} \quad (7)$$

and the derivatives $X_d' = dX_d/dT$ and $X_o' = dX_o/dT$ which are just the inverse slopes of the phase boundaries (see Fig. 1 and appendix 1 for derivation). The first three terms in Eq. (6) correspond to a straight line from point A to D in Fig. 1 bottom, i.e., a weighted sum of the expansivities of ℓ_d and ℓ_o phases. Additionally, there is the term in the rectangular bracket times ΔV which appears suddenly at the phase boundaries and corresponds to the temperature-driven conversion of ℓ_o into ℓ_d phase. At the onset of the coexistence range, at X_d , the degree of ordered molecules is $\xi = 0$ and the step in V' arising from the phase conversion term becomes $V'(B) - V'(A) = \Delta V a X_d'$. If $\Delta V > 0$ (disordering causes expansion) and $X_d' > 0$ (the slope of the X_d boundary is positive), this step is positive (upward) as shown in Fig. 1, bottom. Note that an increasing phase boundary X_d (i.e., $1/X_d' > 0$, $X_d' > 0$, as shown in Fig. 1) means that increasing T shifts the system in the vicinity of the boundary toward the ℓ_d state, i.e., ℓ_o “melts” to ℓ_d . Within the coexistence range, ξ increases linearly with X (lever rule, see appendix, Eq. (10)) so that the phase conversion term follows a straight line. Approaching the X_o boundary, $\xi \rightarrow 1$ and the phase conversion term becomes $V'(C) - V'(D) = \Delta V [2a X_d' + (a - 1) X_o']$ which is positive for $\Delta V > 0$, $a > 1$, and both phase boundaries increasing, $X_d' > 0$ and $X_o' > 0$.

With increasing temperature, the thermal phase conversion per se may become stronger (if the slopes of the boundaries decrease) but ΔV becomes weaker, finally vanishing at the critical point. If, however, the phase boundaries become very steep (i.e., $X_d' \rightarrow 0$, $X_o' \rightarrow 0$), the phase conversion term (and, thus, the steps in V' at the boundaries) vanish also if the system remains in the coexistence

range ($\Delta V > 0$). That means, vanishing steps in V' at the phase boundaries does not necessarily imply the proximity of the critical temperature.

Random-neighbor model

This model is based on the idea that the molecules mix randomly in the membrane and each cholesterol molecule can order up to n PC molecules in its neighborhood. A second cholesterol that interacts with a previously ordered PC has no further effect. That means, the fraction of condensed PC increases linearly with X at low X and shows a saturation when the cholesterol molecules start to interfere with each other. Edholm and Nagle (15) have derived an elegant expression for the cholesterol-dependent area of such a membrane which is analogous to Eq. (2) with a probability of a PC to be ordered, ξ_{PC} :

$$\xi_{PC} = 1 - e^{-nX} \quad (8).$$

If the temperature changes at a given composition X , the amount of ordered lipid changes as:

$$\xi_{PC}' = X \cdot n' \cdot e^{-nX} \quad (9)$$

if n is temperature dependent so that $n' = dn/dT$ does not vanish. The effect on V' is obtained by inserting eqs. (8) and (9) into eq. (3).

RESULTS

Fig. 2A shows the ‘‘PPC curves’’, i.e., the temperature dependencies of the coefficient of thermal volume expansion, $\alpha(T)$, for mixtures of POPC with different amounts of cholesterol. All values are of the order of one per mille per degree, or in other words, increasing the temperature by 10 degrees expands the volume by about 1%. The curve for pure POPC is in good agreement with $\alpha = 0.8 \times 10^{-3} \text{K}^{-1}$ measured for POPC with the neutral buoyancy method (18). However, there are significant systematic differences between cholesterol-containing and pure PC membranes. Two characteristic patterns are found (Fig. 2 A and B) depending on the cholesterol content, X . Moderate addition of cholesterol (Fig. 2A) leads to an enhanced expansion at low temperature which can be explained in terms of a cholesterol-condensed state that is relaxed upon increasing temperature. At higher temperatures, the curves approach that of pure PC. At intermediate X (Fig. 2B), the strong initial decrease of $\alpha(T)$ vanishes and the maximum of α shifts to higher temperatures, suggesting that the condensed state is stabilized by higher cholesterol contents and requires higher temperature to be relaxed. At $X \geq 0.4$, there is virtually no structural transition observed to proceed upon varying temperature.

The range of anomalously enhanced α is illustrated by Fig. 3. The axes of the plot are those of a phase diagram and the range of enhanced α resembles, to some extent, the shape and position of the coexistence range in published phase diagrams. We should however emphasize that the range of enhanced α is not necessarily identical with a phase range (see section on phase model in Theory). In order to elucidate this issue, we have plotted $V'(X)$ for a series of selected temperatures (Fig. 4) and compared it with the phase model, Eqs. (4) - (6).

The solid lines in Fig. 4 were obtained from the phase model by a global, visual optimization of X_d , X_o , ΔV , and V_{cho}' at all selected temperatures (see Fig. 1 for an illustration of the effect of the parameters). V_{PCd}' is identified with the experimental value of V' for pure PC (i.e., $X = 0$). The derivatives X_d' , X_o' , and $\Delta V'$ are obtained from the change in the input parameters from one panel (i.e., temperature) to another. The values for X_d and X_o are visible as steps in Fig. 4. The position of the phase boundaries at, e.g., 20°C (X_d ; $X_o = 0.085$; 0.375) agrees very well with the results of Tauc et al. (12) (0.09; 0.34), which is between the ranges discussed by Henriksen et al. (9) (0.05; 0.3) and measured by de Almeida et al. (13) (0.11; 0.45). It should be noted that different methods may, for example, differ in the minimum size or lifetime of a domain to become detectable. Therefore, they are likely to yield different ‘‘effective’’ phase boundaries in a system that shows no true phase separation but only an approximate two-phase behavior.

The absolute values of ΔV decrease from -10 mL/mol (~ -1.3 vol-%) at 2°C to -9 mL/mol at 10°C and -5 mL/mol (0.7 vol-%) at 40°C, estimated errors are ± 3 mL/mol. The extrapolated expansivity of hypothetical cholesterol membranes, V_{cho}' , increases with T from ~ 0.1 mL/(mol K) at 2°C to ~ 0.4 mL/(mol K) at 40°C.

The random-neighbor model yields the dashed curves in Fig. 4 by choosing values for n , ΔV , and V_{cho}' for each panel. Again, the curves in the panels depend on each other and have to be optimized

globally since n' and $\Delta V'$ are obtained from the variation of n and ΔV between the panels. The parameters for the presented curves are, for example, $n = 3$ at 2°C , 2 at 10°C and 1 at 40°C , $\Delta V = -12$ mL/mol at 2°C , -9 mL/mol at 10°C , and -6 mL/mol at 40°C ; V'_{cho} ranged from 0 at 2°C to 0.3 mL/(mol K) at 40°C .

DISCUSSION

Phase coexistence or gradual transition?

Inspection of Fig. 4 reveals that the behavior of the experimental data is intermediate between the curves obtained by the phase and the random-neighbor model. At very low cholesterol concentration, the condensing effect is weaker than suggested by the random-neighbor model. This implies that the cholesterol molecules do not act fully independently and a concerted action of more than one cholesterol molecule can give rise to a stronger effect. Substantial deviations from the phase model are observed in particular at high X where a gradual decrease of V' is found instead of the sudden drop predicted for a phase boundary. On the other hand, the decrease of V' is still steeper than what can be understood in terms of the random-neighbor model. It must be emphasized that, although the model assumptions and fits are different, the parameters of the two models are consistent with each other (see below). That means our direct, quantitative comparison of the two competing models does not imply one model to be correct and the other to be wrong. Both models are similarly good (or bad) approximations for the real behavior, which is intermediate between the extreme cases represented by the models.

The intermediate behavior found here is in accord with the existence of nanoscopic domains or composition fluctuations that have some properties of a phase but show additional effects that do not apply to true phases. The smaller the domains are and the larger their number, the larger is the entropy gain associated with the freedom to distribute them over the membrane. The phase concept ignores also the contribution to the membrane free energy from domain boundaries which depends on the number and circumference of the domains and the line tension. The complexity of the effects appears to hinder a quantitative description of the system on the basis of structural data.

We emphasize that the significant deviation between the experimental data ($V'(X,T)$) and the behavior expected for a true two-phase as well as a true one-phase system is not a weakness but an advantage of this approach. Although it is theoretically obvious that these models are not perfect, many other observables have been discussed in the literature in terms of one of these models without noticing an inconsistency (see Introduction). These parameters are not applicable to quantify the accuracy of the models. The PPC approach can, in contrast, aid the development of a refined model taking into account the microheterogeneity of the system. For POPC, this refined model is, as expected, not that of condensed, stoichiometric complexes which were reported for other lipids but not for POPC (25,26). Modeling the data on the basis of V' of complex formation (not shown) did, in spite of one additional adjustable parameter, not yield a considerably improved fit.

Cholesterol-induced volume changes

So far, it has been assumed that the well-known chain ordering and stretching effect of cholesterol on PC is fully compensated by an area condensation so that the partial volume of PC remains virtually unchanged, i.e., there would be no excess volume in PC-cholesterol mixtures. Here we detect and quantify this excess volume for the first time. In spite of the limitations of the models discussed above, both yield similar volume changes of cholesterol-induced ordering of PC. At 2°C , we obtained $\Delta V = -(10 \pm 5)$ mL/mol in terms of the phase model and $-(12 \pm 5)$ mL/mol by the random-neighbor model, which corresponds to a relative volume change of $\sim -1.4\%$.

The extent of cholesterol-induced condensation of POPC, up to $\sim -1.4\%$, is much less than the corresponding area and membrane thickness changes (e.g., of the order of 20% (15)) so that it is indeed a reasonable approximation to ignore ΔV upon calculating lipid area changes from changes in order parameter profiles (NMR) or bilayer repeat distances (SAXS) or thickness changes from area data (Langmuir trough). However, the value of -1.4% is large when the volume or packing density changes per se are concerned, since it is close to -2.0% accompanying the freezing of pure POPC into a gel phase (19,27). The latter value can be considered the maximum volume change that is conceivable upon lipid packing changes.

It should be noted that the fact that the orientation of the headgroup is only slightly changed by addition of cholesterol (28) does not mean that it would not contribute to ΔV . Changes in hydration

(see (29)) have a strong influence on the partial volume of the membrane constituents; water molecules bound to polar groups are known to exhibit a larger density than bulk water since the latter establishes a space-consuming network of hydrogen bonds (21,30).

The number of condensed lipid molecules per cholesterol

The phase model suggests a phase boundary to the ℓ_o state proceeding from $X_o \sim 0.3$ at 2°C to 0.35 between 10°C and 20°C and 0.4 at $\sim 40^\circ\text{C}$ (Fig. 3). Since the position of the phase boundary corresponds to the minimum cholesterol content of the ℓ_o phase, we may conclude that one cholesterol molecule may order ~ 2 POPC molecules at 2°C and 1.5 at 40°C . The fits of the random-neighbor model shown in Fig. 3 suggest that a cholesterol can condense $n = 3 \pm 1$ POPC molecules at 2°C , ~ 2 at 10°C and ~ 1 at 40°C . Hence, both models agree within error with the random-neighbor model suggesting a somewhat steeper temperature dependence of n . A larger value of $n \sim 7.5$ was published for DPPC (15), which is in line with many reports indicating that the effect of cholesterol on saturated lipids is stronger than that on unsaturated lipids.

For $\Delta V/V_{\text{PCd}} = -1.4\%$ and $n = 3$ PC molecules per cholesterol, one obtains a volume change by about -4.2 vol-% per cholesterol (in the low X range where the lipid is in excess). This value applying specifically to liquid (ℓ_d or ℓ_o) membranes is close to -4.9 vol-% per cholesterol derived from the slope of the volume change of the gel-to-liquid transition of POPC with increasing cholesterol content (19). This implies that the effect of cholesterol on the lipid volume in the gel phase is much smaller than that in the fluid phase.

CONCLUSIONS

1) Cholesterol-induced ordering of fluid, unsaturated phospholipid is accompanied by a volume condensation and its thermal relaxation is revealed by anomalously enhanced thermal volume expansivity.

2) A quantitative consideration of the expansivity behavior allows for a direct comparison with the predictions for phase separation and random mixing. The real system shows intermediate properties as suggested for nanoscopic de-mixing or domain formation but the two models yield consistent interaction parameters. That means both models are similarly good approximations.

3) The relative volume change of fluid unsaturated lipid (POPC) induced by cholesterol at 2°C amounts to $\sim -(1.4 \pm 0.5)\%$, close to the condensation upon freezing to a gel phase (-2.0%). Each cholesterol molecule can condense $n = 3 \pm 1$ POPC molecules. Both $|\Delta V|$ and n decrease with increasing temperature but the effect remains detectable up to $\sim 70^\circ\text{C}$.

ACKNOWLEDGEMENTS

We are indebted to Halina Szadkowska for excellent technical assistance. We thank S. Keller (FMP, Berlin) and K. Gawrisch (NIH, Rockville) for important comments. Funding by the Swiss National Science Foundation (grant 31-67216.01) is gratefully acknowledged.

REFERENCES

1. Demel, R. A. and B. De Kruffyff. 1976. The function of sterols in membranes. *Biochim Biophys Acta* 457:109-132.
2. Yeagle, P. L. 1985. Cholesterol and the cell membrane. *Biochim Biophys Acta* 822:267-287.
3. McMullen, T. P. W., R. N. A. H. Lewis, and R. N. McElhaney. 2004. Cholesterol–phospholipid interactions, the liquid-ordered phase and lipid rafts in model and biological membranes. *Current Opinion in Colloid and Interface Science* 8:459–468.
4. Veatch, S. L. and S. L. Keller. 2005. Seeing spots: complex phase behavior in simple membranes. *Biochim Biophys Acta* 1746:172-185.
5. Ipsen, J. H., O. G. Mouritsen, and M. J. Zuckermann. 1989. Theory of thermal anomalies in the specific heat of lipid bilayers containing cholesterol. *Biophys J* 56:661-667.
6. Zuckermann, M. J., J. H. Ipsen, L. Miao, O. G. Mouritsen, M. Nielsen, J. Polson, J. Thewalt, I. Vattulainen, and H. Zhu. 2004. Modeling lipid-sterol bilayers: applications to structural evolution, lateral diffusion, and rafts. *Methods Enzymol* 383:198-229.
7. Kahya, N., D. Scherfeld, K. Bacia, and P. Schwille. 2004. Lipid domain formation and dynamics in giant unilamellar vesicles explored by fluorescence correlation spectroscopy. *J Struct Biol* 147:77-89.
8. Veatch, S. L., I. V. Polozov, K. Gawrisch, and S. L. Keller. 2004. Liquid domains in vesicles investigated by NMR and fluorescence microscopy. *Biophys J* 86:2910-2922.
9. Henriksen, J. R., A. C. Rowat, E. Brief, Y. W. Hsueh, J. L. Thewalt, M. J. Zuckermann, and J. H. Ipsen. 2006. Universal behaviour of membranes with sterols. *Biophys J*:in press.
10. Vist, M. R. and J. H. Davis. 1990. Phase equilibria of cholesterol/dipalmitoylphosphatidylcholine mixtures: ²H nuclear magnetic resonance and differential scanning calorimetry. *Biochemistry* 29:451-464.
11. Sankaram, M. B. and T. E. Thompson. 1991. Cholesterol-induced fluid-phase immiscibility in membranes. *Proc Natl Acad Sci U S A* 88:8686-8690.
12. Tauc, P., C. R. Mateo, and J. C. Brochon. 1998. Pressure effects on the lateral distribution of cholesterol in lipid bilayers: a time-resolved spectroscopy study. *Biophys J* 74:1864-1870.
13. de Almeida, R. F., A. Fedorov, and M. Prieto. 2003. Sphingomyelin/phosphatidylcholine/cholesterol phase diagram: boundaries and composition of lipid rafts. *Biophys J* 85:2406-2416.
14. Thewalt, J. L. and M. Bloom. 1992. Phosphatidylcholine: cholesterol phase diagrams. *Biophys. J.* 63:1176-1181.
15. Edholm, O. and J. F. Nagle. 2005. Areas of Molecules in Membranes Consisting of Mixtures. *Biophys J* 89:1827-1832.
16. Melchior, D. L., F. J. Scavitto, and J. M. Steim. 1980. Dilatometry of dipalmitoyllecithin-cholesterol bilayers. *Biochemistry* 19:4828-4834.
17. Nagle, J. F. and S. Tristram-Nagle. 2000. Structure of lipid bilayers. *Biochim Biophys Acta* 1469:159-195.

18. Koenig, B. and K. Gawrisch. 2005. Specific volumes of unsaturated phosphatidylcholines in the liquid crystalline lamellar phase. *Biochim Biophys Acta* in press.
19. Rappolt, M., M. F. Vidal, M. Kriechbaum, M. Steinhart, H. Amenitsch, S. Bernstorff, and P. Laggner. 2003. Structural, dynamic and mechanical properties of POPC at low cholesterol concentration studied in pressure/temperature space. *Eur Biophys J* 31:575-585.
20. Landwehr, A. and R. Winter. 1994. High-pressure differential thermal analysis of lamellar to lamellar and lamellar to non-lamellar lipid phase transitions. *Ber Bunsenges Phys Chem* 98:214-218.
21. Lin, L. N., J. F. Brandts, J. M. Brandts, and V. Plotnikov. 2002. Determination of the volumetric properties of proteins and other solutes using pressure perturbation calorimetry. *Anal Biochem* 302:144-160.
22. Bangham, A. D., M. M. Standish, and J. C. Watkins. 1965. Diffusion of univalent ions across the lamellae of swollen phospholipids. *J Mol Biol* 13:238-252.
23. Huang, J., J. T. Buboltz, and G. W. Feigenson. 1999. Maximum solubility of cholesterol in phosphatidylcholine and phosphatidylethanolamine bilayers. *Biochim Biophys Acta* 1417:89-100.
24. Heerklotz, H. 2004. Microcalorimetry of lipid membranes. *J. Phys.: Cond. Matter* 16:R441-467.
25. Radhakrishnan, A., T. G. Anderson, and H. M. McConnell. 2000. Condensed complexes, rafts, and the chemical activity of cholesterol in membranes. *Proc Natl Acad Sci U S A* 97:12422-12427.
26. Radhakrishnan, A. and H. McConnell. 2005. Condensed complexes in vesicles containing cholesterol and phospholipids. *Proc Natl Acad Sci U S A* 102:12662-12666.
27. Ichimori, H., T. Hata, H. Matsuki, and S. Kaneshina. 1999. Effect of unsaturated acyl chains on the thermotropic and barotropic phase transitions of phospholipid bilayer membranes. *Chemistry and Physics of Lipids* 100:151-164.
28. Brown, M. F. and J. Seelig. 1978. Influence of cholesterol on the polar region of phosphatidylcholine and phosphatidylethanolamine bilayers. *Biochemistry* 17:381-384.
29. Petrache, H. I., D. Harries, and V. A. Parsegian. 2004. Alteration of lipid membrane rigidity by cholesterol and its metabolic precursors. *Macromolecular Symposia* 219:39-50.
30. Chalikian, T. V. 2003. Volumetric properties of proteins. *Annu. Rev. Biophys. Biomolec. Struct.* 32:207-235.
31. Cevc, G. and D. Marsh. 1985. *Phospholipid Bilayers*. E. Bittar, editor. New York: John Wiley and Sons.

APPENDIX: DERIVATION OF EQ. (6)

Let us assume that the lipid volume is smaller in the more densely packed ℓ_o state than in the ℓ_d state. Then, a positive contribution to the thermal expansion will arise if increasing temperature leads to a “melting” of ℓ_o domains to ℓ_d .

We have derived a quantitative model for the thermally induced conversion from ℓ_o into ℓ_d and the subsequent, composition-dependent expansivity, $V'(X)$, at a given T in a system showing phase separation. In the one-phase ranges, there is no phase conversion.

In the coexistence range ($X_d < X < X_o$), the internal composition of the two phases is constant with cholesterol mole fractions of X_o and X_d in the ℓ_o and ℓ_d phase, respectively. What changes as a function of the total cholesterol fraction, X , is only the proportion between the two phases. The fraction of all molecules that is in the ℓ_o phase, ξ (note difference to ξ_{PCd}), is given by the lever rule (4,31):

$$\xi = \frac{[PC_o] + [cho_o]}{[PC] + [cho]} = \frac{X - X_d}{X_o - X_d} \quad (10).$$

Since the local fraction of PC in the ℓ_o phase is $1 - X_o$, we obtain for the fraction of PC in the ordered phase referred to the whole membrane:

$$\frac{[PC_o]}{[PC] + [Cho]} = \xi_{PC} (1 - X) = \xi (1 - X_o) \quad (11).$$

Eq. (3) relates V' to ξ_{PC} and ξ_{PC}' . Differentiating eq. (11) with respect to T (and determining ξ' from eq. (10)) at a given sample composition ($X = \text{const.}$, $X' = 0$), one obtains:

$$(1 - X) \xi'_{PC} = a X'_d - \xi X'_o + a \xi (X'_o - X'_d) \quad (12)$$

with the constant a :

$$a \equiv -\frac{1 - X_o}{X_o - X_d} \quad (13).$$

Insertion into Eq. (3) yields Eq. (6).

FIGURE LEGENDS

Fig. 1, top: Schematic illustration of the phase model. Top: Phase diagram with liquid disordered (ℓ_d), liquid ordered (ℓ_o) and $\ell_d+\ell_o$ -coexistence (dotted area) ranges in the space defined by temperature T and the mole fraction of cholesterol in the membrane, X . The solubility limit of cho in membranes is about $X \leq 0.66$ (23) (temperature dependence unknown). Bottom: The resulting schematic behavior of the expansivity, V' , as a function of X . See text for details.

Fig. 2: The coefficient of thermal expansion, α , as a function of temperature, T , of POPC-cholesterol vesicles with cholesterol mole fractions, X , as specified in the plots. Up to $X \sim 0.2$, $\alpha(2^\circ\text{C})$ increases with X (A) but at higher cholesterol contents, it decreases again (B).

Fig. 3: The relative deviation of thermal expansion coefficients, α , of mixed membranes at given cholesterol content, X , and temperature, T , from the values in the absence of cholesterol.

Fig. 4: The thermal volume expansion, V' , as a function of the cholesterol mole fraction in the membrane, X , at selected temperatures as indicated in the plot. The curves correspond to the phase model (solid lines, perpendicular at phase boundaries) and the random-neighbor model (dashed lines). The corresponding parameters are discussed in the text.

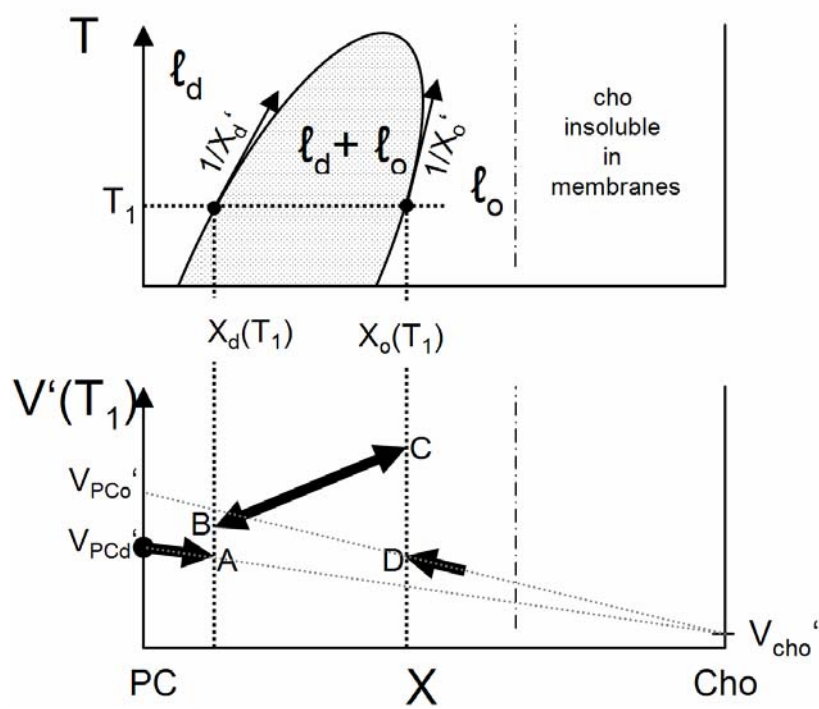


Fig. 1

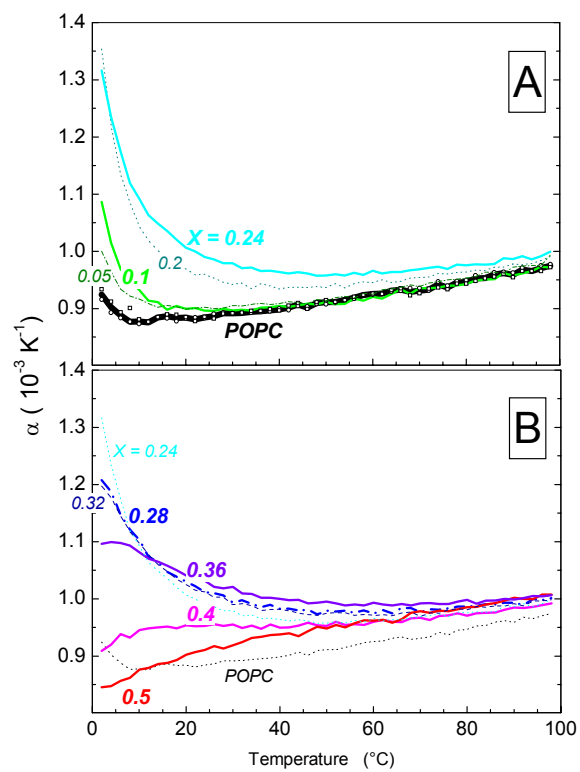


Fig. 2

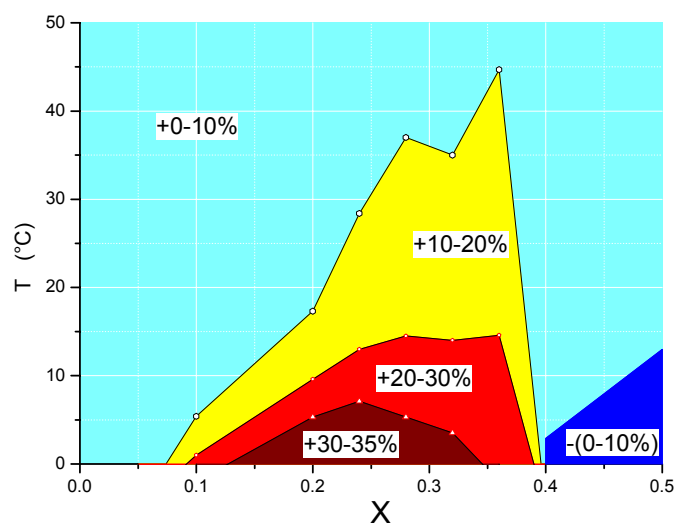


Fig. 3

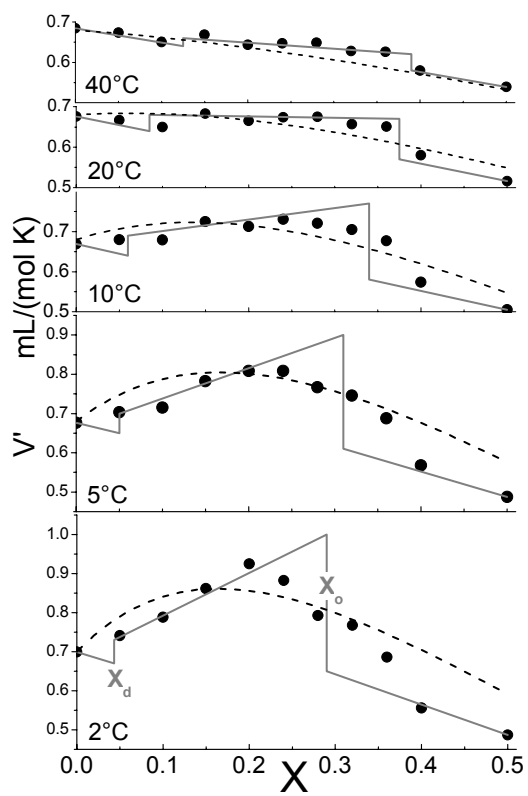


Fig. 4

Tabellarischer Lebenslauf

Persönliche Daten

Alekos D. Tsamaloukas
Blauenstrasse 77
4054 Basel
Geboren am 05. 04. 1975 in Berlin–Ost (DDR)
email: aleko@oxphos.de
Familienstand: ledig
Staatsangehörigkeit: Deutsch

Schulbildung

08/1981–06/1994 Grundschule und Gymnasium in Monheim und Hilden (Leistungskurse Physik und Erdkunde).

Zivildienst

08/1994–10/1995 Mitarbeiter in der Haustechnik im Städtischen Altenheim in Hilden.

Studium

10/1995–10/1996 Studium der Biochemie an der Freien Universität Berlin.
10/1996–9/1998 Studium der Physik an der Freien Universität Berlin, Vordiplom im September 1998, Gesamtnote: sehr gut.
10/1998–9/1999 Studium der Physik an der Rheinischen Friedrich–Wilhelms–Universität im Rahmen des englischsprachigen *Bonn International Physics Programme* (BIPP).
10/1999–9/2000 Studium der Physik an der Freien Universität Berlin.
10/2000–12/2001 Diplomarbeit in der Ag Prof. H. Dau an der Freien Universität Berlin (molekulare Biophysik & Photosynthese) zum Thema: „Fluoreszenzspektroskopie zur Exzitonendynamik in den Chlorophyllantennen des Photosystems II der Pflanzen.“ Gesamtnote: sehr gut.

Berufserfahrung

03/2002 Erhalt eines Promotionsstipendiums der *University of Otago*, Dunedin (Neuseeland); Rückkehr nach Deutschland im Mai 2002.

- 10/2002–03/2003 Wissenschaftlicher Mitarbeiter am Max–Planck Institut für Strahlenchemie in Mülheim an der Ruhr in der Ag von Prof. A. R. Holzwarth. Theoretische Arbeiten zur mathematischen Modellierung der Energietransferprozesse im Photosystem II.
- 4/2003–03/2006 Wissenschaftlicher Mitarbeiter im Biozentrum der Universität Basel in der Ag von PD Dr. H. H. Heerklotz. Promotion über das Thema „Quantifying intermolecular interactions as a basis of domain formation in membranes“, Prädikat: *summa cum laude*.
- seit 4/2006 Postdoktorand am Department of Chemistry & Physics, University of Toronto (Kanada) mittels eines Postdoc–Stipendiums des Deutschen Akademischen Austauschdienstes (DAAD).

Basel, 24. Januar 2006

Alekos Tsamaloukas